ISTANBUL TECHNICAL UNIVERSITY ★ GRADUATE SCHOOL OF SCIENCE ENGINEERING AND TECHNOLOGY

A NOVEL LIQUID LEVEL SENSOR DESIGN USING LASER OPTICS TECHNOLOGY

Ph.D. THESIS

Mehmet Emre ERDEM

Department of Mechanical Engineering

Mechanical Engineering Programme

DECEMBER 2011

ISTANBUL TECHNICAL UNIVERSITY ★ GRADUATE SCHOOL OF SCIENCE ENGINEERING AND TECHNOLOGY

A NOVEL LIQUID LEVEL SENSOR DESIGN USING LASER OPTICS TECHNOLOGY

Ph.D. THESIS

Mehmet Emre ERDEM
(503042002)

Department of Mechanical Engineering

Mechanical Engineering Programme

Thesis Advisor: Prof. Dr. Doğan GÜNEŞ

DECEMBER 2011

İSTANBUL TEKNİK ÜNİVERSİTESİ ★ FEN BİLİMLERİ ENSTİTÜSÜ

LAZER OPTİK TEKNOLOJİSİ İLE YENİ BİR SIVI SEVİYE SENSÖRÜ

DOKTORA TEZİ

Mehmet Emre ERDEM
(503042002)

Makina Anabilim Dalı

Makina Mühendisliği Doktora Programı

Tez Danışmanı: Prof. Dr. Doğan GÜNEŞ

ARALIK 2011

Mehmet Emre Erdem, a **Ph.D.** student of ITU **Institute of / Graduate School of Science Engineering And Technology** student ID **503042002**, successfully defended the thesis entitled "**A NOVEL LIQUID LEVEL SENSOR DESIGN USING LASER OPTICS TECHNOLOGY**", which he prepared after fulfilling the requirements specified in the associated legislations, before the jury whose signatures are below.

Thesis Advisor :	**Prof. Dr. Doğan GÜNEŞ** İstanbul Bilgi University	....
Jury Members :	**Prof. Dr. Ahmet DENKER** İstanbul Bilgi University	....
	Prof. Dr. Nurdil ESKİN İstanbul Technical University	....
	Assis. Prof. Dr. Özgen AKALIN İstanbul Technical University	....
	Prof. Dr. Sezgin Alsan Istanbul Commerce University	....

Date of Submission : 08 July 2011
Date of Defense : 22 December 2011

To my family,

FOREWORD

New materials and technological developments in electronics and computers have changed all of the industries, as well as the world itself. Therefore the types and usages areas of sensors have been spread over a wide variety of applications.
In this thesis, the finite element based development stages of a state-of-the-art liquid level sensor have been performed, while a novel liquid level sensor design using laser optics technology based on Whispering-gallery mode has been presented with the precise experimental results achieved.
I would like to express my deep appreciation and thanks for my advisor Prof. Dr. Doğan Güneş. Without his routing this study could not been achieved.
And very special thanks to Prof. Dr. Volkan Otugen, the Professor and chair of Mechanical Engineering department and director of Micro-Sensors laboratory of SMU, for his valuable contributions, and hosting the experiments in Micro Sensors lab. of Southern Methodist University.
I would also like to thank to Mr. Ulas Ayaz (Ph.D.) for his valuable cooperation & contributions during the experiments, and the manager of manufacturing facilities in SMU, Mr. Necdet Yildirimer for all his advices and contributions during the sensor development stages.
Finally I would like to thank to my family; especially my mother and my father, for their invaluable & continuous supports and love all these years.

December 2011 Mehmet Emre ERDEM
(Mechanical Engineer)

TABLE OF CONTENTS

Page

ABBREVIATIONS

AC	: Alternating Current
CW	: Continuous Wave
ECU	: Electronic Control Unit
DAQ	: Digital-to-Analog Converter
DFB	: Distributed Feedback
FEM	: Finite Element Method
HP	: High Pressure
IR	: Infrared
LED	: Light Emitting Diode
MAP	: Manifold Absolute Pressure
MDR	: Morphology Dependent Resonance
NVH	**:** Noise, Vibration and Harshness
OLS	**:** Oil Level Sensor
PBS	**:** Phosphate Buffered Saline
PD	**:** Photodiodes
PMMA	**:** Polymethyl Methacrylate
PDMS	**:** Polydimethylsiloxane
PULS	: Packed Ultrasonic Level Sensor
RADAR	: Radio Detection and Ranging
SMF	: Single Mode Fiber
UV	: Ultraviolet
WGM	: Whispering Gallery Mode

LIST OF SYMBOLS

a	: Radius of sphere
$\boldsymbol{a_0}$	: Radius of contact area
$\boldsymbol{A_n}$ **&** $\boldsymbol{B_n}$	: Constants
$\boldsymbol{C^*}$	: Compressive wave velocity
D	: Diameter
E	: Young's modulus
F	: Applied force
G	: Shear modulus
J_n	: Bessel functions of first kind,
$\boldsymbol{k_{beam}}$	: Equivalent beam spring constant
$\boldsymbol{k_{sphere}}$	: Equivalent sphere spring constant
L	: Length of the silica beam
$\boldsymbol{P_n}$	: Legendre polynomial,
r	: Radial coordinate
U	: Radial displacement of sphere surface
ν	: Poisson ratio
$\boldsymbol{\lambda}$	: Laser wavelength in vacuum
$\boldsymbol{n_0}$	: Refractive index ,
l	: Integer indicating the circumferential mode number.
$\boldsymbol{\vartheta}$	: Polar coordinate
$\boldsymbol{\delta}$	: Displacement of the translation stage
$\boldsymbol{\lambda_m}$	: Wavelength of He-Ne laser
ω_n	: Angular frequency

LIST OF TABLES

Page

LIST OF FIGURES

Page

A NOVEL LIQUID LEVEL SENSOR DESIGN USING LASER OPTICS TECHNOLOGY

SUMMARY

The discovery of new materials and the technological developments in electronics have changed the whole industry and the world. Today sensors are being used nearly in every application of aeration, space, naval, automotive, civil, mechanical, industrial, electronics and computer engineering as well as advanced medicine, medical sciences and many other areas, and led to innovations and advances to every process when used.

The study has started with the need of highly sensitive, compact liquid level measurement sensor which can be used even in flammable medium. To provide the demand, the positive and negative features and aspects of the current sensors, the literature and similar studies have been investigated. At first, a valid ultrasonic liquid level sensor has been analyzed to meet the requirements by improving its characteristics. For improving and solving the problems of the current sensor, finite element analysis has been performed until reaching a new model, which can be used to build the initial production prototypes. Although consideration of the results has shown that to meet all of the targets, a new and highly sensitive liquid levels sensor has to be developed, which should be the next step of the study.

When looking through the techniques of the liquid level detection, it has been seen that there is a wide variety of detection methods. Some of them are: sensors working mechanically with Archimedes' principle, floating level sensors, magnetic liquid level indicators, liquid level sensors using ultrasound and lambda waves to measure the flight time of the waves, Nuclear level switches using low level radiations emitted by radioactive sources, and various optical detection methods. In some of the optic applications, optic sensors are located at top or bottom level according to liquid existence and some of the fiber optic based systems measure the liquid level by the change of the refractive index.

Other than these, when investigating some other common sensors, capacitive pressure measurement systems based on principle that measures the pressure change between the capasitor plates, strain gage systems which measure the pressure by shape changes, load cell type systems and piezoelectric pressure measuring systems has been evaluated.

These systems usually have sensitivity problems. As an example, ultrasonic liquid level systems in automotive applications have ±1mm liquid height sensitivity values, while most of the precise pressure measurement sensors are sensitive to measure 50-100 kpa.

The theory of this study was found many years ago when it was seen that sound waves in whispering tone bounce along the circular gallery of St Paul's Cathedral with very little loss, and this phenomenon was named as Whispering Gallery Mode

(WGM). Today WGM theory has been introduced into modern electronics, and as a result, it has become an advanced theory including optical physics and electronics. In modern WGM applications, when laser light comes into the microsphere in its contact point with the tapered film, the light undergoes total internal reflections in the sphere. After repeated total internal reflections at the curved boundary, the electromagnetic field can close on itself and a resonance occurs on the light signal going to the photodiode.

More importantly these resonances change when there is a change on the refractive index or geometry. The resonance frequencies shift with the changes of the microsphere size and/or the optical properties of the surrounding medium. One of the biggest advantages of the WGM theory is that very small values such as 10^{-5} N can be detected by using this method.

For evaluating the possibility of developing a higly sensitive novel liquid level sensor using WGM phenomenon Southern Methodist University Microsensors lab. has been visited. After many meetings and discussions, it has been considered that a new kind of highly sensitive liquid level sensor can be developed by using the WGM phenomenon, in the Micro sensors lab. facilities of Southern Methodist University, where the experiments of the novel sensor have been performed.

The novel sensor shows that the dependence of WGM shifts to liquid levels can be assumed as perfectly linear all the measurement range without being affected by the amount of liquid in the container. A Pa change in liquid pressure, results as high as 3,12 pm WGM shifts, which have been observed during the liquid level experiments. When the axis have been switched, it can be estimated that the values are ranging between 0,033-0,053 mm of water level per pm WGM shift of the Laser Spectrum, again with a perfect linear correlation. It has also been calculated that the total uncertainity of the experiments is assumed to be around ±1,12%, which might be improved with the usage of equipments with higher accuracy.

Also nother advantage relies on the WGM phenomenon, in which this novel sensor can be worked in any environment without being affected by the availability of flammable liquids and gasses etc.

As a result of this study, a novel high-tech laser-optic technology based liquid level measurement sensor has been designed which can be used in automotive, aerospace & aviation industries, medicine, defense, civil engineering, and many other fields.

LAZER OPTİK TEKNOLOJİSİ İLE YENİ BİR SIVI SEVİYE SENSÖRÜ

ÖZET

Elektronik ve bilgisayar sektörlerindeki teknolojik gelişmeler ve yeni malzemelerin keşfi bütün endüstri kollarını değiştirdiği gibi, dünyayı da baştan aşağı değiştirmiş ve değiştirmeye de devam etmektedir. Günümüzde sensörler, havacılıktan otomotive, uzay çalışmalarından, makine, inşaat sektörlerine ve hatta tıp alanına kadar, mühendisliğin kullanıldığı her alana girmiş ve girdiği alanlarda, sadece mevcut metodları kolaylaştırmakla kalmamış, aynı zamanda büyük yeniliklere ve ilerlemelere yol açmıştır.

Bu çalışmaya yüksek hassasiyete sahip, yanıcı ve patlayıcı ortamlardan etkilenmeden çalışabilecek yeni bir sıvı seviye sensörü ihtiyacı ile yola çıkılmış, bu talebi karşılayabilmek icin mevcut sensörlerin artı ve eksi yönleri, bunun yanında literatürde benzeri çalışmalar incelenmiştir. İlk önce mevcut ultrasonik bir seviye sensöründeki sorunları çözebilmek adına sonlu elemanlar analizleri yapılmış ve çalışma ilk imalat prototipleri üretilip testler yapılacak noktaya kadar getirilmiştir. Ancak bu çalışma sonucunda istenen hassasiyet noktasına ulaşılamayacağı görüldüğü için tamamen yeni bir sıvı seviye sensörü geliştirme fikri ortaya çıkmıştır. Sensörü geliştirme aşamaları planlanmış ve daha sonra detaylarıyla anlatılacak olan deneysel sonuçlarla fikrin doğrulanması sağlanmıştır.

Tekniğin bilinen durumuna göz atıldığında sıvı seviyesi tespit yöntemlerinin çok çeşitli olduğu gözlemlenmiştir. Bunlardan bazıları, Arşimed prensibiyle mekanik olarak sıvıların kaldırma kuvvetini ölçen sistemler, şamandıralı sıvı seviye tespit sistemleri, manyetik seviye indikatörleri, ultrasonik ses ve lambda dalgalarıyla bu dalgaların gidiş-geliş sürelerine göre mesafeyi ölçen sistemler, düşük enerjili gamma ışıması ile nükleer sıvıların seviyesini ölçmekte kullanılan sistemler ve çeşitli temel optik uygulamalarıdır. Bu optik uygulamaların bazıları, sıvının mevcudiyetine göre üst veya alt seviyede konumlandırılan optik sensörler ve akademik çalışmalarda da göze çarpan ortamdaki kırılma indisi değişiminden yararlanarak sıvının mevcudiyetini tespit etmekte kullanılan fiber optik sistemlerdir.

Bunun haricinde belli başlı basınç sensörleri incelendiğinde ise temelde kondansatör plakalarının arasındaki alanın basıncındaki değişim sonucu kondansatör kapasitesinin değişmesi prensibine dayanan kapasitif basınç ölçme sistemleri, strain gage (gerilim ölçer) kullanarak şekil değişikliğinden yararlanan basınç sensörleri, Load Cell (Yük Hücresi) tipindeki sistemler ve üzerine gelen basınca göre elektrik akımı/gerilim oluşturan Piezoelektrik basınç ölçme sistemleri göze çarpar.

Bu sistemler genellikle hassasiyet sorunlarına sahiptirler. Örneğin ultrasonik sıvı seviye sistemlerinin otomotiv uygulamalarında sıvı yüksekliği ±1mm hassasiyetine sahipken basınç ölçümünde kullanılan sensörler 50-100 kPa hassasiyetlerde çalışırlar.

Bu noktada sıvı seviyesi tespit yöntemlerinde bir eksiklik olduğu görülmüş, ve yüksek teknolojiye sahip, hassasiyet açısından sorunu olmayan bir alternatif

arayışına girilmiştir, ve sıvı seviyesi ölçümünde uygulamaları olmasa da, farklı alanlarda çığır açan yepyeni bir yönteme rastlanmıştır.

Bahsedilen çalışmanın teorisi, bundan uzun yıllar önce fısıldama tonundaki seslerin dairesel bir galerinin çevresi boyunca yansıyarak çevresel olarak uzak mesafelerde duyulması sonucu bulunmuş olup Fısıldayan Galeri Modu (Whispering Gallery Mode (WGM)) ismini almıştır. Günümüzde ise WGM uygulamalarında, lazer ışığı, mikro küreciklere temas ettiği noktada tam yansımalar meydana getirip dairesel bir yörünge izlemektedir. Dairesel yörünge boyunca tam yansımalarla ilerleyen lazer ışığı dalga boyunun tam katlarında mükemmel bir şekilde üst üste gelerek ilerlemeye devam eder. Ancak bu mükemmel çakışmaların bir sonucu olarak, küreciklerin yörüngelerinden geçen ışık sinyalinde rezonanslar meydana gelir.

Teorinin gereği olarak, kürenin kırılma indisi veya şekli değiştiği zaman bu rezonanslar da yer degiştirmektedir. Bu durumda kürenin üzerine uygulanan basınç veya kuvvet sonucu kürenin şeklinde veya yarıçapında bir farklılık olduğu taktirde, mevcut rezonansların yeri değişecek, ve bu değişim bir yazılımla takip edildiği taktirde mikro küreciğe uygulanan basınç veya kuvvet bulunabilecektir. Bu yöntemin en önemli avantajlarından biri, bu prensibe göre çalışan sensörlerin yüksek hassasiyete sahip oluşlarıdır. Diğer bir önemli avantaj ise sensörün giriş ve çıkışında sadece düşük enerjili lazer ışığı olmasından dolayı her türlü patlayıcı veya yanıcı ortamda sorunsuz ve tehlikesiz çalışabilecek olmasıdır.

Bu tip bir sıvı seviye sensörü geliştirmek fikriyle Southern Methodist Üniversitesi (SMU, Dallas, TX) Makine Mühedisliği bölümü Mikro Sensörler laboratuarı ziyaret edilmiş, ve benzeri WGM uygulamaları üzerinde çalışmalar yapılarak yöntemin sıvı seviyesi ölçümüne uygulanabilirliği incelenmiştir. Bu konuda çok sayıda makale incelendikten, ve SMU’daki konunun uzmanları ile fikir alışverişinde bulunulduktan sonra WGM prensibinin sıvı seviyesi ölçümünde kullanılabileceği kararına varılmıştır. Bu kararın alınmasının ardından teorinin detaylarına inilerek, çalışma prensibi doğrultusunda en uygun deney düzeneği ve sensör prototipinin nasıl olması gerektiğine dair ön çalışmalar yapılmıştır. Bu teorik çalışmalarda da bir fikir birliğine varıldığı noktada, SMU Mikrosensörler laboratuarlarına bizzat gidilmiş, ve WGM prensibi ile çalışan yeni bir sıvı seviye sensörü geliştirme üzerinde çalışmalara başlanmıştır. Geliştirilen çeşitli sensör prototipi ve deney düzeneği kullanılarak nihai tasarıma ulaşılmış, ve nihai tasarımla ilk önce sıvı olmayan ortamda gaz basınçlarını ölçmek üzere bir düzenek kurularak ilk deneyler yapılmıştır. Deneylerde başarılı sonuçlar elde edilmesini takiben sıvı seviye ölçümü dene düzeneğinin kurulması çalışmalarına başlanmış, ve bu aşamada özellikle sensörün sıvı altında çalışacak şekilde sızdırmazlığa karşı korunmasına özen gösterilmiştir. Bu aşamalardan sonra bir konteynır içine yerleştirilen sensör çalışmaya başlamış, ve çok çeşitli kereler konteynıra su doldurma ve boşaltma sağlanarak, sensörün çeşitli durumlardaki davranışı gözlemlenmiş, ve bütün bu deneyler süresince veri toplanmıştır.

Deneylerde toplanan datalar göstermiştir ki WGM rezonans kaymalarının sıvı seviyesi değişimlerine verdiği karşılık, diğer bir değişle sensörün hassasiyeti lineer bir eğri halini almaktadır. Grafikler incelendiğinde eğriler, 0,9967-0,9993 arasında değişen R^2 değerleri ile mükemmele yakın bir korelasyon ile doğru teşkil etmektedir.

Üstelik bu davranış sıvı seviyelerine veya doldurma boşaltma sürelerine bağlı olmaksızın çeşitli seviyelerde tekrar etmektedir, ki bu durum sonuçların güvenilirliği açısından son derece önemlidir.

Elde edilen değerler fiziksel olarak incelendiğinde ise, 1 Pa seviyesindeki değişimin gaz basıncı deneylerinde 5,93 pm seviyelerinde rezonans kaymalarına sebep olduğu, sıvı basıncı deneylerinde ise 3,12 pm seviyelerine kadar rezonans kaymalarına ulaşılabileceği görülmektedir. Bir başka değişle eksenler yer değiştirdiğinde özellikle sıvı seviyesi ölçümü deneylerinde 0,033-0,053mm'lik su seviyesi değişimlerinin, laser spektrumunda 1 pm'lik kaymaya neden olduğu görülebilir. Burada belirtmek gerekir ki sonuçlar yine mükemmele yakın bir lineerlikle ortaya çıkmaktadır.

Bu sonuçlara ek olarak hata hesabı yapıldığında deney düzeneğine sıvı doldurulurken % ±1,126, deney düzeneğindeki sıvı boşaltılırken ise % ±1,137 seviyelerinde doğruluk değerleri elde edilmiştir. Burada dikkat edilmesi gereken bir husus, gerek gaz basıncı, gerekse de sıvı seviyesi ölçümlerinde kullanılan referans cihaz olan basınç dönüştürülerin üretici verilerine bakıldığında bu cihazların %±1 doğruluğa sahip olduklarıdır. Dolayısıyla ileride yapılacak çalışmalarda deney düzeneğinde daha yüksek doğruluğa sahip ekipmanların kullanılması ile beraber doğruluk değerlerinin daha da iyileşeceği tahmin edilmektedir.

Bu çalışmanın sonucunda, otomotivden uzay-uçak sanayi ve havacılığa, tıptan savunma sanayine, ve benzeri çok çeşitli alanlarda basınç ve sıvı seviyesi ölçümü yapabilecek lazer-optik teknolojisi temelli yepyeni ve ileri teknoloji ürünü hassas bir basınç sensörü tasarımı, deneysel sonuçları ile beraber sunulmuştur.

1. INTRODUCTION

In today's world, electronics are developing much faster than anything, which enables us to develop better systems, and control them precisely. Technological developments are affecting every industry one by one, therefore sensors are being used nearly in every application of aeration, space, naval, automotive, civil, mechanical, industrial, electronics and computer engineering as well as advanced medicine, medical sciences and many other areas.

There are many sensors controlling the mechanical systems. This study is focused on specific techniques for liquid level measuring. For example oil level sensor used in automotive industry has a critical importance due to the fact that it controls the oil levels and warns the driver for dangerously low levels. Otherwise oil loss without detection, may cause extensive damage.

Although there are many different applications for liquid level measuring, two of them are the most common techniques. There is a wired resistive sensor which works with the principle of resistance difference. When the current passes the resistance, it creates a voltage, which is different than the reference, or in other words it measures the difference in output and input voltages due to changing oil levels. But the main problem of the sensor is it is not capable of making any precise measurements, the best it can reach is ± 5 mm of liquid height difference.

The second type of sensor is an ultrasound transmitting one which works with the sonar principle; the sensor sends ultrasonic waves from the mounted locations which is the bottom of the sump, and when the sound waves reach the liquid surface, they reflect back to the sensor. When the sensor gets the reflected waves the sofware just calculates the distance out of the time of wave transmitting in the liquid. This is a better technology a higher precison of ± 2mm.

To improve sensitivity, cooperative studies have been started with one of the main sensor developers in the industry, Hella GmbH. Hella uses the ultrasonic principle in their sensors, and they have a sensor which is being mounted to the bottom of the oil sump, which has been redesigned to work inside oil with higher precision. Many studies have been performed with Hella, and developed a new sensor by using Finite Element Analysis. After making numerous analysis on the current sensor, a new design was developed. The new design was safe under engine vibrations, to keep stress and strain levels very much below of tensile limits of the material. Also, when analyzing according to fatigue conditions, the new sensor has been designed as safe as the current one. The main problem was the restrictions of the manufacturer about keeping the damping cap design same, to be able not to affect the ultrasonic wave propagations. Development studies performed on the sensor excluding the damping cap, therefore there is no way to improve sensitivity of the sensor.

When considering these issues, many different techniques used in the industry analyzed one bye one. There are many different types of approaches to sensors detecting the validity and level of the liquids: there are sensors working with archimedes' principle [2], sensors using transmittal of lambda waves [18], sensors using ultrasound waves in aero space applications [10], and even optical methods detecting the validity of the liquid using the changes in the refractive indexes [6], [5], and etc.

There is another method, called the Whispering Gallery Mode, which has been founded theoretically many years ago, but it has been started using in advanced electronics by using laser optics just a few years ago [19-23]. This method, has been investigated in detail and used for developing a novel liquid level sensor.

1.1 Purpose of the Thesis

The main objective of this study is to develop a novel liquid level sensor, with high precision and safety against explosion to be able to operate in many different fields of industry. For this aim, by using laser optics technology based on Whispering gallery mode phenomenon, a unique liquid level sensor has been built, which has precise measurement results, and can also work under flammable liquid conditions.

1.2 Background

The first studies about Whispering Gallery Mode (WGM) theory was started almost a century ago with the work of Lord Rayleigh, who studied propagation of soundwaves over a curved gallery surface. Earlier researchers have found that microresonators used in WGM have extremely high quality factors (Q) in the optical domain [43].

In a related study, Microspherical (50-500 μm diameter) glass resonators with Q factors excessing 10^{10} values have been demonstrated, and Q factors as high as 10^{11} are, in principle, possible [44].

In recent times whispering gallery modes have found new fame with the development of nano-optics. In the modern version of a Whispering Gallery Mode, laser light is coupled into a circular waveguide, such as a glass ring. When the light strikes the boundary of the ring at a grazing angle it is reflected back into the ring. The light wave can make many trips around the ring before it is absorbed, but only frequencies of light that fit perfectly into the circumference of the ring can do so. If the circumference is a whole number of wavelengths, the light waves superimpose perfectly each trip around.

This perfect match between the frequency and the circumference is called a resonance, or whispering-gallery mode.

Whispering gallery modes occur at particular resonant wavelengths of light for a given droplet size. At these wavelengths, the light undergoes total internal reflection at the particle surface and becomes trapped within the particle. In other words, WGM occurs when light travels in a dielectric medium of circular geometries. The droplet behaves like a low-loss optical cavity with the light circulating for timescales on the order of nanoseconds [46].

Whispering Gallery Modes of dielectric microspheres have attracted interest with proposed applications in a wide range of areas due to the high optical quality factors that they can exhibit.

In mechanical sensing application, the dielectric microsphere is optically coupled to a single mode fiber which carries light from a tunable laser and serves as an input/output port for the microsphere. When the microsphere comes into contact with an exposed section of the fiber core, its optical resonances are observed extremely narrow (with very high Q values) and thus are highly sensitive to any change in the morphology of the sphere (shape, size, or refractive index) . Moreover, the resonance frequencies will shift with the changes of the microsphere size and/or the optical properties of the surrounding medium.

A study about geometrical theory of whispering gallery modes indicates that, axisymmetric dielectric bodies have very high quality-factors, when sphere and torus shapes have been examined by Richtmyer. However, it has been seen that in the case of simplest axisymmetric geometry, different from ideal sphere or cylinder, no closed analytical solution has been found. While the microspheres in the theory of WGMs, are well established and allows precise calculations [54].

In the literature, there are many WGM based measurement techniques, which have been proposed for biological applications, especially detection of various molecules, mechanical sensing including temperature, force, pressure, acceleration, wall shear stress, magnetic field etc which will be discussed further in detail.

2. SENSORS

Sensors are essential components of electronic control systems. Sensors are defined as "devices that transform (or transduce) physical quantities such as pressure or acceleration into output signals (usually electrical) that serve as inputs for control systems". Starting in the late 1970s, microprocessor-based engine control modules were phased in to satisfy federal emissions regulations. These systems required new sensors such as MAP (manifold absolute pressure), air temperature, and exhaust-gas stoichiometric air-fuel-ratio operating point sensors. Today the need for sensors is evolving and progressively growing. For example, in engine control applications, the number of sensors used will increase from approximately 10 in 1995, to more than 30 in 2010 [8].

Computer controlled systems continually monitor the operating condition of today's mechanical systems. Sensors convert temperature, pressure, speed, position and other data into either digital or analog electrical signals. The computers use the sensor data to control different systems through the use of actuators, which is an electromechanical device such as a relay, solenoid or motor.

2.1 Sensor Types

In general, there are three main categories of sensors [35]:

2.1.1 Switch sensors

2.1.1.1 Phototransistor

A phototransistor is a transistor that is activated or turned on by light. When combined with a LED and a rotating slotted wheel in a vehicle speed sensor, a phototransistor can supply vehicle speed data to a computer [35].

2.1.1.2 Reed switches

The reed switch is an electrical switch actuated by the field from an external permanent magnet or electromagnet placed in close proximity. This field causes the reeds to become magnetic, the ends are attracted and the contacts either open or close. Removal of the magnetic field allows the springy reeds to restore the contacts to their original state.

2.1.2 Resistive sensors

2.1.2.1 Thermistor

It is a type of resistor whose resistance varies significantly with temperature, more so than in standard resistors. Thermistors are widely used as inrush current limiters, temperature sensors, self-resetting overcurrent protectors, and self-regulating heating elements.

2.1.2.2 Potentiometer

A potentiometer is a variable resistor that is commonly used as a sensor.It is a mechanical device whose resistance can be varied by the position of the movable contact on a fixed resistor. The movable contact slides across the resistor to vary the resistance and as a result varies the voltage output of the potentiometer. The output becomes higher or lower depending on whether the movable contact is near the resistor's supply end or ground end [37].

2.1.2.3 Piezo-resistive

A piezo resistive sensor is a resistor circuit constructed on a thin silicon wafer. Physically flexing or distorting the wafer a small amount changes its resistance. This type of sensor is usually used as a pressure sensing device such as a manifold pressure sensor, although it may also be used to measure force or flex in an object such as the deceleration sensor located in the SRS air bag center sensor.

2.1.3 Voltage generating sensors

2.1.3.1 Piezo electric

Piezo electricity is generated by pressure on certain crystals, such as quartz, which will develop a potential difference, or voltage, on the crystal face. When the crystal flexes or vibrates, an AC voltage is produced [35].

2.1.3.2 Oxygen sensors

The oxygen sensor located in the exhaust manifold of an engine, senses whether the air-fuel ratio is rich or lean, and sends signals to the ECU which in turn makes minor corrections to the amount of fuel being metered. This is necessary for the three-way catalytic converter to function properly. There are two kinds of oxygen sensors: Zirconia oxygen sensor and Titania oxygen sensor.

2.1.3.3 Magnetic inductance

Magnetic inductance sensors consist of a coil of wire around an iron core plus a permanent magnet. The magnet can be either stationary or movable. If the magnet is the moving member, as it passes the coil the magnetic lines of force cut through the coil and a voltage is produced. Since the north and south poles of the magnet alternate as they pass the coil, the voltage41 polarity also alternates. As the speed of the magnet rotating past the coil is increased a larger voltage is produced and the frequency of the voltage polarity changes is increased.

3. LEVEL MEASUREMENT SENSORS

Level is measured at the position of the interface between phases of liquid/gas, solid/gas, or liquid/liquid, and where the level is simply a measure of height. It defines the position of the interface, that is, the surface where the two phases meet with respect to a reference point.

The level measurement can either be continuous or point values. Continuous level sensors measure level within a specified range and determine the exact amount of substance in a certain place, while point-level sensors only indicate whether the substance is above or below the sensing point [30].

Direct level measurement methods employ physical properties such as fluid motion and buoyancy, as well as optical, thermal, and electrical properties. [29].

Indirect level measurement involves converting measurements of some other quantity, such as pressure to level by determining how much pressure is exerted over a given area at a specific measuring point, the height of the substance above that measuring point can also be determined.

3.1 Level Sensor Types

Level sensors detect the level of substances that flow, including liquid, granular materials, and powders.

When selecting a measuring device, it is important to consider the operating parameters and the physical and chemical properties of the process materials.

There are many different types of level sensors summarized in the following sections.

3.1.1 Mechanical sensor

3.1.1.1 Floating system

Floats work on the simple principle of placing a buoyant object with a specific gravity intermediate between those of the process fluid and the headspace vapor into the tank, then attaching a mechanical device to read out its position. While the float itself is a basic solution to the problem of locating a liquid's surface, reading a float's position (i.e., making an actual level measurement) is still problematic. Early float systems used mechanical components such as cables, tapes, pulleys, and gears to communicate level. Today magnet-equipped floats are the most popular types [27].

3.1.1.2 Buoyancy method

Buoyancy is an upward acting force exerted by a fluid, that opposes an object's weight an it is based on Archimede's principle .

The mechanical level indicator consists of the immersion body with calibrated measuring spring which transmits the change of level to the mechanical or electrical indicator [27].

3.1.1.3 Vibrating level systems

An electronic circuit excites the blade of probe to its resonant frequency, and when material comes into contact with the blade, vibration is damped causing switching of the relay. This device is suitable for control maximum levels of solids and liquids in many types of applications (e.g. foods, grains, granules, pellets, cement, powder)

3.1.2 Hydrostatic pressure methods

Displacers, bubblers, and differential-pressure transmitters are all hydrostatic measurement devices. Any change in temperature will therefore cause a shift in the liquid's specific gravity, as will changes in pressure that affect the specific gravity of the vapor over the liquid [41].

3.1.2.1 Bubbler systems

This technology is used in vessels that operate under atmospheric pressure. A dip tube having its open end near the vessel bottom carries a purge gas into the tank. As gas flows down to the dip tube's outlet, the pressure in the tube rises until it overcomes the hydrostatic pressure produced by the liquid level at the outlet. That pressure is monitored by a pressure transducer connected to the tube [41].

3.1.2.2 Differential pressure level detectors

The differential pressure detector method of liquid level measurement uses a detector connected to the bottom of the tank being monitored. The higher pressure, caused by the fluid in the tank, is compared to a lower reference pressure (usually atmospheric) [38].

3.1.2.3 Displacers

Displacers work on Archimedes' principle. The displacer's density is always greater than that of the process fluid (it will sink in the process fluid), and it must extend from the lowest level required to at least the highest level to be measured. As the process fluid level rises, the column displaces a volume of fluid equal to the column's cross-sectional area multiplied by the process fluid level on the displacer. A buoyant force equal to this displaced volume multiplied by the process fluid density pushes upward on the displacer, reducing the force needed to support it against the pull of gravity. The transducer, which is linked to the transmitter, monitors and relates this change in force to level.

3.1.3 Electrical methods

3.1.3.1 Conductivity probes

The Conductivity Probe determines the ionic content of an aqueous solution by measuring its conductivity. It consists of two main parts: the anode (positive) and the cathode (negative). The probe is activated when a voltage is applied to the system. This puts force onto the charged ions in the solution, which pushes them to either the anode or cathode depending on their charge [39].

3.1.3.2 Capacitance probes

A capacitor is formed when a level sensing electrode is installed in a vessel. The metal rod of the electrode acts as one plate of the capacitor and the tank wall (or reference electrode in a non-metallic vessel) acts as the other plate. As level rises, the air or gas normally surrounding the electrode is displaced by material having a different dielectric constant. A change in the value of the capacitor takes place because the dielectric between the plates has changed.

3.1.3.3 Optical level switches

An optical level switch works by emitting a beam of infrared light within a prism and measuring the amount of light received. When the measured fluid reaches the sensor the amount of emitted light received drops thus triggering the contacts. As the sensor is detecting the state between material covering or not covering the prism it can be used to detect the presence or absence of fluid thus preventing damage to pumps.

3.1.3.4 Microwave level systems

Radar level measurement is based on measuring the transit time of high frequency (GHz) electromagnetic energy transmitted from an antenna at the top of the tank and reflecting off the surface of the level medium; the higher the dielectric of the medium, the stronger the reflection.

3.1.3.5 Nuclear level systems

The nuclear level switch is based on the detection of radiations emitted by a radioactive source. When radiation transmit through material it will be absorbed, scattered or transmitted without any reaction.

3.1.3.6 Ultrasonic level detectors

Ultrasonic level sensors measure the distance between the transducer and the surface using the time required for an ultrasound pulse to travel from a transducer to the fluid surface and back.

3.2 Literature Review

In the literature, there are also many different techniques for measuring the liquid levels. Some of them are: Archimedes' principle, ultrasonic wave propogation techniques, radar, fiber optics etc.

In the study of Prune University, India [2], a cantilever beam is mounted into the liquid tank, and Archimedes's principle rises the beam through the liquid, and load cell measures the deflection. Generally these kind of easy to build basic type sensors have low accuracies around %2, but this system has a lot better in accuracy ± 0.5%, and still works in a wide temperature range: -40c +80C. This sensor is an example for easy to build, cheap, easily calibrateable liquid level sensor.

Another method uses ultrasonic lambda waves was developed in Russia, 2002 with the cooperation of Radio engineering and electronics instute of Russia, Gazavtomatika company of Russia and Milwaukee University's Electics and Computer department [18].

Principle of this study based on the changing characteristics of lambda waves in the liquid environment. Lambda waves has an advantage that they can continue their ways(or in other ways propogate) in such situations that acoustic waves do reflect because of various obstacles.

There are a couple of upper level detector transducers, and lower level transducers. The main principle is the difference of the wave characteriscits of lambda waves in the liquid and in the air are different, so by this differecence min and max levels can be easily detected. This sensor works well in North of Russia's oil areas bewteen -40°C and +60°C [17].

Another method developed and performed by NASA Langley research center and Old Dominion University is called and ultrasonic level sensor for liquids working under high pressure. [11].

Liquid level sensors are generally make continious measurements under up to 1000 psi of pressure, but such situations like liquid oxygen transfer to the rocket engine, etc. needs high amounts of liquids to be transferred by high pressure around 6000 psi. For this aim, new and special sensors have been generated.

The principle is basic, transducer send an ultrasonic wave, and propogating waves are being reflected from the liquid surface. The transit time can be easily converted to distance $(H=C_L T/2)$ and the liquid level can be calculated by this equation.

Another method using ultrasonic wave propogation was developed in 2001 by BFGoodrich airplane advanced sensors department [10]. The importance and difference of this study comes from the application field rather than the working principle. In the airplane industry because the weights are very important, the importance of this study can be easily understood.

The principle is the same with the study before, sending and collecting ultrasonic waves, and finding the liquid levels according to the wave transfer times. The difference comes from the importance of temperature difference, where a newly landed airplane is around -30°C, water/fuel on the ground is around 12°C.

With ±1mm accuracy, measurement error reduces with the increasing amount of water into the tank. This sensor works well between -40°C and +70°C.

A totally different method is the usage of fiber optics in liquid level measurement was performed by Gauhati University in 2007 [6].
Fiber optic cables reflects the laser/light signal when in the air, but when the density difference reduces, it transfers the laser light to the liquid environment, therefore sensor detects the liquid environment as shown in Figure 3.1.

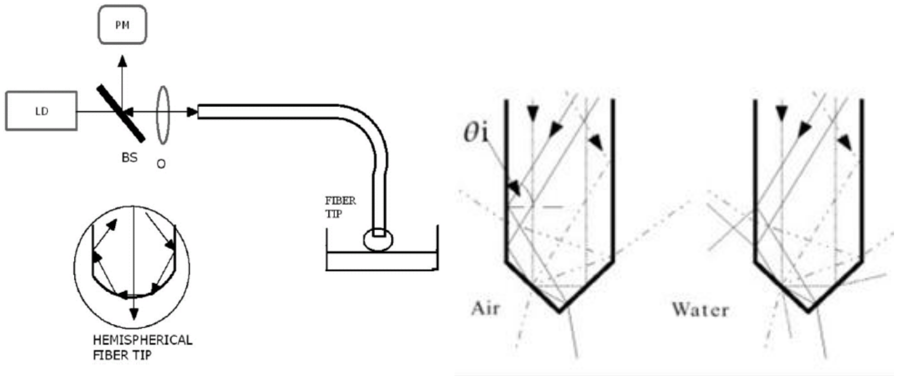

Figure 3.1 : Fiber optical liquid level measurement experiment setup [6].

One obstacle may be the dirt in the liquid, another can be the length of the fiber optic cable which can reduce the light signal reponse. In ideal conditions, fiber optic cables are capable of reaching 5 micron precision, with high accuracy and repeatability, that no other sensor can match.
Another study made by Parma university in Italy, 2005 [5]. When in air, most of the light rays reflect back, but when located in water light rays continue their way, therefore reflected signals' decrease shows that the optical fiber tip is inside water.
That means within the materials natural boundaries (-20°C ile +70°C) usage of optical fibers are easy, accurate and inexpensive.

4. OIL LEVEL SENSOR

When looking at the current oil level sensors used in automotive industry, two main OLS types appear:

- Wire resistance type level sensors
- Ultrasonic type level sensors

The sensor using resistance wire, are mainly reliable in statical measurements, but are not capable of getting dynamic measurements.

A resistance wire which is designed to cover both the maximum and minimum liquid levels is heated by sending a constant current through it. The voltage drop across the wire depends on the amount of heat that is dissipated from the wire to the surrounding medium. The voltage drop value is compared to values in a look-up table where voltage-drop versus temperature is listed.

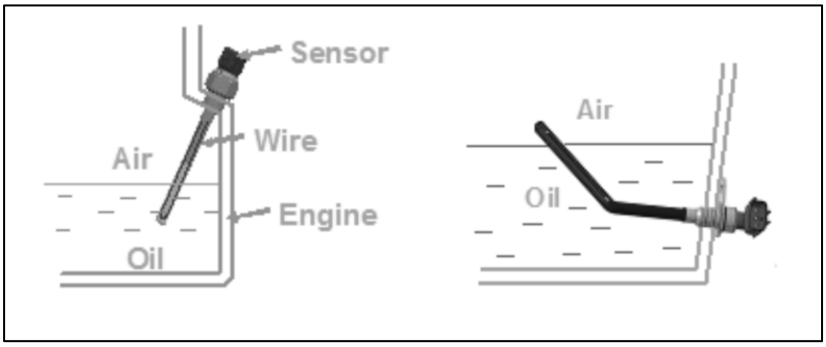

Figure 4.1 : Different types of resistance wire OLS [23].

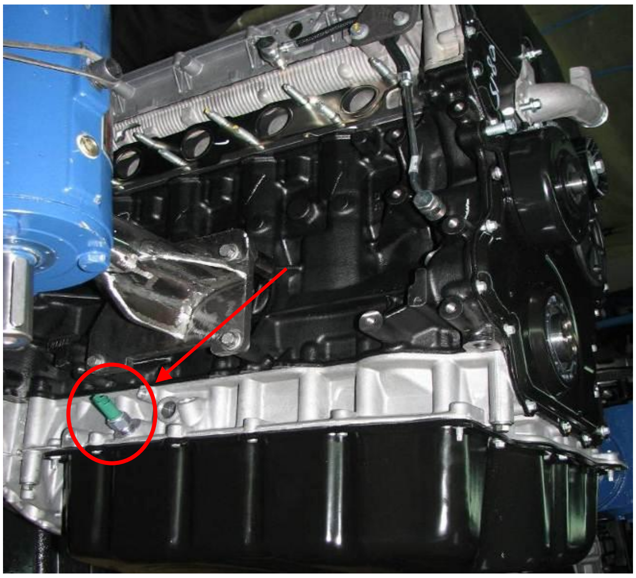

Figure 4.2 : Resistance Wired Level Sensor in its assembled position [23].

When focused on the ultrasonic level sensor, it can be seen that it’s principle is measuring the time frame between transmitting and receiving of ultrasound wave. The ultrasound wave reflects from the liquid surface, and returns back to the receiver, and because if the speed of sound is known in the specific environment, which is oil in this situation, so the distance from receiver to the liquid surface can be calculated easily.

Ultrasonic type level sensors have advantages in dynamic measurements, nevertheless they are more complex and more expensive when compared to the resistance wire type level sensors. However, Ultrasonic sensors are not suitable for using in every application. When the container vibrates under certaiın conditions, air bubbles get formed in the liquid. Therefore, the soundwaves propagating from the sensor reflects from these bubbles instead of reflecting from the surface and cause false signals.

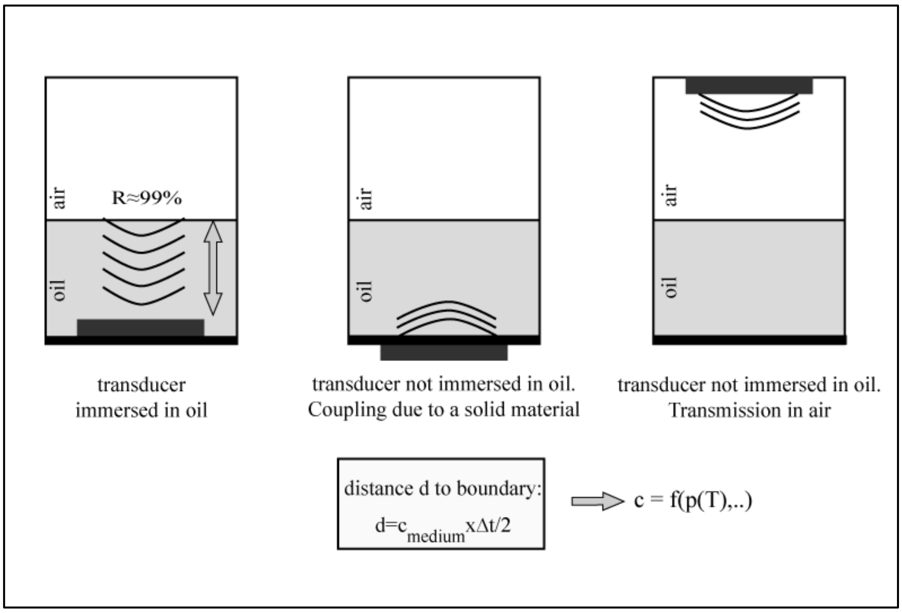

Figure 4.3 : The working principle of the ultrasonic level sensors.

4.1 Hella Oil Level Sensors

Oil-level sensors ensure that the engine oil does not become dangerously low without being noticed. Current Hella sensors work according to the delay principle of ultrasound waves in liquid medium [22]. Ultrasound technology has already been used successfully for years in different applications. The challenge for liquid level measurement applications is in the special adaptation of wavelength and pick-up characteristics as well as the choice of suitable structure and connection technology [34].

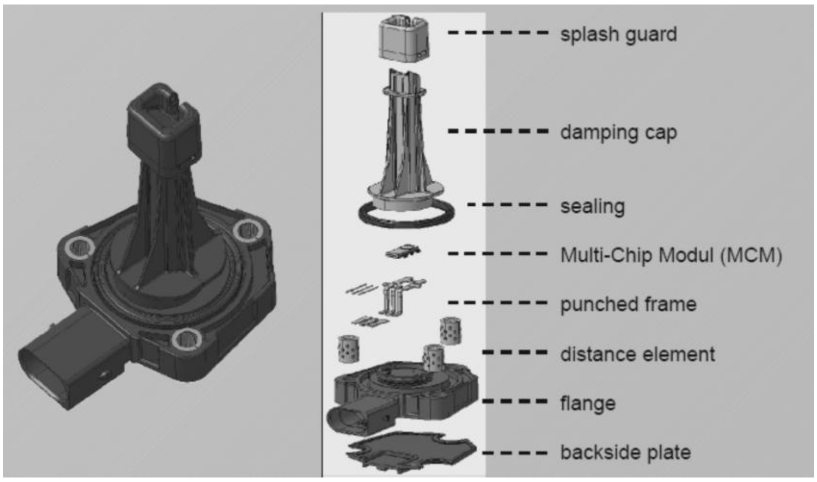

Figure 4.4 : The components of a specific Hella's oil level sensor [34].

The ultrasonic oil level sensor can measure the oil level continuously, i.e. both in the dynamic and in the static range. It thus provides information about the oil level within the whole period of engine operation, which can often be several hours in the case of construction machinery, tractors and fork lift trucks.

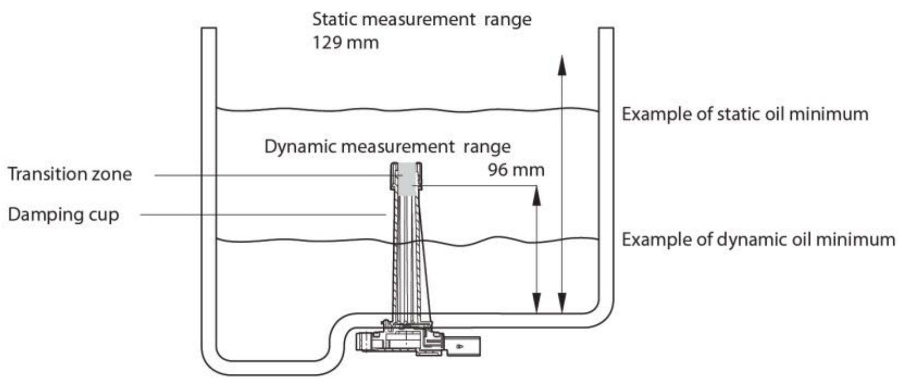

Figure 4.5 : Sketch of ultrasonic level sensor [33].

4.2 Oil Level Sensor Design Concept & Fem Analysis

The current ultrasonic sensor has many problems including bubbling, sensitivity etc. Therefore the target of the Hella cooperated study was to work on the mechanical design (material, sealing, mounting) and integrate the ultrasonic oil level sensor inside the liquid container.

In the FE analysis, the worst case scenario is having an outside temperature of -40°C, while the temperature of the oil in the container is 160°C. During the analysis, it is going to be pretended that there is not enough oil in the container, to minimize the damping effect.

For FEM simulation, material properties have been assigned to sensor parts. A composite of Polyamide and Glassfiber (PA66-GF35) has been used for the main body parts, while fixings are CuZn39Pb3 and grounding is CuNi10Fe1Mn. (APPENDIX A)

As expected, current design can withstand vibrations when the base is outside, and the sensing part is inside the oil pan.

Sensor manufacturer insisted on keeping the damping cap design. Therefore after making various analysis, it has been agreed to keep the damping cap section, which propagates the sound waves, so a new sensor design has been developed as shown in Figure 4.6.

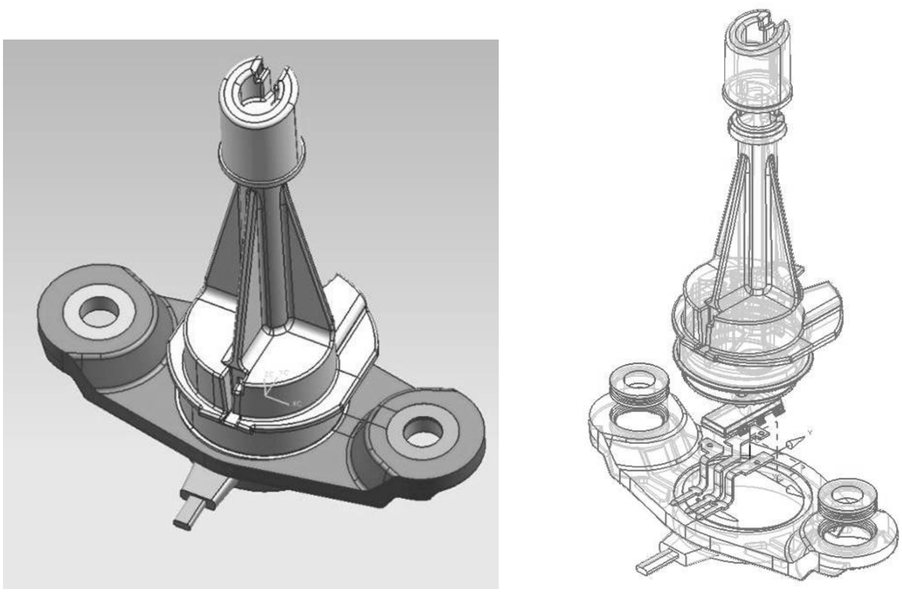

Figure 4.6 : The new oil level sensor design.

4.3 Meshing

The first part of the anaylsis is the meshing stage. Each part of the sensor have been meshed separetly, for having optimum element size.

After meshing, all of the sensor parts assembled by glueing operation. In glueing operation, distance between the surfaces have been assigned to be lower than 0.25 mm.

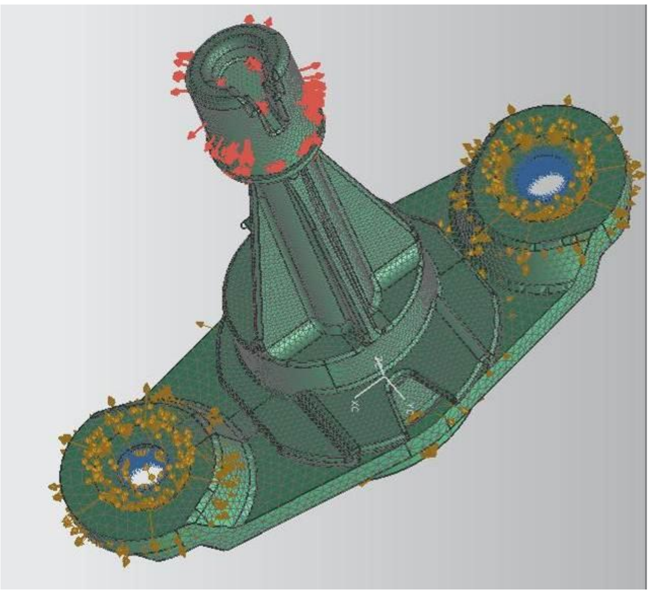

Figure 4.7 : Meshing.

In the Figure 4.8., brown arrows demonstrate the "Surface-to-surface gluing", which bonds the solid bodies together.

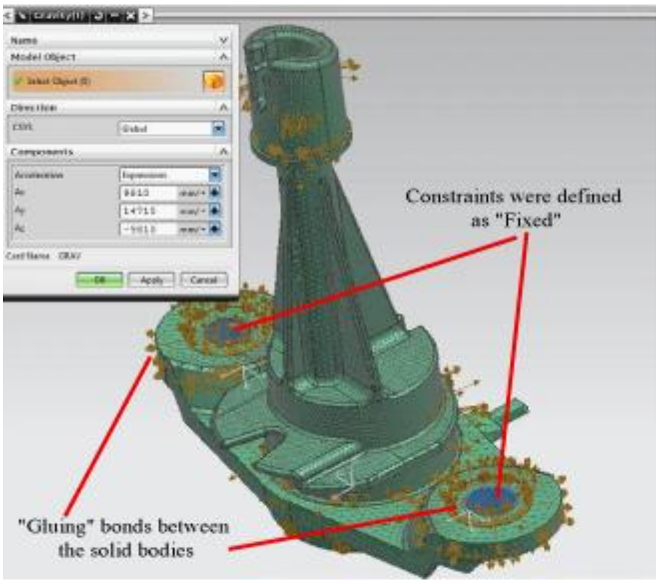

Figure 4.8 : Gluing operation.

4.4 Modal Analysis

The goal of modal analysis is to determine the natural mode shapes and frequencies of an object or structure during free vibration. It is common to use the finite element method (FEM) to perform this analysis because, like other calculations using the FEM, the object being analyzed can have arbitrary shape and the results of the calculations are acceptable. The types of equations which arise from modal analysis are those seen in eigensystems [24].

The physical interpretation of the eigenvalues and eigenvectors which come from solving the system are that they represent the frequencies and corresponding mode shapes. Sometimes, the only desired modes are the lowest frequencies because they can be the most prominent modes at which the object will vibrate, dominating all the higher frequency modes.

4.4.1 Modal analysis results

By solving the model, the natural frequencies and the stress-strain values of each mode have been found.The results of the modal analysis can be seen in Table 4.1.

According to the results, modes 7,8,9 having the frequencies 1635 Hz, 2187Hz, and 2413Hz have higher stress and strain values exceeding the material limits. But because these frequencies are all over the testing limits according to DIN EN 60068-2-6, the new design is safe according to modal analysis.

Table 4.1 : Displacements/strains of all modes.

Load Case 1 : Number of Iterations = 9

	Displacement (mm)				Stress (mN/mm²(kPa))			
	X	Y	Z	Magnitude	Von-Mises	Min Principal	MaxPrincipal	Max Shear
Mode 1 ,1.456e+000 Hz								
Max	1.093e+000	4.554e-001	5.137e+000	1.482e+001	2.616e+000	1.121e+000	2.542e+000	1.377e+000
Min	-1.442e+001	-2.322e+000	-9.734e+000	1.799e-001	4.679e-004	-3.626e+000	-1.945e+000	2.588e-004
Mode 2 ,2.303e-001 Hz								
Max	3.953e+000	1.944e+000	2.508e+000	1.138e+001	9.552e-001	1.809e-001	1.185e+000	5.213e-001
Min	-3.804e+000	-1.129e+001	-1.709e+000	4.182e-001	1.497e-005	-8.029e-001	-1.715e-001	7.821e-006
Mode 3 ,4.830e-001 Hz								
Max	4.320e+000	3.877e+000	2.337e+000	7.462e+000	2.237e+000	2.408e+000	4.457e+000	1.161e+000
Min	3.271e+000	-1.019e+000	-5.399e+000	4.122e+000	1.771e-005	-1.940e+000	-6.088e-001	1.008e-005
Mode 4 ,1.100e+000 Hz								
Max	3.075e+000	9.187e+000	2.359e+000	1.018e+001	2.057e+000	1.259e+000	2.804e+000	1.115e+000
Min	-5.783e+000	-1.145e+000	-6.669e+000	3.863e+000	1.779e-004	-1.815+000	-6.019e-001	9.967e-005
Mode 5 ,1578e+000 Hz								
Max	2.324e+000	1.709e+001	9.184e+000	1.767e+001	4.182e+000	2.432e+000	4.853e+000	2.329e+000
Min	-4.456e+000	-2.895e+000	-3.438e+000	1.264e+000	4.969e-004	-4.102e+000	-2.121e+000	2.805e-004
Mode 6 ,3.160e+000 Hz								
Max	5.013e+000	7.102e+000	-.108e-001	1.329e+001	1.635e+000	8.248e-001	2.228e+000	8.946e-001
Min	-7.524e+000	-1.327e+001	-6.563e-001	1.146e-001	1.924e-004	-3.150e+000	-1.361e+000	1.102e-004
Mode 7 ,1.635e+003 Hz								
Max	3.673e+000	4.716e-001	1.146e+001	2.247e+001	1.549e+006	1.346e+006	2.520e+006	8.143e+005
Min	-2.237e+001	-4.544e-001	-1.202e+001	2.242e-002	2.537e+001	-2.883e+006	1.550e+006	1.437e+001
Mode 8 ,2.187e+003 Hz								
Max	5.794e+000	7.376e-001	1.749e+001	1.840e+001	2.877e+006	3.308e+006	6.018e+006	1.468e+006
Min	-5.770e+000	-2.644e+000	-3.929e+000	1.535e-001	2.439e+002	-3.612e+006	-1.459e+006	1.396e+002
Mode 9 ,2.413e+003 Hz								
Max	7.191e-001	2.481e+001	8.345e+000	2.538e+001	3.133e+006	6.241e+005	3.328e+006	1.673e+006
Min	-7.208e-001	-9.215e+000	-1.320e+001	2.434e-002	-9.336e+002	-3.260e+006	-1.010e+006	5.381e+002
Load Case 1 Summary								
Max	5.794e+000	2.481e+001	1.749e+001	2.538e+001	3.133e+006	3.308e+006	6.018e+006	1.673e+006
Min	-2.237e+001	-1.327e+001	-1.320e+001	2.242e-002	1.497e-005	-3.612e+006	-1.550e+006	7.821e+006

4.5 Stress-Strain Analysis

The frequency vs acceleration values obtained from the Volkswagen Automotive test spec, according to DIN EN 60068-2-6 which is accepted as an industry standart have been used during the analysis.

Table 4.2 : The frequency vs. acceleration values.

Frequenz (Hz)	Amplitude der Beschleunigung [m/s²]
100	100
150	150
200	200
240	200
255	150
440	150

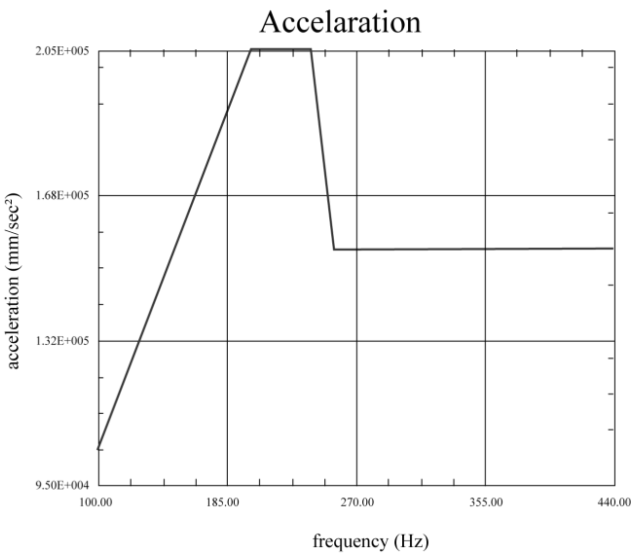

Figure 4.9 : Frequency vs. acceleration values.

Frequency vs. Acceleration used in the analyzing software can be seen in Table 4.2 and Figure 4.9.

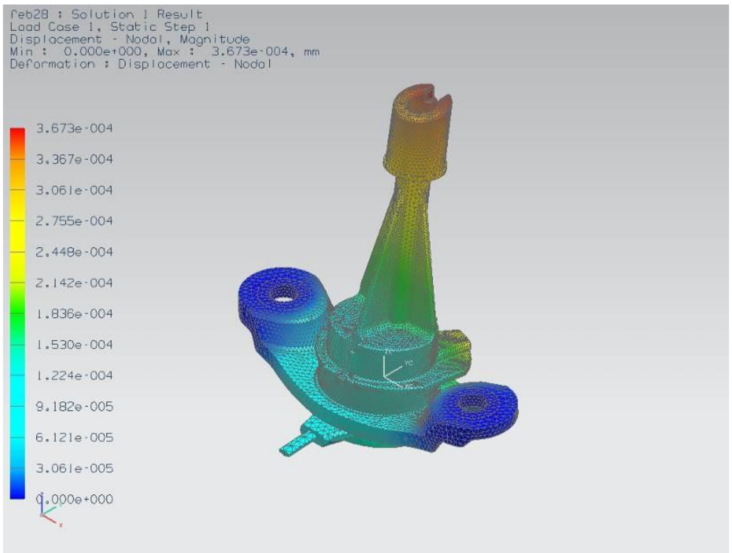

Figure 4.10 : Displacement, strain and stress figures at both temperature limits (-40º C and +160º C).

4.5.1 Stress-strain analysis results

According to the stress-strain analysis under test conditions, oil level sensor faces a stress value under 0.21 MPa, which makes no deformations when compared with Yield Stress & Ultimate Tensile Strength values of the materials which have values between 150-200MPa.

When considering these results, the design is completely safe.

4.6 Fatigue Analysis

To see the effects of the cycling loads, the model has been analyzed according to the Fatigue conditions.

For this aim Fatigue Strength Coefficient, Fatigue Strength Exponent, Fatigue Ductility Coefficient and Fatigue Ductility Exponent values have been inserted into the material database.

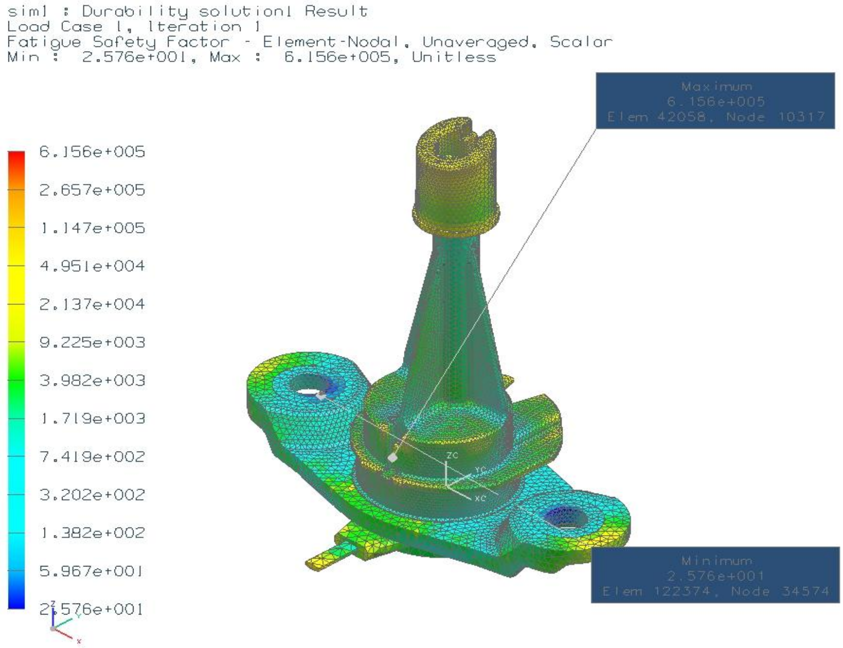

Figure 4.11 : Fatigue safety factor – Element – Nodal.

4.6.1 Fatigue analysis results

The expected lifetime is above 10^36 cycles, and safety factors have minimum values of 25.76 for fatigue and 2.796 for strength. According to these findings,it can be said that, the new desing is absolutely safe according to fatigue properties under cycling loading of test conditions.

Although this new ultrasound sensor design is safe, it is indifferent by means of sensitivity and has similar problems with the current sensor. So it has been agreed that a completely new sensor should be designed to get rid of the current problems and to reach higher sensitivity values.

For this aim, different sensor applications in the literature has been investigated and finally a unique theory has been differentiated with high sensitivity and wide range of applications.

This method which is named as Whispering Gallery Mode, will be evaluated in the following sections in detail.

5. WHISPERING GALLERY MODES THEORY

5.1 Whispering Gallery Mode: Background/Development Stages

The whispering gallery is located in the dome of St Paul's Cathedral, London, and has the curious property that if two people stand at opposite sides of the gallery, at a distance of 42 meters, and one whispers into the wall of the dome, then the other person can hear what is being said. Interestingly the effect does not work if one speaks normally, giving the gallery its name. The reason for this strange effect is that the sound bounces along the wall of the gallery with very little loss, and so can be heard at a great distance. The reason it does not work if you speak normally is that the increased amplitude of the noise allows it to circulate the gallery multiple times, and so the sounds all get mixed up and can no longer be heard properly. It can be viewed that there is a narrow region near the edge of the dome where the waves propagate most efficiently, and this is known as a 'whispering gallery mode' in honour of gallery where it was discovered [25].

The study of WGMs was started almost a century ago with the work of Lord Rayleigh, who studied propagation of sound over a curved gallery surface. In 1909, Debye derived equations for the resonant eigenfrequencies of free dielectric and metallic spheres that naturally take into account WGMs. Generalized properties of electromagnetic resonances in dielectric spheres were widely discussed afterwards, with emphasis on the microwave, not optical, modes of the spheres.

The first observations of WGMs in optics can be attributed to solid-state WGM lasers. Laser action was studied in Sm:CaF2 crystalline resonators. The size of the resonators was in the millimeter range. In liquid resonators, WGMs were first observed by elastic light scattering from spherical dielectric particles. It was recognized that WGMs could help in measurements of spherical particle size, shape, refractive index, and temperature. Earlier researchers have been found that Whispering gallery modes of micro spherical and other micro-resonators are known to have extremely high quality factors (Q) in the optical domain [42].

Microspherical (50-500 μm diameter) glass resonators with Q factors excessing 10^{10} values have been demonstrated, and Q factors as high as 10^{11} are, in principle, possible [44].

In recent times whispering gallery modes have found new fame with the development of nano-optics. In the modern version of a whispering gallery, laser light is coupled into a circular waveguide, such as a glass ring. When the light strikes the boundary of the ring at a grazing angle it is reflected back into the ring.
The light wave can make many trips around the ring before it is absorbed, but only frequencies of light that fit perfectly into the circumference of the ring can do so. If the circumference is a whole number of wavelengths, the light waves superimpose perfectly each trip around.
This perfect match between the frequency and the circumference is called a resonance, or whispering-gallery mode.

Whispering gallery resonators always experience a certain amount of tunnel-leakage of the radiation from the confined mode. This leakage or radiation loss increases as the diameter of the cavity is reduced (scaled by the wavelength). It also depends on the refractive index contrast between the resonator material and the surrounding medium. Whispering gallery loss is therefore controlled by appropriate selection of the resonator diameter, the refractive index, and also the operational wavelength of the laser [46].

Whispering gallery modes occur at particular resonant wavelengths of light for a given droplet size. At these wavelengths, the light undergoes total internal reflection at the particle surface and becomes trapped within the particle. The droplet behaves like a low-loss optical cavity with the light circulating for timescales on the order of nanoseconds.

Whispering Gallery Modes of dielectric microspheres have attracted interest with proposed applications in a wide range of areas due to the high optical quality factors that they can exhibit. WGM occurs when light travels in a dielectric medium of circular geometries. After repeated total internal reflections at the curved boundary, the electromagnetic field can close on itself and give rise to resonances. If the dielectric medium is a microsphere, one obtains a very small mode volume and high finesse. In order to couple light in or out of the microsphere, it is necessary to utilize overlapping of the evanescent radiation field of WGMs with the evanescent field of a phase-matched optical fiber or waveguide. Photons tunnel from the eroded optical fiber to the microsphere if their refractive indices are very close.

In mechanical sensing application, the dielectric microsphere is optically coupled to a single mode fiber which carries light from a tunable laser and serves as an input/output port for the microsphere. When the microsphere comes into contact with an exposed section of the fiber core, its optical resonances are observed extremely narrow (with very high Q values) and thus are highly sensitive to any change in the morphology of the sphere (shape, size, or refractive index) . An interesting phenomenon in WGM is that the resonance peaks in the light intensity spectrum curve is very sharp and the intervals between two successive peaks are very stable. Moreover, the resonance frequencies will shift with the changes of the microsphere size and/or the optical properties of the surrounding medium.

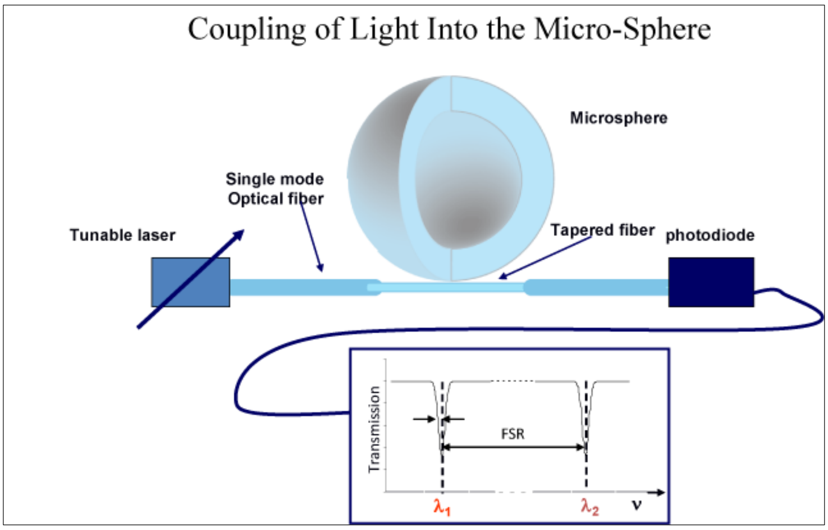

Figure 5.1 : WGM shifts.

WGM shifts have caused by the total internal reflections occured in the microsphere. The laser light comes into the microsphere in its contact point in the tapered film, and the light undergoes total internal reflections in the sphere.

5.2 Geometrical Theory Of Whisperıng Gallery Modes

A study about geometrical theory of whispering gallery modes indicates that, axisymmetric dielectric bodies have very high quality-factors, when sphere and torus shapes have been examined by Richtmyer.

However after this study, it has been seen that in the case of simplest axisymmetric geometry, different from ideal sphere or cylinder, no closed analytical solution has been found. While the microspheres in the theory of WGMs, are well established and allows precise calculation of eigenmodes, radiative losses and field distribution both analytically and numerically [53] .

There are many studies regarding high Q WGM dielectric disk resonators [53] and cylindrical optical microcavity resonators [56]

Figure 5.2 shows a Summary of the Most Commonly Used Whispering Gallery Mode Resonant Cavity Geometries, along with the Materials Used to Fabricate Them and the Corresponding Quality Factors.

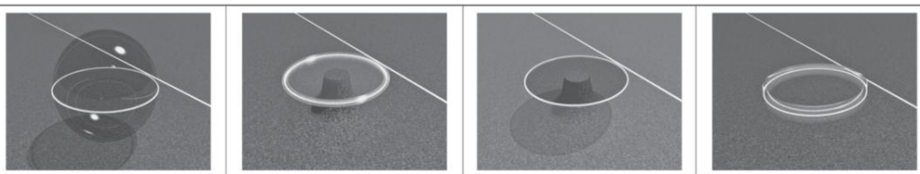

Geometry	Microsphere [2]	Microtoroid [7]	Microdisk [5,7,39]	Microring [8,10,21]
Possible material	Silica	Silica	Silica, silicon, silicon nitride, AlGaAs	Polymeric materials, silicon
Quality factor	$>10^9$	$>10^8$	$\sim 10^5–10^7$	$\sim 10^3–10^5$
Fabrication method	Reflow	Lithography/ reflow	Lithography	Lithography/ molding

Figure 5.2 : Most commonly used wgm resonant cavity geometries [53].

5.3 Applications And Studies Based On Wgm Principles

In the literature, there are many studies regarding WGM phenomenon, a number of WGM based measurement techniques have been proposed for biological applications, especially detection of various molecules, mechanical sensing including temperature, force, pressure, acceleration, wall shear stress, magnetic field, etc.

5.3.1 Microlasers

An early study in year 2000 indicates that an angle-polished fiber coupler can be implemented to couple an optical fiber to the microsphere to generate Whispering Gallery Modes. [49]

Another early study about microlasers in completed in 2001 indicates that, a novel hybrid-fiber-taper based laser coupling configuration has been proposed, in which the microsphere has been coupled using a single fiber taper that was a combination of 980-nm single mode fiber (SMF) and 1550-nm SMF [50].

5.3.2 Optical switching

In an early study, a high-Q nonlinear cylindrical microcavity resonator has been proposed, and the transmission of an integrated optical waveguide close to a microcavity has been measured and related to the resonances of the cylindrical microcavity. Which can be accepted as a base to coupling phonemenon [53].

Optical microsphere resonators are also attractive systems for both fundamental physics research in the field of cavity quantum electrodynamics and for the use in optoelectronic devices [56].

5.3.3 Biosensor

A biosensor is an analytical device for the detection of an analyte that combines a biological component with a physicochemical detector component. Optical Biosensors provides the most comprehensive analysis of optical biosensors and relevant technologies to date. There are some studies about optical biosensors based on WGM principles.

One of studies about biosensors, which uses disk shaped resonators, that has been used for the detection of biological materials with high sensitivity. The principle of the device depends on monitoring the change in transfer characteristics of the disk resonator when biological materials fall onto its active area [51].

Another study related with optical biosensors shows that, the need for miniaturized and sensitive instruments for bio-detecting has accelerated the development of micrometer-scale optical biosensors. According to the researchers, in biosensor applications microspheres have some problems like lack of size control during fabrication, and difficulty in integration with other optical components, but microdisk shaped resonators can work successfully in biosensor applications. Researchers indicate that SiO2 microdisks with high Q factors and diameters ranged from 400-1200 micron and thicknesses of 1 and 15 microns have been fabricated on Si substrates. Also since the fabrication process used in the study is compatible with that in standard microfabrication, the sensors can be easily integrated with other electronic and optical components on a semiconductor chip [32].

As a means of determining the sensitivity and feasibility of the microdisk structure as a sensing device, Q-factor was calculated and sensing performance was observed. The optical resonances of the WGM modes in the disks were evidenced by dips in the intensity and an increase in the temperature resulted in longer resonant wavelengths. This effect is reversible; a decrease in temperature results in shorter resonant wavelengths [40].

The results of an another study about biodetection show that silica resonators provide the lowest material losses and highest Q factors. Also semiconductors such as silicon have been used to reach Q factors of more than 500,000 [5] and polymer-ring resonators have been used to achieve Q factor values of more than 100,000 [23–25]. However, these Q factors are several orders of magnitude lower than for the silica ultrahigh-Q microcavities, such as microtoroids [6] or microspheres [2], which reach Q factor values ranging from 500 million to 10 billion [46].

Another study about the High-Q Whispering-Gallery Mode Sensor In Liquids shows that optical biosensors are typically transducers that detect the presence of molecules at a surface. The basic detection scheme is that binding of molecules to the micro-resonator surface induces an optical change proportional to the amount of bound molecules, so in short researchers just measure the change on the characteristics of the resonator, such as Q factor [43].

The results of the study about detecting biomolecules optically shows that, it is required to use micro fabricated glass surfaces with surface coatings to minimize nonspecific binding, without changing the optical properties of the sensor. According to this study, Q factor factors of the WGM microspheres have values greater than 1010 in air, and greater than 109 in a variety of solvents, including methanol, H20 and phosphate buffered saline(PBS). In other words WGM type optical biosensors are extremely sensitive, nondestructive, and capable of sensing almost any kind of molecule, chemical and pre-biotic as well as biological. [42]

5.3.4 Micro sensors

A study about micro-optical force sensor concept shows that WGMs can be excited evanescently coupling light from a tunable diode laser using a tapered single-mode fiber, and applying a compressive force generates a change in both the shape and the index of refraction of the sphere leading to a shift in WGM. By tracking these shifts, the force magnitude can be determined using solid silica as well as solid and hollow Polymethyl-methacrylate (PMMA) microsphere resonators [14].

Another paper investigates the feasibility of a WGM-based microsensor for electric field measurement. It has been found by the elastic deformation (strain) of a dielectric material occurred under the force exerted by an electrostatic field. The results of the analysis indicates that detection of electric fields as small as ~500V/m may be possible using water filled, hollow solid polydimethylsiloxane (PDMS) microspheres. The electric field sensitivities for solid spheres, on the other hand, are significantly smaller, resulting that solid PDMS spheres work well for electrostriction, which is the elastic deformation (strain) of a dielectric material under the force exerted by an electrostatic field [3].

In the study of Iopollo, Ayaz and Ötügenin the name of High Resolution force based on morphology dependent optical resonances of polymeric spheres, performance characteristics of a force sensor concept based on the morphology dependent resonance (MDR) shifts of micro-optical resonators have been investigated. It has been stated that the microsphere sensors with diameters ranging between 300 and 950 microns may have force resolutions reaching 10^{-5}N. According to the study, MDRs can be observed as sharp dips in the transmission spectrum with very high Q factors. According to the study, when the resonances are extremely narrow, with very high Q factors, they become highly sensitive to any change in the morphology of the sphere. Therefore any instantaneous change in the morphology of the microsphere will cause a shift in the resonance position allowing for the precise measurement of the mechanical effect.As an important result of this study shows that decrease of both sphere diameter and young's modulus results in increasing sensitivity. [4].

Another study which belongs to Iopollo, Ötügen, and Marcis, shows that the mechanical modes of dielectric microspheres can be excited by simultaneously imposing static and harmonic magnetic fields. Therefore by monitoring and tracking WGM shifts, the detection of small magnetic fields is possible [15].

There are some studies analyzing the effect of hydrostatic pressure on solid and hollow microsphere optical resonators. The researchers have expressed that the pressure-induced WGM shifts of hollow polymethyl methacrylate (PMMA) microspheres were monitored, and found that the effect of atmospheric pressure variations on silica resonators is negligible, but hydrostatic pressure may be effective in the optical tuning of hollow polymer spheres, because of the higher sensitivity of the hollow microspheres [13].

In an another study about resonators shows that, when applications of whispering-gallery mode resonators in photonics and nonlinear optics have been investigated, it has been seen that open dielectric resonators based on complete internal reflection has become an alternative to the usual optical resonators. Modern dielectric optical resonators have cylindrical, spherical, spheroidal/toroidal, ring, and other shapes and topologies with various confining principles [58]

A method has been developed to fabricate microtube resonators with strong whispering-gallery-mode emission but with quality factors only up to 3000. The microcylindrical or microcapillary dielectric resonators have generated significant interest due to their small size and material compatibility with telecommunication optical fibers [59]

5.3.5 Solar cells

Light Absorption Enhancement In Thin-Film Solar Cells Using Whispering Gallery Modes In Dielectric Nanospheres indicates that whispering gallery modes in dielectric nanospheres can be used for the enhancement of light absorption (light trapping) in thin film solar cells. When resonant dielectric spheres are in proximity to a high-index photovoltaic absorber layer, incident light can be coupled into the high-index material and can increase light absorption. another important benefit of this structure for photovoltaic application is its spherical geometry that naturally accepts light from large angles of incidence. [57]

5.4 Q Factor

In physics and engineering the quality factor or Q factor is a dimensionless parameter that a higher Q indicates a lower rate of energy loss relative to the stored energy of the oscillator In other words oscillators with high quality factors have low damping so that they ring longer. [45]

The quality factor ratio ($\lambda / \Delta\lambda$) can also be demonstrated as the fraction of resonant wavelength (λ) over width of the resonance wavelength ($\Delta\lambda$)[16]. As pointed above, “Quality Factor” is a measure of how well an optical resonance is. In other words, when the Q factor is high, then the determination of very small morphology dependent shifts (WGM) of optical spheres become possible.

The very high quality factors Q of microspheres may be attributed to several factors. One is that the dielectric materials for microspheres, fiber grade fused silica, have ultra-low optical loss at the frequencies of the supported whispering gallery modes. Another is that the surface of the sphere is specially fabricated to minimize the size of any surface inhomogeneities, e.g., on the order of a few A by processes such as fire polishing; these can scatter photons out of the WG mode and decrease the Q.

Although Q-values approaching material loss limits of 10^9 have been reported in the Literature, calculations and experimental results generally pointed values around 10^6-10^7 , and accepted as 10^7 in WGM experiments [12]

5.5 Evanescent Field Phenomenon

The evanescent field is coupled, (bound) to an Electromagnetic Wave or mode, propagating inside the waveguide. It is a kind of surface wave, and thus in Fiber optics, the evanescent field may be used to provide coupling to another fiber. [47]

In optics, evanescent-wave coupling is a process by which electromagnetic waves are transmitted from one medium to another by means of the evanescent, exponentially decaying electromagnetic field. That means Coupling is a process, that is usually accomplished by placing two or more electromagnetic elements close together so that the evanescent field generated by one element does not decay much before it reaches the other element [48].

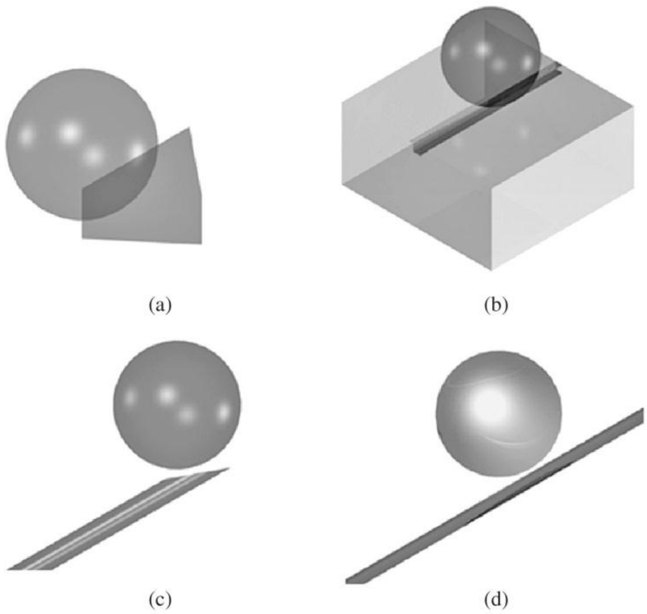

Figure 5.3 : Coupling devices (a) Prismcoupler, (b) half block coupler, (c) angle polished fiber coupler, and (d) fiber taper coupler [53].

5.6 Fiber Optic Coupler

A Fiber optic coupler is a device used in optical fiber systems with one or more input fibers and one or several output fibers. Light entering an input fiber can appear at one or more outputs and its power distribution potentially depending on the Wavelength and polarization. Such couplers can be fabricated in different ways, for example by thermally fusing fibers so that their cores get into intimate contact. If all involved fibers are single-mode (supports only a single mode per Polarization direction for a given wavelength), there are certain physical restrictions on the performance of the coupler. In particular, it is not possible to combine two or more inputs of the same optical Frequency into one single-polarization output without significant excess losses. However, such a restriction does not occur for different input wavelengths: there are couplers which can combine two inputs at different wavelengths into one output without exhibiting significant losses. Such couplers are used. Wavelength-sensitive couplers are used as multiplexers in wavelength-division multiplexing (WDM) telecom systems to combine several input channels with different wavelengths, or to separate channels. [26]

5.7 Laser Physics

The word ‘laser‘ is an acronym for light amplification by stimulated emission of radiation. It is worth noting that the term ‘light’ refers to a wide spectrum of wavelengths from soft x-ray, through ultraviolet (UV) and visible to far infrared (IR). The two most important basic principles for laser science are the quantum nature of light and a process called stimulated emission (both accredited to Einstein). The quantum nature of light refers to light quantised into photons.

The laser is a light source that exhibits unique properties. Since the first demonstration of a ruby laser by Maiman in 1960, there has been a phenomenal development in the field of lasers. Lasers are used in thousands of applications in every section of modern society, including consumer electronics, information and communications technology, entertainment, science and industry, the medical field and defence. The laser triggered the photonics revolution and is the foundation of modern photonics [49].

Lasers range in size from tiny diode lasers to large systems the size of a football field. All of these have three basic properties in common, which separate lasers from ordinary light sources: monochromaticity, directionality, coherence.

Conventional light sources emit light consisting of a broad range of wavelengths (i.e. colours); a laser, on the other hand, emits only a very narrow range of wavelengths.

Conventional light sources, like a light bulb, emit light in all directions, while lasers can emit light that spreads (‘diverges’) only very little with distance. However, all laser beams eventually diverge as they move through space.

Some consider coherence to be the most fundamental property of laser light, i.e. where all parts of the electromagnetic waves are in phase.

A laser basically consists of three parts: a resonant optical cavity called the optical resonator, a laser gain medium (also called active laser medium) and a pump source to excite the particles in the gain medium.

The optical resonator consists of at least two mirrors between which the light bounces up and down resonantly. In most cases, one or more mirrors are curved, so that a resonant optical mode forms. This mode defines the laser beam. Modern dielectric mirrors used in lasers typically have a reflectivity of up to 99,9%.

However, one of the end mirrors is usually only partially reflective, so that a portion of the light is transmitted. This mirror is called the output coupler. The transmitted part forms the laser output.

In order to operate, the laser requires a gain medium in the resonator, which amplifies light and thus compensates for the loss through the output coupler. Lasers are typically classified by the type of gain medium they employ (gas laser, solid-state laser, dye laser, semiconductor laser, etc.). The stimulated emission process takes place in the gain medium.

The gain medium amplifies light of any direction. However, only the light that bounces up and down between the resonator mirrors is amplified many times and therefore reaches a high intensity. In a continuous wave (CW) laser, the gain in the laser gain medium and the loss from the output coupler plus other losses are in equilibrium. The fact that the photon energy has to match a given energy transition makes the laser monochromatic. Since the amplification process maintains the phase and direction of the light, the laser output is directional and coherent.

The active particles in the laser gain medium need to be in a state of inversion for the laser to operate. To reach this state requires some pumping process, which lifts them into the required energy state. Typical pumping processes are electrical current in a gas or semiconductor laser or optical pumping in a solid-state or dye laser. Optical pumping is typically achieved either by flash lamps or by another laser.

5.8 Theory And Equations

Geometric optics provides the simplest interpretation of the WGM. The laser light from the optical fiber is coupled to the microsphere nearly tangentially, and approaches the interior surface of the sphere beyond the critical angle, thereby experiencing a total internal reflection along the interior surface of the microsphere. Trapped inside the microsphere, the light circumnavigates the interior surface of the sphere. A resonance is realized when light returns to its starting location in phase. Thus, the approximate condition for resonance is [4]:

$$2\pi n_0 a = \mathrm{I}\lambda \qquad \textbf{(5. 1)}$$

λ = vacuum wavelength of laser,

n_0 = refractive index ,

a = radius of sphere,

l = integer indicating the circumferential mode number.

Equation 5.1 [4] is a first order approximation and holds for $a \geq \lambda$.. At resonance, light experiences constructive interference in the sphere which is observed as dips in the transmission spectrum through the optical fiber. A minute change in the size or the refractive index of the microsphere will lead to a shift in the resonance wavelength as:

$$\frac{d\lambda}{\lambda} = \frac{dn_0}{n_0} + \frac{da}{a} \tag{5.2}$$

In a WGM-based force sensor concept, uniaxial force is applied on the sphere along the polar direction (normal to the plane of light circulation) through two high-stiffness plates. The applied force induces a change in both the radius (strain effect) and the refractive index (through mechanical stress) of the sphere.

The studies reported in 2008 by Southern Methodist University, Mechanical Engineering Department , an analytical framework was developed for the force sensors. Specifically, expressions were developed for WGM (Morphology dependent resonances, WGM) shifts in sphere sensors due to force applied in the polar direction. The analysis accounts for both the strain and stress effects in determining the WGM shifts. Using these expressions, a systemic analysis is carried out to determine the sensitivity, resolution, an bandwidth limits of force sensors based on WGM shifts of polymeric microspheres.

5.8.1 Systemic analysis

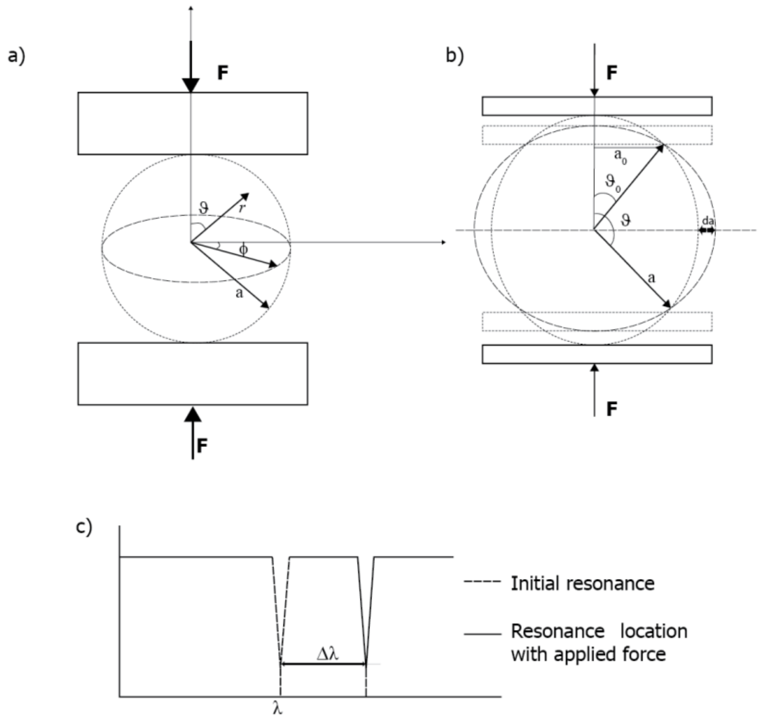

Figure 5.4 : a) Microsphere with applied force; (b) contact geometry; (c) transmission spectrum [4].

5.8.1.1 Stress and strain in a solid dielectric microsphere

When a solid dielectric sphere of radius *a* that is compressed by two pads made of high stiffness material. The applied force *F* will lead to a mechanical stress field inside the microsphere.

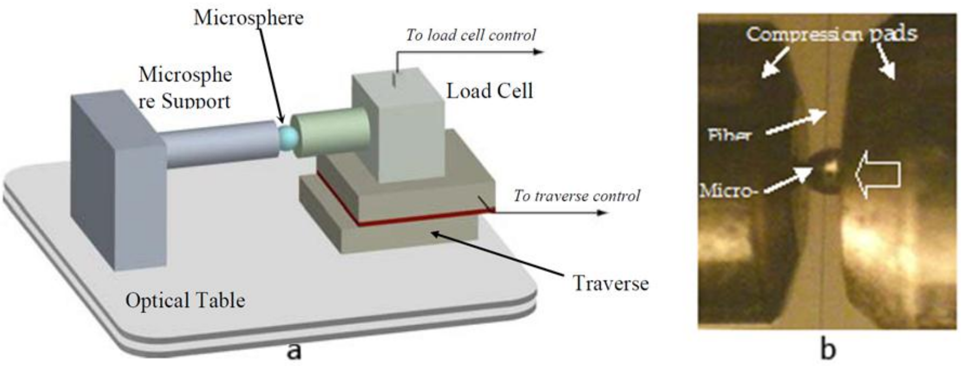

Figure 5.5 : An experiment setup of a WGM force sensor (a), microsphere and its tapered fiber in detail (b) [14].

It will also deform the sphere (strain), leading to a WGM shift, as depicted in Fig.5.2(c). The deformation of the sphere can be obtained by solving the Navier equation [4]:

$$\nabla^2 u + \frac{1}{1-2\nu}\nabla\nabla.u = 0, \tag{5.3}$$

u = displacement of a given point within the sphere,

ν = Poisson ratio.

For a symmetric loading, the expresion is:

$$u_r = \sum_n [A_n(n+1)(n-2+4\nu)r^{n+1} + B_n n r^{n-1}]\, P_n(\cos\vartheta), \tag{5.4}$$

rr = radial coordinate,

ϑ = polar coordinate,

u_r = radial component of displacement,

Pn = Legendre polynomial,

An Bn = constants determined by the boundary condition at the sphere surface.

For an elastic body along with the stress-displacement relationship, the stress distributions within the sphere are obtained as:

$$\sigma_{rr} = 2G\sum[A_n(n+1)(n^2-n-2-2\nu)r^n + B_n n(n-1)r^{n-2}]P_n(\cos\vartheta),$$

$$\sigma_{\vartheta\vartheta} = -2G\sum\left\{[A_n(n^2+4n+2+2\nu)(n+1)r^n + B_n n^2 r^{n-2}]P_n(\cos\vartheta) + [A_n(n+5-4\nu)r^n + B_n r^{n-2}]\cot(\vartheta)\frac{dP_n(\cos\vartheta)}{d\vartheta}\right\},$$

$$\sigma_{\vartheta\vartheta} = -2G\sum\left\{[A_n(n^2+4n+2+2\nu)(n+1)r^n + B_n n^2 r^{n-2}]P_n(\cos\vartheta) + [A_n(n+5-4\nu)r^n + B_n r^{n-2}]\cot(\vartheta)\frac{dP_n(\cos\vartheta)}{d\vartheta}\right\}$$

$$\sigma_{r\vartheta} = 2G\sum\{[A_n(n^2 + 2n - 1 - 2\nu)r^n + B_n(n-1)r^{n-2}]\}\frac{dP_n(\cos\vartheta)}{d\vartheta} \qquad \textbf{(5.5)}$$

G = shear modulus of the sphere material.

Neglecting the friction at the contact point between the sphere and the plates, the boundary conditions are:

$$\sigma_{rr}(a) = \begin{cases} -p(\vartheta), & 0 \le \vartheta \le \vartheta_0 \text{ and } \pi - \vartheta_0 \le \vartheta \le \pi \\ 0, & \vartheta_0 \le \vartheta \le \pi - \vartheta_0, \end{cases}$$

$$\sigma_{r\vartheta}(a) = 0 \qquad 0 \le \vartheta \le \pi, \qquad \textbf{(5.6)}$$

where angle ϑ_0 defines the extent of the contact between the plate and the sphere. The pressure *p* exerted by plates of infinite stiffness on the sphere is given by

$$p(\vartheta) = \frac{3F}{2\pi a_0^3}\sqrt{a_0^2 - a^2 sin^2(\vartheta)}, \qquad \textbf{(5.7)}$$

a_0 = the radius of contact area, as shown in Fig. 5.2(b).

It should also be noted that F in the formula, consists of hydrostatic pressure, times the area of the metal boss $F = P_{External} x A_{Boss}$ (which is constant) used in the liquid level experiments.

In order to obtain coefficients A_n and B_n in Eqs. (5.4) and (5.5), the boundary condition given in Eq. (5.6) has to be expanded in terms of the Legendre polynomial in the following form:

$$\sigma_{rr}(a) = \sum_n H_n P_n\,(cos\,\vartheta) \qquad \textbf{(5.8)}$$

Then the coefficient H_n is obtained as:

$$H_n = (2n+1)$$

$$x\int_0^{\pi/2} P_n(\cos\vartheta)\frac{3F}{2\pi a_0^3}\sqrt{a_0^3 - a^2\sin^2(\vartheta)}\,sin\,\vartheta d\vartheta \qquad \textbf{(5.9)}$$

By satisfying the boundary condition, Eq. (5.6), for Eqs. (5.5) and (5.8), coefficients A_n and B_n are obtained as follows:

$$A_n = \frac{H_n}{2Ga^n[(n+1)(n^2-n-2-2\nu)-n(n^2+2n-1+2\nu]}.$$

$$B_n = \frac{H_n}{2G[(n+1)(n^2-n-2-2\nu)-n(n^2+2n-1+2\nu]} \times \frac{(n^2+2n-1+2\nu)a^{2-n}}{(n-1)} \quad \textbf{(5.10)}$$

Once coefficients A_n and B_n are obtained, strain (displacement) and the stress fields can be calculated by substituting Eq. (5.10) into Eqs. (5.4) and (5.5), respectively.

5.8.1.2 Force-induced WGM shift in a solid dielectric microsphere

For the solid microsphere, the last term in Eq. (5.2) can be calculated by evaluating Eq. (4.4) at *r*=*a* and then dividing it by the sphere radius *a* [4]:

$$\frac{da}{a} = \sum_n \frac{H_n}{4G(n^2+2n\nu+n+\nu+1)} \times \left[\frac{2-4n^2+\nu(4n^2-2n-4)}{n-1}\right] P_n(0) \quad \textbf{(5.11)}$$

Next determining the effect of stress on refractive index perturbation, dn_0/n_0, in Eq. (5.2). Neumann–Maxwell equations provide the relationship between stress and refractive index as follows:

$$n_r = n_{0r} + C_1\sigma_{rr} + C_2(\sigma_{\vartheta\vartheta} + \sigma_{\phi\phi}) \quad \textbf{(5.12)}$$

$$n_\vartheta = n_{0\vartheta} + C_1\sigma_{\vartheta\vartheta} + C_2(\sigma_{rr} + \sigma_{\phi\phi})$$

$$n_\phi = n_{0\phi} + C_1\sigma_{\phi\phi} + C_2(\sigma_{\vartheta\vartheta} + \sigma_{rr})$$

Here n_r ,n_ϑ ,n_ϕ are the refractive indices in the direction of the three principle stresses and n_{0r} ,$n_{0\vartheta}$,$n_{0\phi}$ are those values for the unstressed material. Coefficients C_1 and C_2 are the elasto-optical constants of the material, and for both PMMA and PDMS, C_1=C_2. For PMMA C_1=C_2=C=–10−10 m^2 /N and for PDMS this value is C_1=C_2=C= −1,75x10^{-10} m^2/N. Thus, for a spherical sensor, the fractional change in the refractive index due to mechanical stress is reduced to:

$$\frac{dn_0}{n_0} = \frac{n_r - n_{0r}}{n_{0r}} = \frac{n_\vartheta - n_{0\vartheta}}{n_{0\vartheta}} = \frac{n_r - n_{0\phi}}{n_{0\phi}} = \frac{C(\sigma_{rr} + \sigma_{\vartheta\vartheta} + \sigma_{\phi\phi})}{n}. \quad \textbf{(5.13)}$$

There are different kinds of sphere materials showing different responses to the measurements.

Table 5.1 shows the different sphere materials and their specific values like Young's modulus, index of refraction and Elasto-optical constant – which all are related with the WGM measurement results. (Below)

Table 5.1 : The different sphere materials and their specific values.

Material	Young's Modulus (Kpa)	Poisson coef.	Density (kg/m³)	Index of refraction	Elasto-Optical constant (m²/N)
Silica	73×10^{6}	0.17	2200	1.467	$C_1=4.22 \times 10^{-12}$
PMMA	3.18×10^{6}	0.35	1170-1200	1.489	$C1=C2=10 \times 10^{-11}$
PDMS	3-1000	0.5	1050	1.375	$C1=C2=-1.75 \times 10^{-10}$
PnHMA	-	-	1010	1.481	-

In the present WGM optical sensor, light is traveling in a plane that is normal to the applied force. Thus, evaluating the appropriate expressions for stress in Eq. (5.5) at $\vartheta=\pi/2$ and *r*=*a*, and introducing them into Eq. (5.13), the relative change in the refractive index due to force *F* is obtained as [4]:

$$\frac{dn_0}{n_0}=\frac{C}{2n_0}\sum_n\left[\frac{H_n(n+1)(n^2+3n+4+4\nu n)}{(n^2+2\nu n+n+\nu+1)}\right]P_n(0) \tag{5.14}$$

Equations (5.11) and (5.14) represent the effect of strain and stress, respectively, on the WGM shift of the solid dielectric sphere. Plugging these into Eq. (5.2), the total WGM shift is obtained as:

$$\frac{d\lambda}{\lambda}=\sum_n\frac{H_n}{2(n^2+2n\nu+n+\nu+1)}\times\left[\frac{2-4n^2+\nu(4n^2-2n-4)}{(n-1)2G}+\frac{C(n+1)(n^2+3n+4+4\nu+4\nu n)}{n_0}\right]P_n(0). \tag{5.15}$$

Pressure is the force per unit area applied in a direction perpendicular to the surface of an object (P=F/A) [63]. Equation (5.15) shows the change of total WGM shifts, while Hn includes force (F) term, therefore the theory shows that there is a direct proportion between the Force/Pressure applied on the sphere, and the WGM shifts as $d\lambda/\lambda$. When the equations come together, $d\lambda/\lambda$ becomes:

$$\frac{d\lambda}{\lambda} = \sum_{n} \frac{(2n+1) \times \int_0^{\pi/2} P_n(\cos\vartheta) \frac{3\boldsymbol{P_{Ext}} \times A_{Boss}}{2\pi a_0^3} \sqrt{a_0^3 - a^2 \, sin^2(\vartheta)} \sin\vartheta \, d\vartheta}{2(n^2 + 2n\nu + n + \nu + 1)} \times \left[\frac{2 - 4n^2 + \nu(4n^2 - 2n - 4)}{(n-1)2G} + \frac{C(n+1)(n^2 + 3n + 4 + 4\nu + 4\nu n)}{n_0}\right] P_n(0) \quad \textbf{(5.16)}$$

In the formula above, PDMS spheres have elasto-optical constant values as,

$$C_1 = C_1 = C_2 = C = -1{,}75 \times 10^{-10} \; {m^2}/{N}, \quad \textbf{(5.17)}$$

Shear Modulus:

$$G = \frac{E}{2(1+\nu)} = \frac{1000 \; kPa}{2\;(1+0{,}5)} = 333{,}33 \; kPa$$

values, and angle ϑ_0, which defines the extent of the contact between the plate and the sphere varies between 0 and π.

Therefore this relationship indicates a direct proportion between the external pressure applied on the sphere and WGM shifts, which will be investigated further by experimental methods.

5.8.2 PDMS

PDMS is an elastomer that is a mixture of two components: a base and a curing agent. By changing the ratio between the base and the curing agent, it is possible to obtain elastic materials with Young’s modulus ranging between 3 and 1000 kPa (corresponding to a base to- curing agent volume ratio of 60:1 and 10:1, respectively).

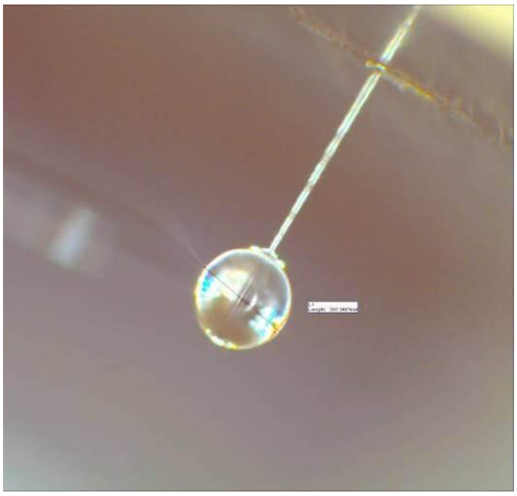

Figure 5.6 : A typical PDMS sphere.

A typical PDMS sphere between 200-600 micrometer can be seen above.The sphere diameters can be arranged according to the type of measurement and required sensitivity.

5.8.2.1 PDMS sensor

Polydimethylsiloxane (PDMS) belongs to a group of polymeric organosilicon compounds that are commonly referred to as silicones. PDMS is the most widely used silicon-based organic polymer, and is particularly known for its unusual flow properties.

The PDMS microspheres were manufactured by dipping the tip of a silica fiber inside a freshly mixed PDMS polymer pool. A number of PDMS microspheres were manufactured using different mixture ratios, thereby having different Young's moduli [36].

The Young modulus of a PDMS microsphere is substantially smaller than that of PMMA sphere of the same diameter resulting in comparable sphere deformations at much smaller force levels. Thus, determining the sensitivity of the PDMS force sensors is a more challenging task; the load-cell based measurement setup of would not provide sufficient resolution for sensor calibration. Moreover, since the force levels in these calibrations are ($<10^{-6}$ N), even the aerodynamic forces due to air currents (air drafts and natural convection) would have considerable adverse effect.

In order to account for the sphere deformation, a Hertz-contact analysis was carried out on the spheres for a range of force values. Using this force versus deformation data and modeling the sphere as a linear spring system, the equivalent spring constant k_{sphere} was determined for each sphere size and PDMS mixture ratio used in the experiments. Then, the equivalent spring constant of the beam-sphere system was determined as [4]:

$$\frac{1}{k_e} = \frac{1}{k_{sphere}} + \frac{1}{k_{beam}}, \tag{5.17}$$

Where the spring constant for the beam is:

$$\frac{1}{k_{beam}} = \frac{3E\pi D^4}{64L^3}. \tag{5.18}$$

Here, E is the Young modulus, D is the diameter, and L is the length of the silica beam. The force exerted on the sphere is then calculated as

$$F = k_e\delta\,, \tag{5.19}$$

where δ is the displacement of the translation stage and is determined by the Michaelson interferometer signal as:

$$\delta = l\frac{\lambda_m}{2} \tag{5.20}$$

Here, l is an integer and λ_m is the wavelength of the He–Ne, laser (632.8 nm). The WGM shift dependence on the applied force for a solid PDMS microsphere of 910 μm diameter with base-to-curing agent volume ratio of 50:1 (E =10 kPa). The figure indicates a strong agreement between the experiments and Eq. (5.15).

6. EXPERIMENTAL METHOD

6.1 Sensor Design

Southern Methodist University Mechanical Engineering Faculty’s micro sensors lab has been visited to investigate their studies regarding WGM microsensors for the first time, and for the second time it was revisited for a longer period of time to develop the actual novel liquid level sensor.

WGM based Micro Sensors technology is suitable for many different applications, therefore after studying deeply on the theory, and making further discussions with the researchers, a novel liquid level sensor based on WGM principle has been designed, and successful results have been achieved in the experiments.

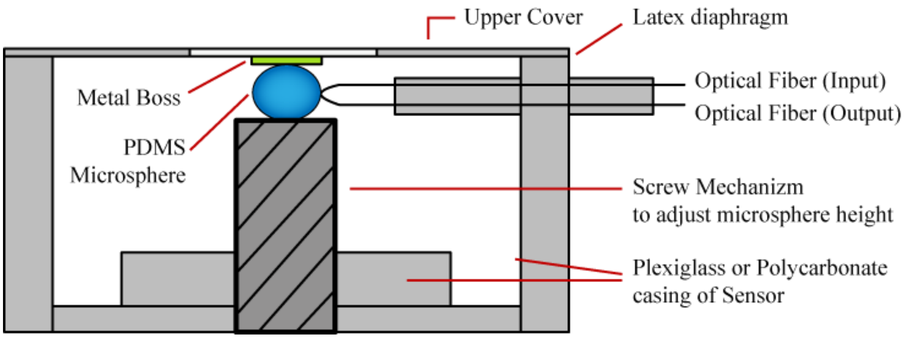

Figure 6.1 : WGM sensor sketch [7].

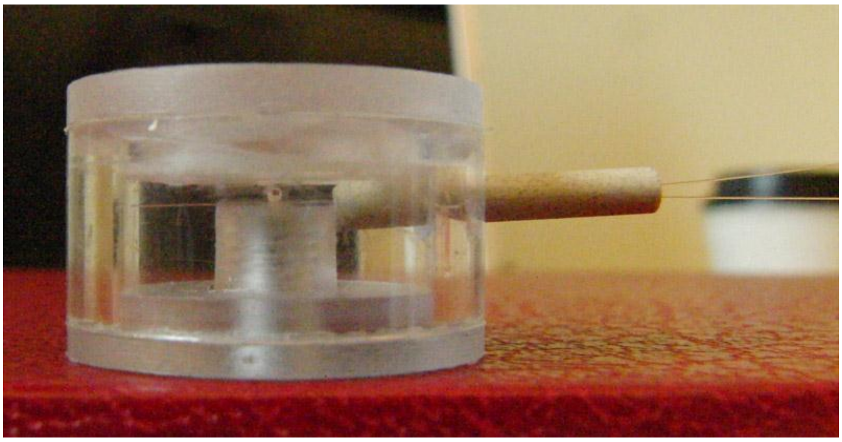

Figure 6.2 : Sensor design.

After defining the properties of the experiments, many different prototype sensors have been designed. According to the results of these prototype sensor development studies, it has been considered that, when designing the actual liquid level sensor, a cylindrical case which has a hole for the inlet and outlet of laser light through the fiber cables, another hole for precise observations; a PDMS microsphere; an elastic membrane both to resist the liquid molecules outside the sensor, but also to enable the sphere to feel/detect every little pressure change; a metal boss inside the membrane to obtain an equal force distribution on the sphere as seen in the formulas, and lastly a screw mechanism enabling the microsphere to move vertically until it touches the metal boss on the membrane had been used.

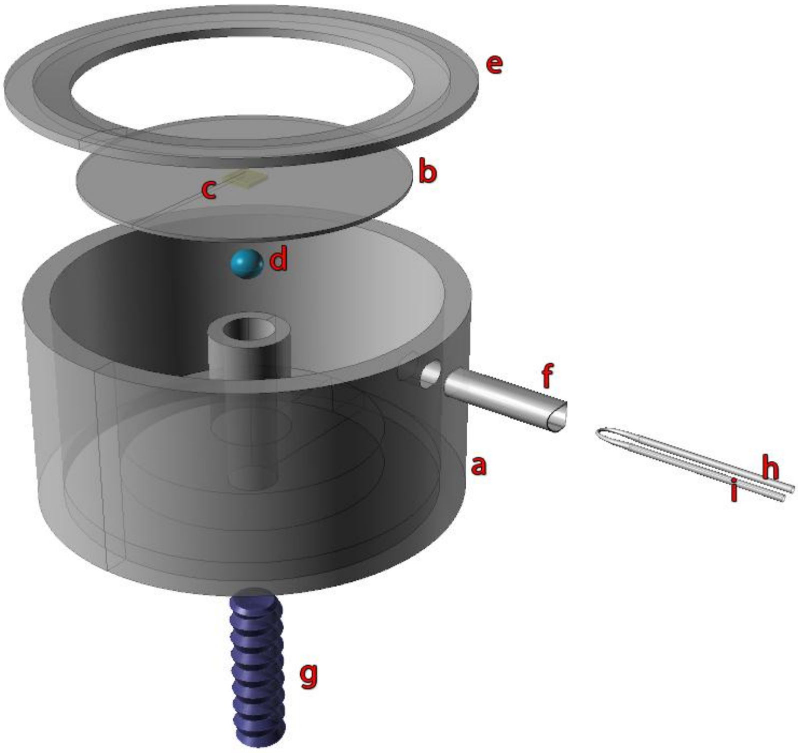

Figure 6.3 : Sensor case (a); Latex diaphragm (b); Metal Boss (c); PDMS microsphere (d); Upper cover (e); Fiber protector (f); Screw Mechanism (g); Optical fiber input (h); Optical fiber output(i).

6.1.1 Micropshere

The concept of liquid level sensor is based on the optical resonance shifts (WGM) of dielectric spheres. Therefore as mentioned earlier, these shifts are generated by the perturbations in the sphere morphology, occurred in shape, size or the refractive index. These microspheres used in the WGM theory are actually dielectric resonators with very high quality factors.

These spheres can be made of different materials including Polydimethylsiloxane (PDMS), Polymethyl methacrylate (PMMA) and Silica. Table 5.1 shows the different sphere materials and their specific values like Young's modulus, index of refraction and Elasto-optical constant – which all are related with the WGM measurement results. PDMS sensors have been tested in the experiments, and proven that PDMS is definetly a suitable material for liquid level experiment setup because of it's mechanical properties and ease of production.

PDMS is an elastomer that is a mixture of two components: a base and a curing agent. By changing the ratio between the base and the curing agent, it is possible to obtain elastic materials with Young's modulus values ranging between 3 and 1000 kPa.

The experiments have been defined so that the minimum liquid level should be 0mm which means there is no liquid in the container, up to a limit of 300 mm liquid height. After examinations it has been seen that using a PDMS sphere with 10:1 volume ratio would be the best choice both to have 0-3000 Pa pressure range, and have the best possible sensitivity using the force detection concept.

For this aim 10 ml of Sylgard 184 Silicone Elastomer base and 1ml of Sylgard curing agent have been mixed for 10 minutes in lab room conditions until a homogeneous mixture is formed.

Microspheres were manufactured by dipping the tip of a silica fiber inside a freshly mixed PDMS polymer pool. After this step PDMS spheres on fiber tips, have been located into lab ovens preheated to 400^{o}F (200^{o}C) for over 5 hours. After this process spheres were examined carefully under microscopes, and the ones with clear content, circular shape, and suitable sizes have been selected to be used in sensor production.

6.1.2 Sensor case

It has been agreed that cylindirical shaped sensor case would be suitable both for ease of sensor production and supply of materials. In the first trials, plexiglass material was used to produce casing. But because of the breakage failures during manufacturing, the final material has been changed to polycarbonate which is a more durable and machinable material. Also fiber protectors have been produced using this material, which holds and protects the input and output fibers.

6.1.3 Elastic membrane

During sensor design and production, an elastic membrane was required to transfer the outside pressure to the microsphere, without letting any liquids or gasses leak inside the sensor case. Therefore many different materials have been tried as elastic membrane, and latex has become the best alternative with its water and oil resistance, moreover still thin and elastic characteristics. As a result after building the sensor casing, latex membrane was assembled on top of the sensor by using suitable adhesives.

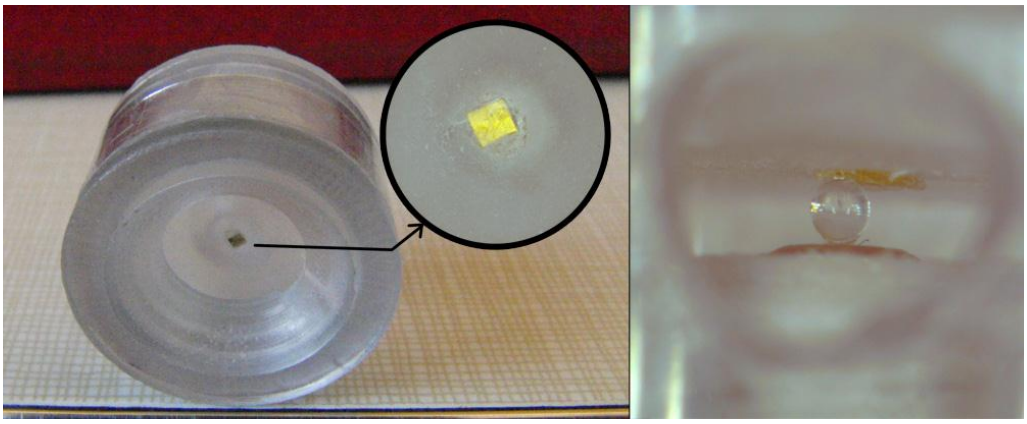

Figure 6.4 : Metal boss added to the latex membrane for greater sensitivity (a).The microsphere touching metal boss (b).

A metal boss has been cutted as 1x1mm from a copper sheet, and assembed in the center of the membrane by using suitable adhesives. The reason for adding this metal boss was to increase sensitivity and to obtain a stiff surface for a balanced pressure distribution over the microphere, resulting to match the force sensor equations shown in the previous chapter. Figure 6.4 above, shows metal boss assembled inside the membrane center, where the detailed view has been taken by an electro-microscope. Figure 6.4(b) shows the exact touching condition of the microsphere located between the screw mechanism, and the metal box. With this setup, any liquid level change makes a balanced pressure increase on microsphere without letting any liquid inside, hence changing the sphere morphology, which is what was expected from the design.

6.1.4 Fiber

To be able to obtain evanescent-wave coupling, which was explained earlier [47], two optical elements, like the fiber and the sphere in this case, should be placed close together so that the evanescent field generated by one element (fiber) does not decay much before it reaches to the other element (sphere). Therefore the glassfiber should be stripped by using fiber strippers, and thinned by using fire torch to be able to obtain optical coupling. The thinning process is done by clamping the fiber's edges by fiber holders and pulling/streching the fibers very slowly until making it thinner enough to interact the core of the fiber with the sphere. The typical radius drops from a standart 125 micron fiber thickness to around 10 microns, allowing the evanescent-wave coupling to occur between fiber and optic resonator- which is the microphere in this case.

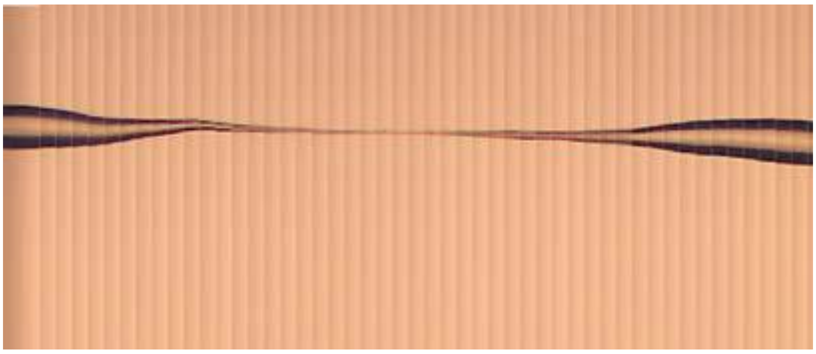

Figure 6.5 : Tapered fiber.

6.1.5 Screw mechanism

As expressed in the theory before, any small pressure increase can be detected by the changes on the morphology, either size or shape of the sphere. To be able to detect the pressure changes, the metal boss on the membrane should be surface to surface touching to microsphere. Therefore microsphere has been placed on top of a screw mechanism, located in its centerline hole which fixes the sphere location with the fiber tip. After locating the sphere on the screw mechanism, it has been finely tuned for touching the metal boss precisely. The touching condition should not to be too tight not to create any fake pretension, or any morphology change on the micropshere.

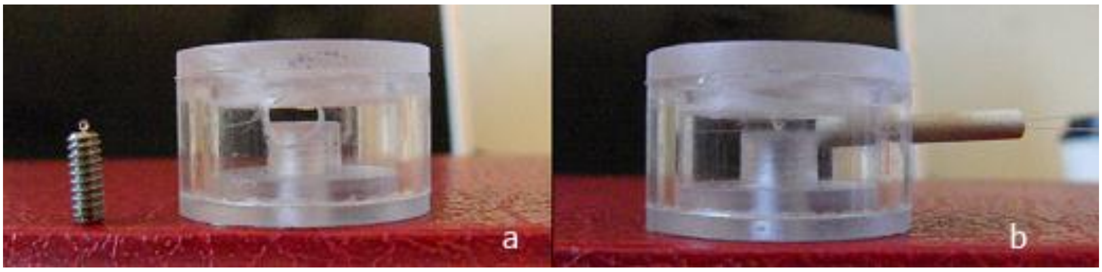

Figure 6.6 : Screw mechanism (a), Optical fiber placed in sensor body (b).

Also many elements have been used such as the translational stages shown below, helping to couple the fiber core into the sphere.

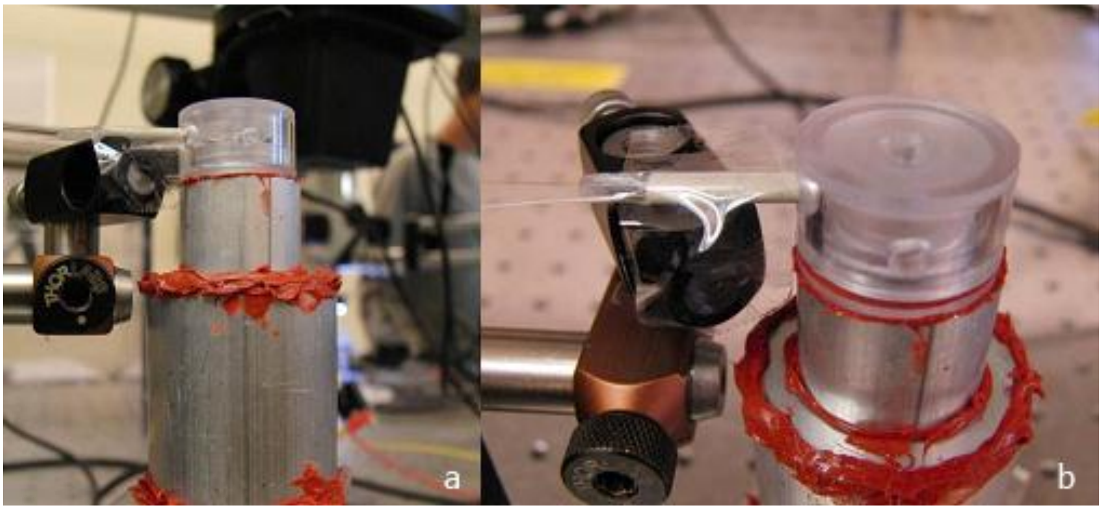

Figure 6.7 : Sensor production (a), Fiber core inside the sensor (b).

6.2 Experiment Setup

After reaching the final sensor design, and manufacturing the actual sensors, tracking of WGM shifts has become possible, and hence pressure changes of the surrounding medium can be measured with a suitable experiment setup. For this aim, the most suitable experiment set up has been built to measure the pressure changes of the medium, which is related with the height of the liquid.

A schematic of the experiment setup is shown below. The output of a laser diode having a laser wavelength of ~1312nm, has been coupled into a single mode optical fiber, and approximately 90% of the light is used to obtain WGM shifts in the sensor, while remaining 10% is used as the reference signal.

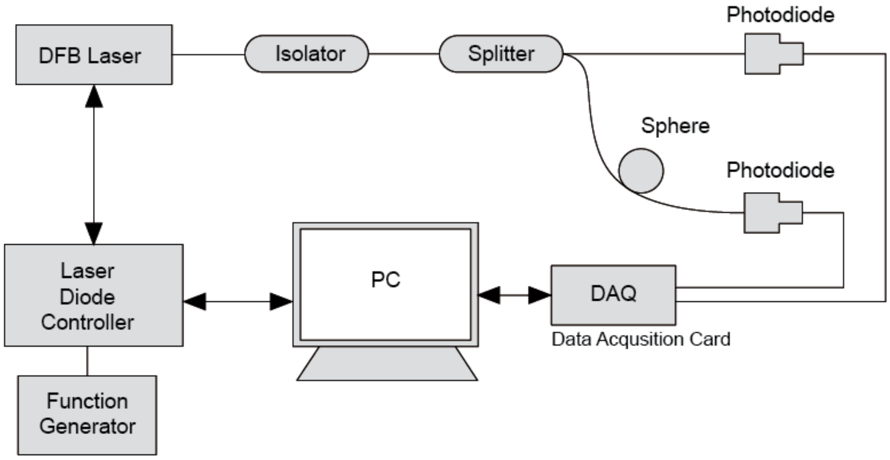

Figure 6.8 : The experiment setup [4].

The laser controller has been driven by a function generator, where a sawtooth input was used in the experiments. The output ends of the sensor signal and reference optical fibers have been coupled to photodiodes (PD).

The main purpose of the photodiodes are to detect and convert the light signals into electric signals. Then PD outputs and the function generator outputs have been sampled by using an analog-digital converter and the DAQ card in the PC.

For producing the microspheres, 10 ml Silicone Elastomer base has been mixed with 1 ml of Silicone Elastomer curing agent. Just after preparing this mixture, a fiber piece, which has been stripped to obtain an even smaller diameter, has been dipped into it and formed a liquid PDMS sphere. After preparing many liquid/droplet spheres, they have been cured about five hours in an oven heated up to 400F, to form the solid PDMS spheres.

After obtaining the sensing elements, the microspheres, the experiment setup have been designed. It has been decided to have two steps: Air Presssure Meaurements, and relatively more difficult but more important Liquid Level Measurements.

6.2.1 Equipment

6.2.1.1 Main equipment

While the eqipments, and their purposes have been generally summarized above, these equiments can be listed below as they have used in the experiments:

- Distributed Feedback (DFB) Laser with Analog, 10mW Output

- Precision Laser Diode Controller
- Function/Arbitrary Waveform Generator
- Special computer tracking software generated in LabView.
- SM1FC Fiber Adapters
- OM99T-V15 Trinocular, Stereo Microscope
- NI PCI-6232 Series Multifunction DAQ Device

6.2.1.2 Additional equipment to build the setup

- Esk03 Mounting Posts Essentials Kit (Posts , Rods, bases, Post holders)
- 2x PDA10CS Amplified InGaAs Detector, Variable Gain
- 250 μm Bare fiber
- 250 μm single mode coupler
- 14-Pin Butterfly Laser Diode Mount
- Current Source Laser Diode Mount Interconnect Cable
- TE Controller/Laser Diode Mount Interconnect Cable
- Cable, Type SH68-78-EP Shielded cable
- BNC-2110 Noise Rejecting, Shielded BNC Connector Block
- XYZ translation stage. (PT3 - thorlabs)
- SM1FC SM1 (1.035"-40) to FC Fiber Connector Adapter Plate
- 10140A Multimode SMA905 Connectors for 140 μm Fiber
- 10230A Multimode SMA905 Connectors for 230 μm Fiber
- 30126D1 FC/PC Single Mode Connector, Ø125 μm,Ceramic Ferrule, Ø3 mm Boot
- IO-H-1310FC-APC-SP Fiber Isolator, 1310nm, low power, FC/PC input endAPC on output end
- Fiber strippers, screwdrivers, blades and many other general lab tools.

Detailed technical specifications of these devices can be found in the Appendix B.

Figure 6.9 shows most of the devices related with the laser signal conditioning. The laser coming from laser source is controlled optically by the laser diode controller, where the signal shape is conditioned with the function/wave form generators.

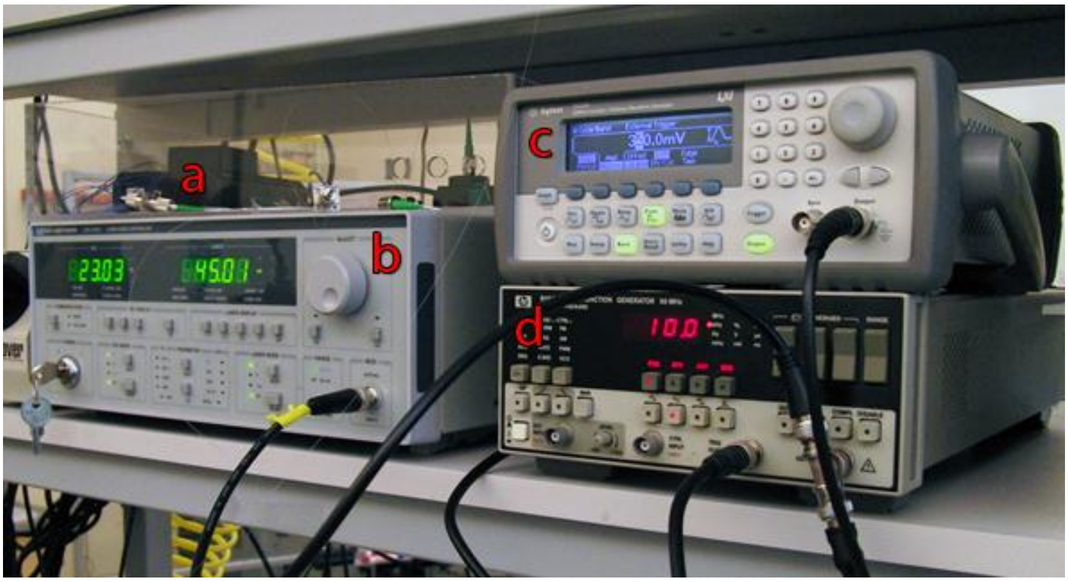

Figure 6.9 : Laser source (a), Laser diode controller (b), Pulse function generator (c), Arbitrary wave form generator (d).

6.2.2 Air pressure measurement setup

Air pressure experiments have been performed by applying pressure to a cylindrical chamber assembled on top of the sensor, by using a syringe. The cylindrical chamber is used for increasing the pressure linearly and for getting rid of any kind of noise such as pressure fluctations during applying pressure. The reference pressure signal is measured by a pipe, which is also connected to the cylindrical chamber, while the other side is connected to a pressure transducer. The accuracy of pressure transducer is known as ± 1.0% according to the data sheet included in table A.9 of the Appendix section.

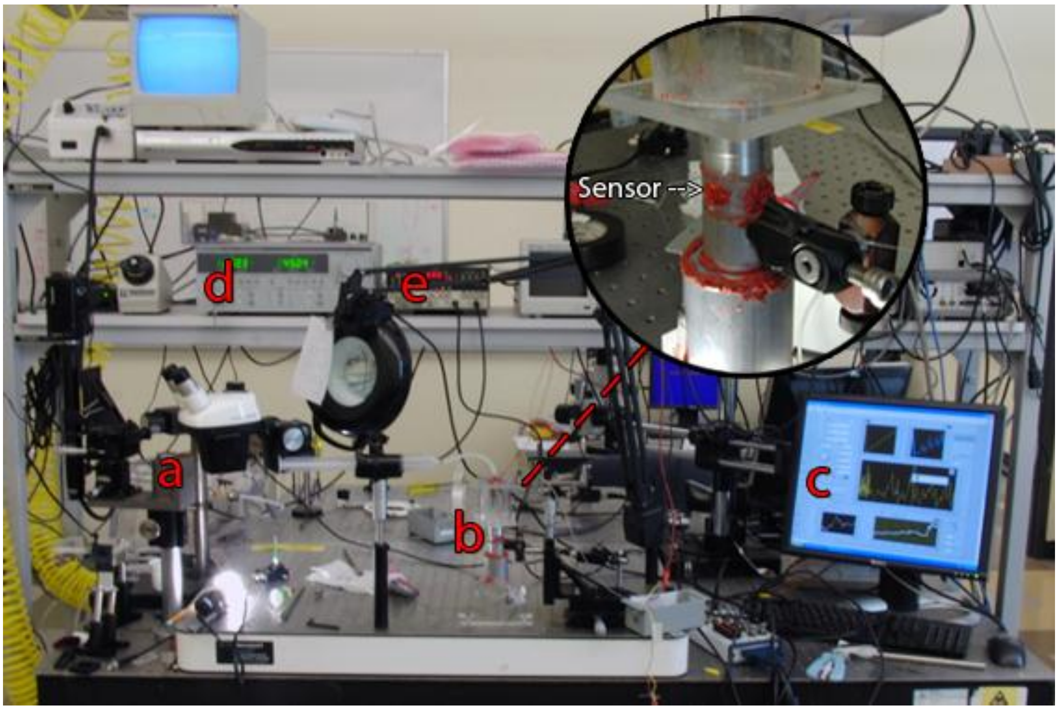

Figure 6.10 : The experimental setup used in “Air Measurements” (Trinocular, stereo microscope (a), Sensor located under the cylindrical chamber (b), Tracking software (c), Laser diode controller (d), Arbitrary wave form generator (e).

The figure 6.3 shows the general experiment setup used in the air pressure experiements, which is the first step showing that the sensor design is working in air. In the setup the thinned glass fiber has been touched and fine tuned to the microsphere physically by the help of magnifying glasses and also the stereo microscope untill catching any resonances on the tracking software.

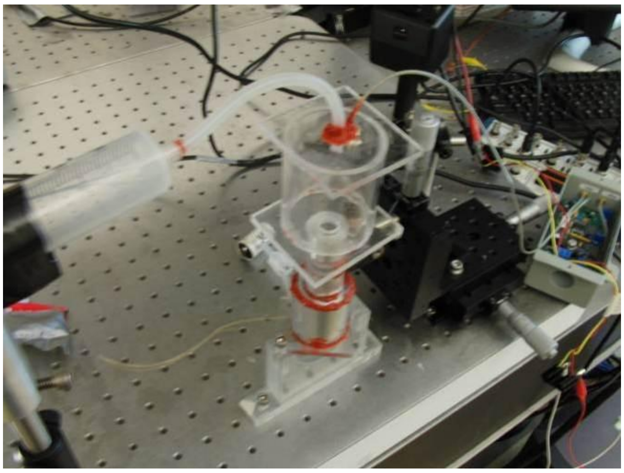

Figure 6.11 : Air pressure measurements using syringe and pressure box in detail.

After getting the WGM shifts or in other words getting the resonances on the LabView sofware, the detection of pressure changes phase can be started. As shown in the figure 6.12, the sensor then has been located under the cylindrical chamber, which is connected to both the pressure transducer and the syringe. Therefore any pressure change generated by the movements of syringe, can be detected by the sensor, and can be controlled by the pressure transducer, which works as the reference.

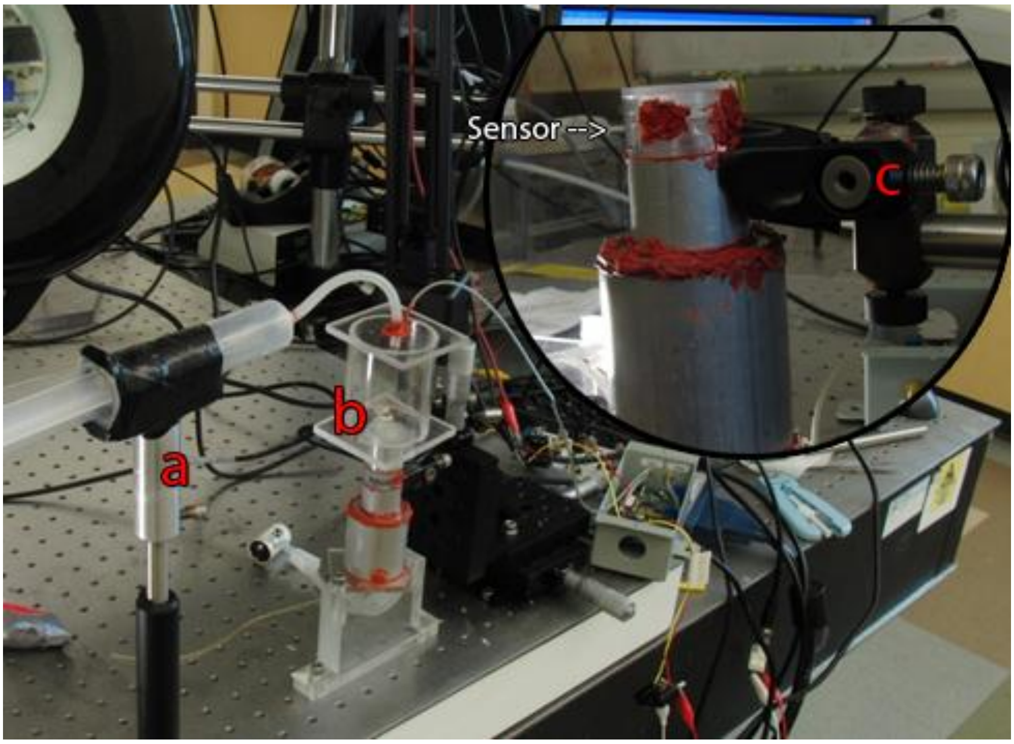

Figure 6.12 : Syringe for applying pressure (a), Cylindrical chamber (b), Translational stages used during the sensor building (c).

As it can be seen in the Figure 6.12, the pressure is being applied to the sensor through the cylindrical container by moving the syringe. Therefore a controlled pressure increase has been obtained on the sphere, which the results will be shown in the results section.

6.2.3 Liquid level measurements setup

The most important difference of the liquid level experiment setup is the content container and it's ingreedients. The liquid container was selected to be transparent for observing the setup simultaneously, during adding or draining water, and to have higher walls to contain liquid levels above 300mm, resulting a liquid pressure range between 0-3000 Pa.

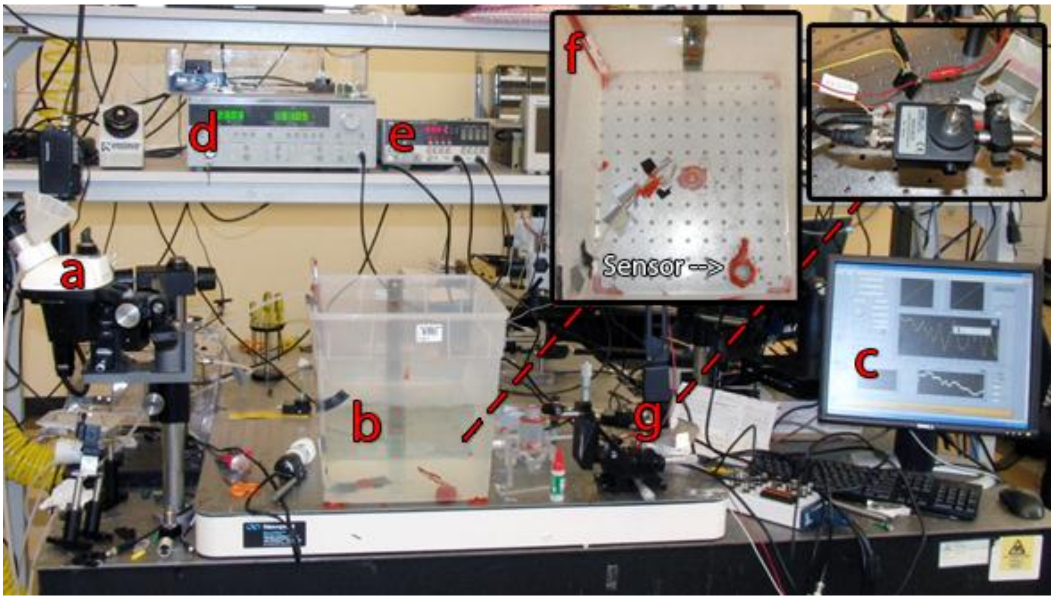

Figure 6.13 : Trinocular, stereo microscope (a), Liquid container (b), Tracking software (c), Laser diode controller (d), Arbitrary wave form generator (e), Liquid container having the level sensor, u tube, and the scale ruler (f), Photodiode (g).

For increasing or decreasing the liquid levels with the same flow rate, a piping system was used for both water inlet and water outlet. For this experiment water has been selected because of its easiness to use in laboratory conditions, cheapness to obtain, as well as it's cleanness for the test medium and electronic devices around. For increasing the water levels, a piping system has been developed and used to add water from a tap with a constant flow rate, and also to drain the water to a sink, when the pipe end lowered.

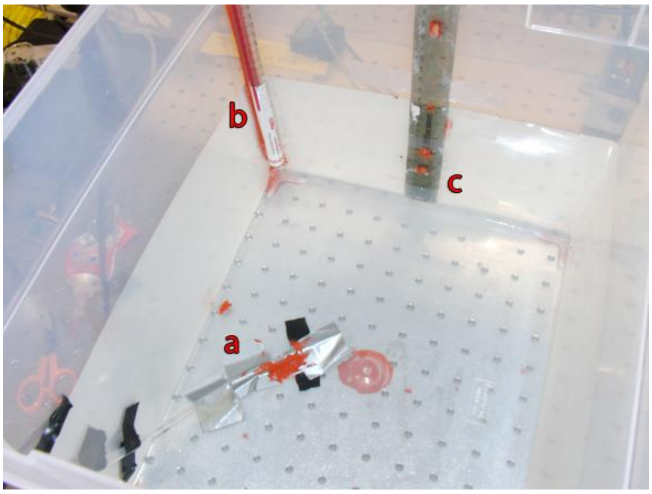

Figure 6.14 : Drain pipe (water inlet and outlet) (a), U tube connected to pressure transducer (b), Scaled ruler for calibration of pressure transducer and converting the pressure values into liquid levels (c).

After designing the water inlet and outlet, two measurement devices has been added to the system for reference and calibration as it can be seen in the figure above. First of all a u tube has been inserted into the setup, which is sealed and connected to the pressure transduces, which is giving the exact pressure increase occurred because of the liquid level increase in the tank performing as the reference device, and a basic scaled mm ruler for the calibration of the pressure transducer, as well as the transformation of the pressure values into liquid levels. In summary u tube principle in classical college physics [60] has been applied in this section for calibrating the pressure transducer and referencing it to the WGM laser optics sensor.

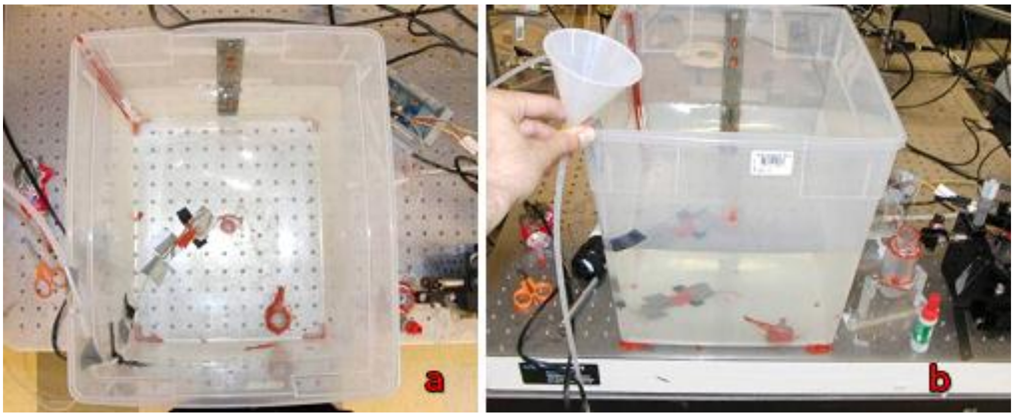

Figure 6.15 : Water pressure/depth experiments(a), For draining and adding water same pipe has been used, which was fixed in the bottom of the container 8 (b).

More figures related with the liquid level measurements can be seen above & below.

Figure 6.16 : Obtaining linear flow (a), Two sensors under water (b).

Temperature resistant silicon was used for sealing during the experiments as well as other adhesives and duct tapes.

6.2.4 Software tracking

The software used in the experiments, had been generated by using National Insturments' LabView software, which is a visual programming environment to develop and design measurement, test, and control systems using graphical icons and wires that resemble flowcharts. [61]

The software in the experiments uses a method making cross-correlation of two different optical spectra to determine the amount of resonance shifts. This method of detecting sample shift is very similar to template matching or phase correlation techniques in image processing.

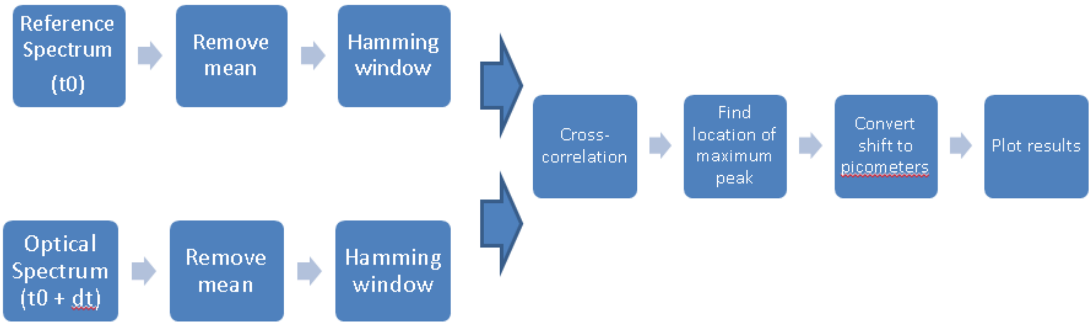

Figure 6.17 : Method for WGM shift tracking.

As schematized in the Figure 6.17, an optical spectrum has been obtained by a photodiode, which is a type of photodetector, that converts light signal into electrical signal such as current or voltage. In this spectrum obtained through a microscope, resonances exhibit after one scan of the laser. This spectrum has been acquired at time t0, and it has been chosen as the "Reference" spectrum. Another spectrum has also been obtained at time t1. By computing the mean and subtracting it from each waveform, it will be available for the cross-correlation of the two waveforms either in the time domain or in the frequency domain. The result of the cross-correlation computation is a waveform that is twice as long (minus one sample) as the two spectra. This new waveform will have an absolute maximum which represents the shift amount where the two spectra are most similar. If the resonances had not shifted at all from time t0 to time t1, this absolute peak would be in the horizontal center of the cross-correlation waveform. If the resonances have shifted, the peak will have moved a certain number of samples away from the center of the cross-correlation waveform. This distance is proportional to the amount of resonant shift that has occured from time t0 to time t1.

Because the error, or uncertainity of the resonance shifts tracking has been obtained by 14 bit DAQ card, the precision of the data should be $1/(2^{14})$. The method for tracking the WGM shifts uses seven calculation steps as shown in figure 6.17 above, so the error folds seven times. Therefore resulting WGM shift data obtained by the algorithm contains an uncertainity of

$$\sum_{n=7} \frac{1}{2^{14}} = \frac{7}{16384} \ ,$$

which equals an accuracy level around ±0.043%.

Figure 6.18 below, demonstrates the Labview program generated for the WGM sensor experiments. Software for tracking the WGM rezonance shifts has five main screens: Reference signal screen, Sensor signal screen, Normalized Signal screen, Applied force control screen, and WGM Shift Tracking screen.

The box on upper left indicates the saw tooth profile which was selected as the signal directly going to the photodiode, while the box on the upper right indicates the sensor signal after evanescent-wave coupling of process with the microfiber. Resonances can be seen even on this box. The larger rectangular box, shows the normalized signal, and tracks the sharp dips, WGM resonances. The box on the lower left indicates the applied force control device, which is the pressure transducer in both liquid level and air pressure experiments, while box on the lower right indicates the force control of the sensor generated by the movement of the WGM resonances.

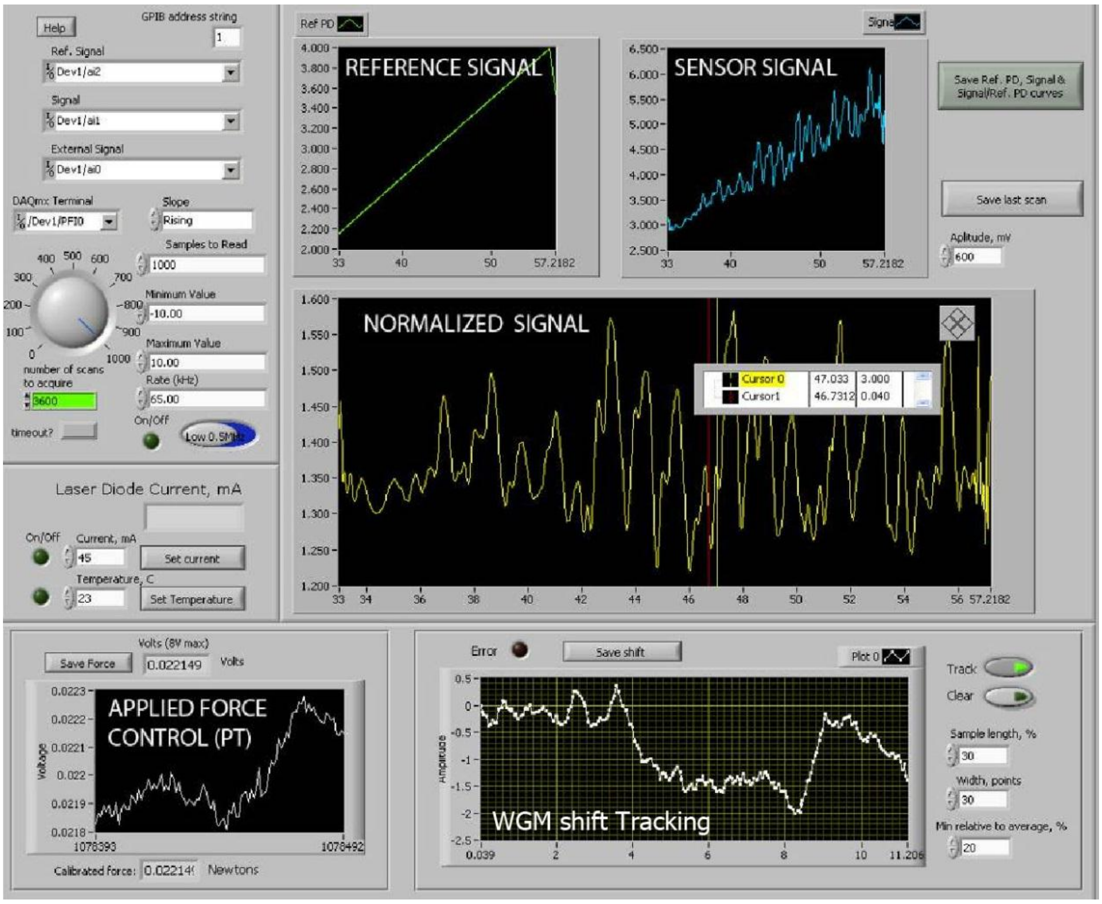

Figure 6.18 : Softw are for tracking the WGM resonance.

When looking at the software screen above, the first thing that should be done is to obtain the resonances on sensor signal and normalized signal screens, which demonstrates the signals coming from the sensor. To be able to do this, a careful tuning of the sensor is required for coupling the fiber into microsphere, which is a very though process and needs care and expertise. After obtaining trackable resonances, then any pressure increase or decrease create shifts of the resonances as demonstrated above. These shifts are tracked in the normalized signal box. It should be noted that the X axis of the normalized signal box is in Volts scale, while the X axis is mA. This changing mA value is being changed according to the formula 6.1 as shown below [4]:

$$\frac{d\lambda}{\lambda} = \frac{dn_0}{n_0} + \frac{da}{a} \qquad \textbf{(6.1)}$$

According to the formula, the resonance shift values can be tracked and read from the normalized signal box, but the because the figures in are raw demonstrating mA values, later they have been calibrated into pm scaled shifts. These shifts are then being tracked and recorded by the sofware and the WGM shift tracking screen demonstrates the WGM shifts through time. The Applied Force Control screen, shows Pressure Transducer signals during these increases or decreases. In other words, while the Pressure Transducers have been used as the reference device, these Applied Force Control screens demonstrates the reference pressure change values for the WGM liquid level sensor.

The data obtained from the software consists of three main columns, showing time, WGM shift tracking and Pressure transducer signal. The WGM shifts and pressure transducer data can be used as the tracking graph through time. More importantly the WGM shifts in pm versus the converted pressure transducer values showing the liquid level in mm graph gives the sensitivity curve of the sensor. The processing and implementation of the data is shown in the following chapter with greater detail.

7. RESULTS

As expressed in the previous section, after building the experiment setups, many different trials have been performed .

But before that it would be better to explain the data collecting process a little bit further to understand the results.

For example when water level starts to rise continously, then resonances in the normalized signal screen starts shifting forward. The amount and speed of these shifts are directly related with the flow rate and increasing the amount of liquid in the container.

The most important function of the software depends on the tracking mechanism of the resonance shifts. The software tracks these resonance shifts continuously, as a result, plots a graphic of these changes. The slope of the sensor signal shown in the lower right box increases during liquid level increase, and also because system tracks the pressure transducer signal as the control value, the slope also increases in the lower left box.

During draining, because the water level drops, resonances starts to shift to the opposite direction, causing a decrease in the slope, in other words a negative slope in the sensor signal box located on lower right. Similarly decreasing slope can be observed in the pressure transducer signal during draining.

Because the data collection had been performed continuously & automatically by LabView software, and data colletction intervals are within 0,02-0,03 second range, each graphs shown in this study consists of up to 52000 data points according to the length of each data set.

7.1 Air Pressure Measurement Results

Before expressing the results, it would be better to define some important concepts like Sensitivity, Accuracy, Linearity and Resolution.

Sensitivity, is a measure of the change in output of an instrument for a change in input. Generally speaking, high sensitivity is desirable in an instrument because a large change in output for a small change in input implies that a measurement may be taken easily. Sensitivity must be evaluated together with other parameters, such as linearity of output to input, range and accuracy. The value of sensitivity is generally, indicated by the transfer function. Thus, when a temperature transducer outputs 5 mV per degree C, the sensitivity is 5 mV/C. [17]

Accuracy of a measurement system is the degree of closeness of measurements of a quantity to that quantity's actual (true) value. [64] [65]

Linearity is the behavior of a device, in which the output varies in direct proportion to the input. In a linear device, the output-to-input signal amplitude ratio is always the same, no matter what the strength of the input signal is. [66]

In other words, linearity defines how well the device's actual performance (across a specified operating range) approximates a straight line. [67]

Resolution, determines the ability to see fine details in the measurement, which is the minimum detected pressure level in the experiments indicated in this section. [21]

After giving these definitions, it will be better to review some examples of the data obtained fom the experiments. First some examples to Air Pressure Measurements can be seen in the figures below.

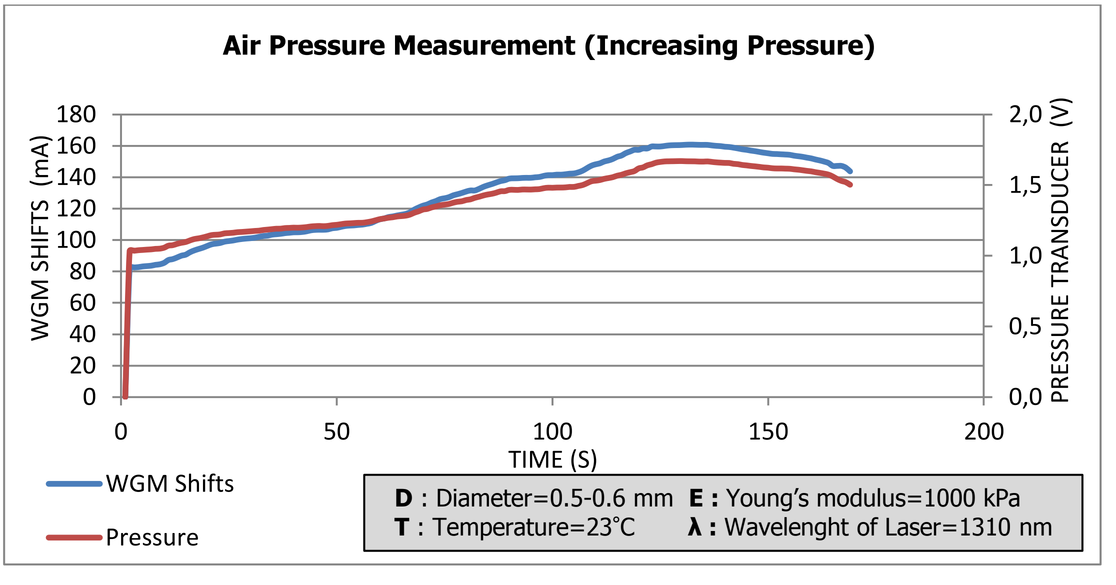

Figure 7.1 : Air pressure measurements.

In the graph above, red line represents the pressure transducer, while the blue line represents the WGM resonance shifts in miliampers. In this graph the pressure transducer signal is already calibrated for the air pressure measurements. Therefore the relationship between the WGM shifts of the sensor signal in pm scale and pressure values in Pa scale obtained from the reference pressure transducer signal results to draw the sensitivity curve, which can be seen below. As expressed in the previous chapter, while a mA change of resonances equals to 5pm shifts, the WGM shifts have been converted into pm values, while the pressure transducer signal has been converted from Volts to Pa scale.

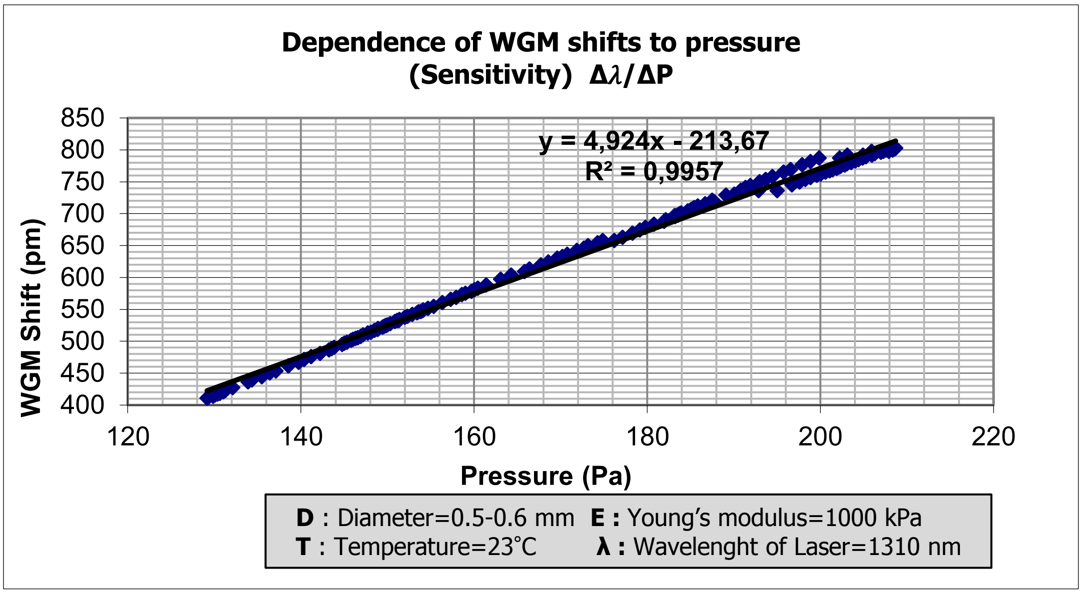

Figure 7.2 : The dependence of WGM shifts to pressure changes.

In the graph above, WGM shifts demonstrate a linear response with no discernible hysteresis in the pressure range tested, thus providing a reliable pressure reading essential for sensor performance. The corresponding resonance shift as a function of applied pressure is plotted above.

Y axis represents the resonance shifts in pm scale, while X axis represents the pressure changes in Pa scale. The R-squared value, which is a coefficient in statistics that demonstrates the degreee of correlation between two varibales. As an example while R^2=0 means there is no correlation between the two variables, R^2=1 means there is a perfect (100%) correlation between these variables. In the graph above, because the R=quared value is 0,9957, that means the data obtained from the experiment, near-perfectly correlates to the trendline. Thefeore according to the data above, a linear relationship between the WGM shifts and applied pressure appears with a slope of 5 pm/Pa.

7.2 Liquid Level Measurements

In the Liquid level measurements, pressure on the sensor changes due to increasing or decreasing amounts of liquid levels. Therefore it can either be called as liquid level measurements or water pressure measurements.

In air pressure measurements, the reference value had been air pressure, there was no need for any conversion. But in liquid level measurements, the experimental setup is much more complex, hence pressure transducer signal's conversion to liquid levels is required to evaluate the results.

7.2.1 Conversion of pressure transducer signal

In liquid level measurement setup, the pressure transducer is connected to a perfectly sealed U tube. One side of this U tube is open to the bottom of the container, while the other side is sealed, and piped to the pressure transducer. This setup enables when the liquid level increases, it also increases the pressure in the U tube, and hence the pressure transducer signal increases. When draining water, also the pressure in U tube decreases, resulting a decrease in the Pressure Transducer signal.

Conversion data have been collected each time by recording the Pressure transducer signal with the Labview software, and the actual liquid levels read from the scale simultaneously, during both increasing and decreasing liquid levels. The data obtained, have been used to develop the conversion of the Pressure transducer signal into liquid heights. Conversion curve during filling has been shown in Figure 7.3, while conversion curve during draining has been demonstrated in Figure 7.4.

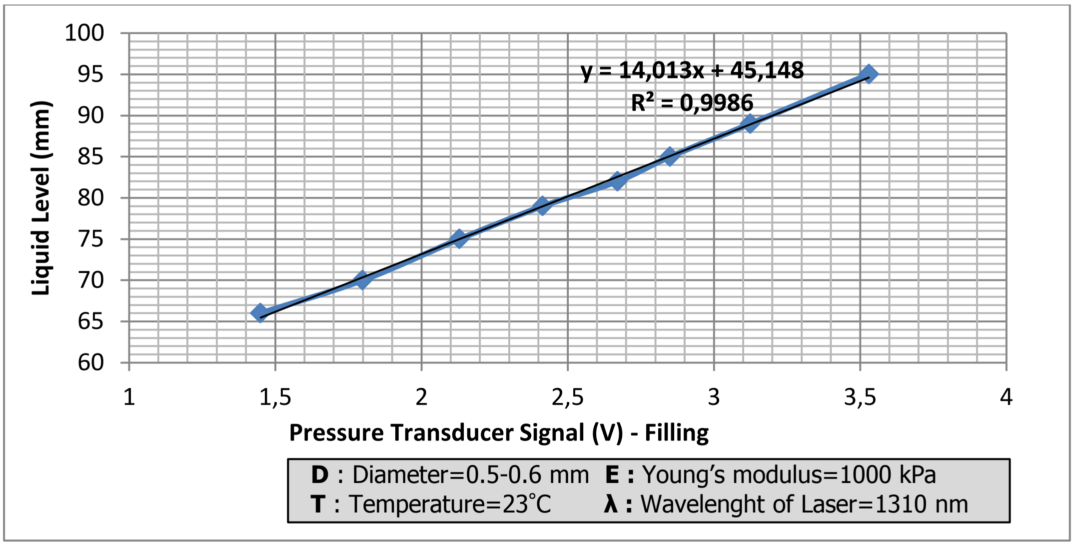

Figure 7.3 : Conversion of pressure transducer signal to liquid level during filling.

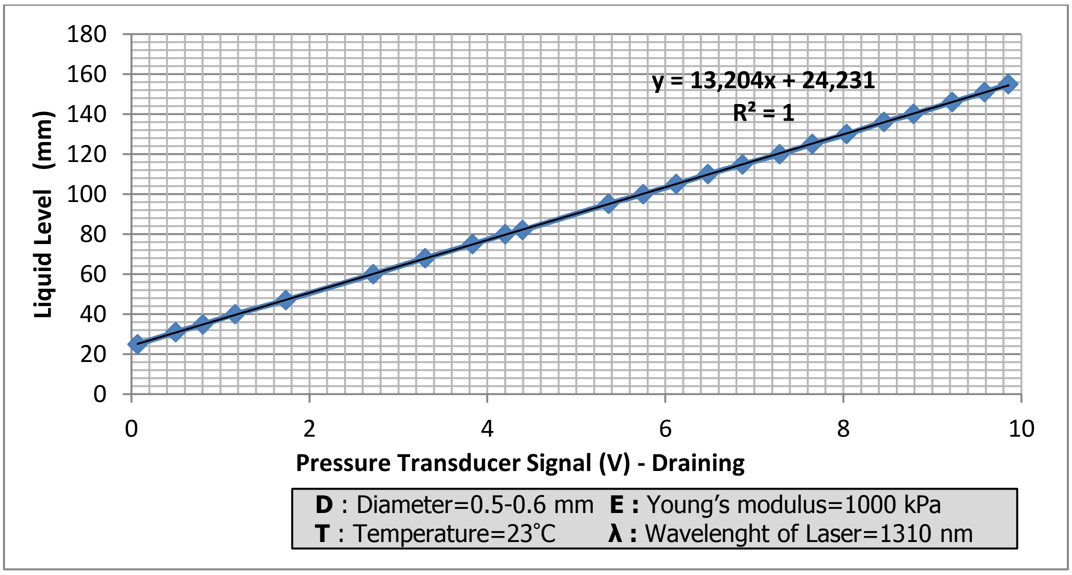

Figure 7.4 : Conversion of pressure transducer signal to liquid level during draining.

For reliability of the results, pressure trandsucer conversion data has been taken very precisely during each experiment either when filling or draining liquid. The data collection has been performed precisely, without having any sparse distribution around the curve. As it can be seen in the figure above, although the time intervals are not homogenous, the conversion curve forms a perfect linear function with great R Squared values.

7.2.2 Liquid level measurement results

The liquid level measurements have been performed during filling and draining water to the container. Some sample graphics is be given in this thesis for interpreting the results. Fiorexample in the graphs below, red line represents the pressure transducer, while the blue line represents the WGM resonance shifts, similarly as shown in the air pressure measurements earlier.

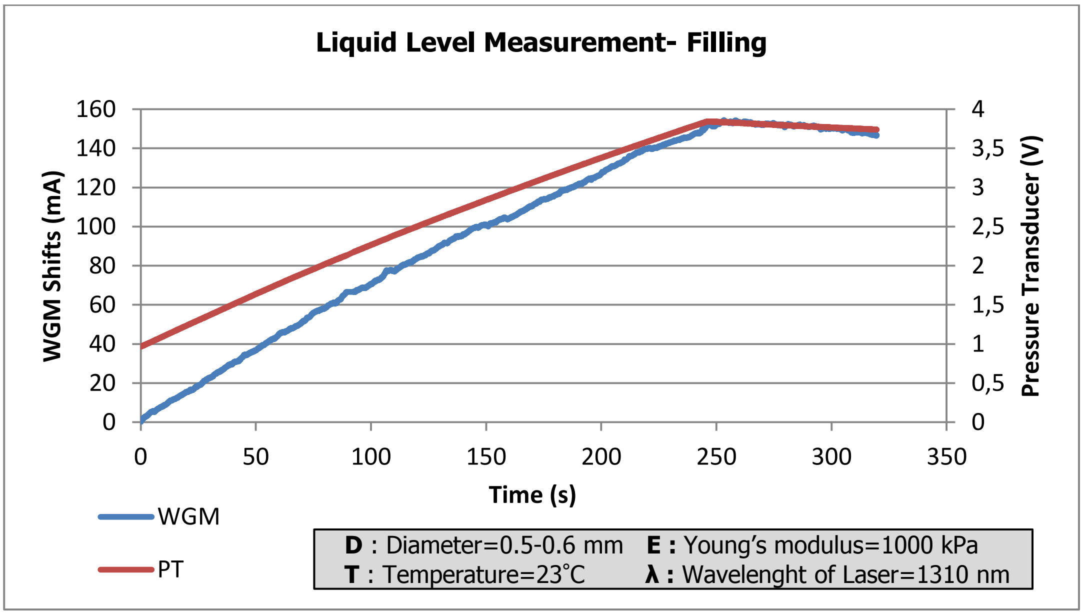

Figure 7.5 : Liquid Level Measurements – Fillling.

In the figure above, either the pressure transducer signal or the sensor signal is not already converted, which demonstrates the raw data obtained from the software during filling the container with water.

Later sensor signal, representing the WGM shifts has been converted into pm scale, while the Pressure Transducer representing the reference signal has been converted into liquid levels in mm scale. Therefore after these conversions, the relationship between the WGM shifts of the sensor signal in pm scale and liquid levels in mm scale can be visualized as shown below in the figures.

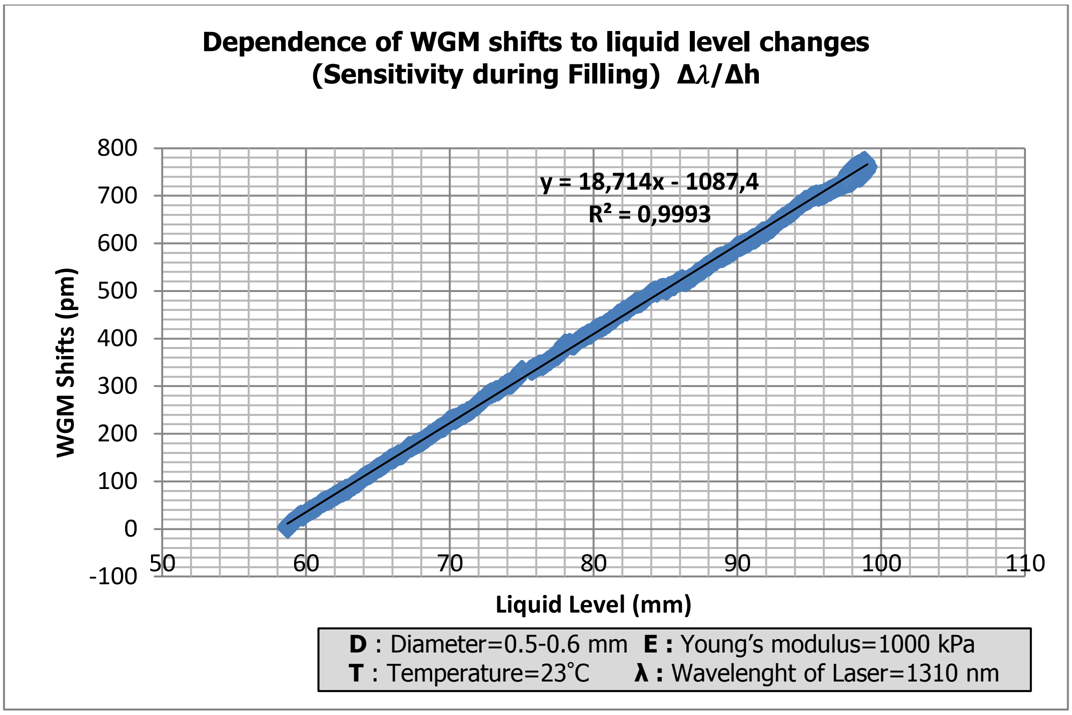

Figure 7.6 : The dependence of WGM shifts to liquid level changes (mm).

The liquid levels can easily be converted to Pa, with the basic conversion ratio of 9,8065 Pa/mmH_2O as follows:

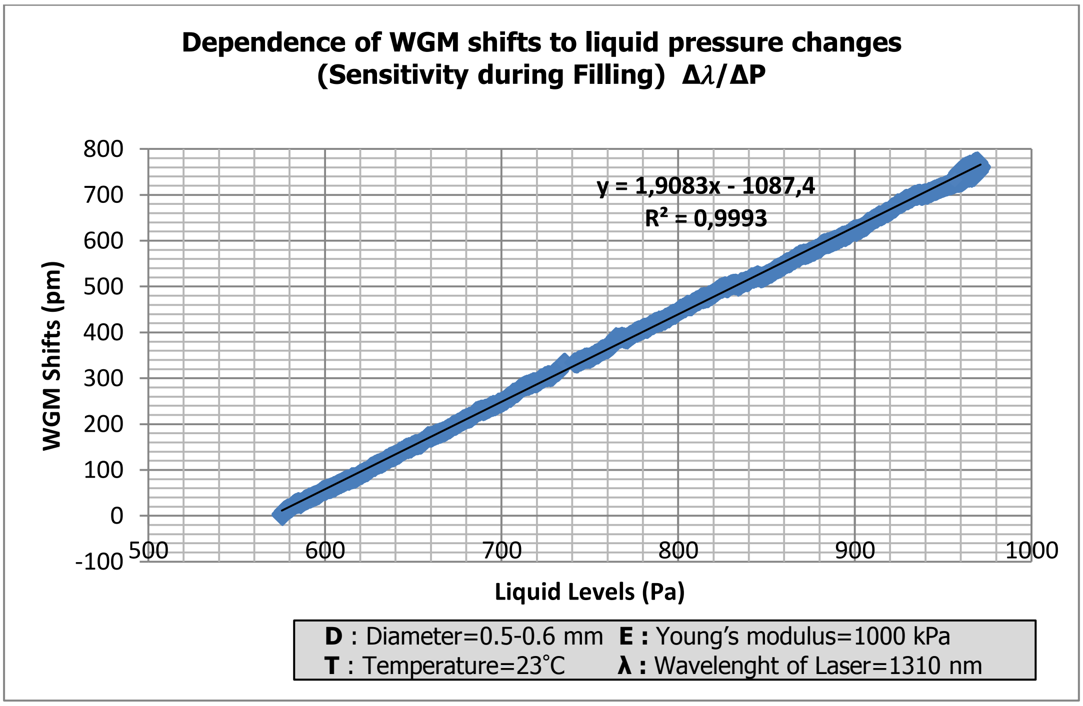

Figure 7.7 : The dependence of WGM shifts to liquid pressure changes (Pa).

In the graph above, WGM shifts demonstrate a linear response with no discernible hysteresis in the pressure range tested, thus providing a reliable pressure reading essential for sensor performance. The corresponding resonance shift as a function of applied pressure is plotted above.

The worst sensitivity dependence of the sensor obtained in liquid level measurements during filling the container with water has been presented above. In the graph, Y axis represents the resonance shifts in pm scale, while X axis represents the liquid levels in the container both in mm and Pa scales. Therefore the linear dependence of WGM shifts due to liquid levels can be observed.

The best sensitivity dependence has been observed during draining water, as expected due to the smoother level change characteristics of draining. Therefore the dependence of WGM shifts to liquid levels changes is better, in other words higher sensitivities has been obtained during draining.

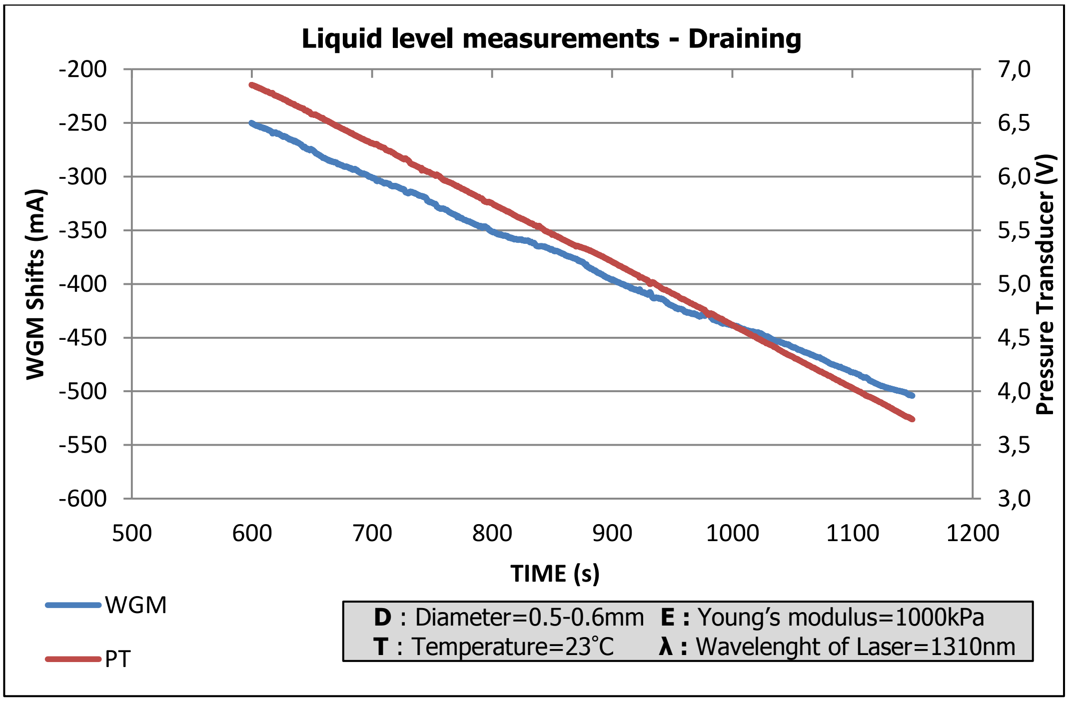

Figure 7.8 : Liquid level measurements during draining water.

The red line represents the pressure transducer, while the blue line represents the WGM resonance shifts.

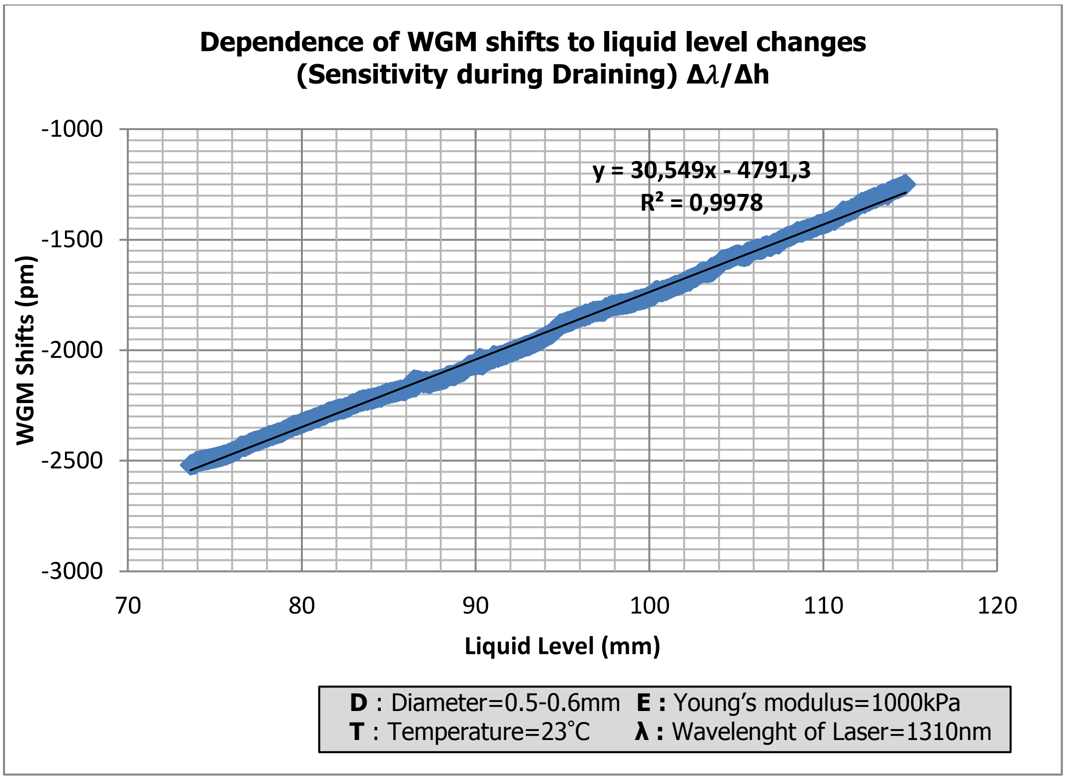

Figure 7.9 : The Dependence of WGM shifts to liquid level changes (mm).

Again, the liquid levels have been converted to Pa (1mmH_2O=9,8065 Pa) as follows:

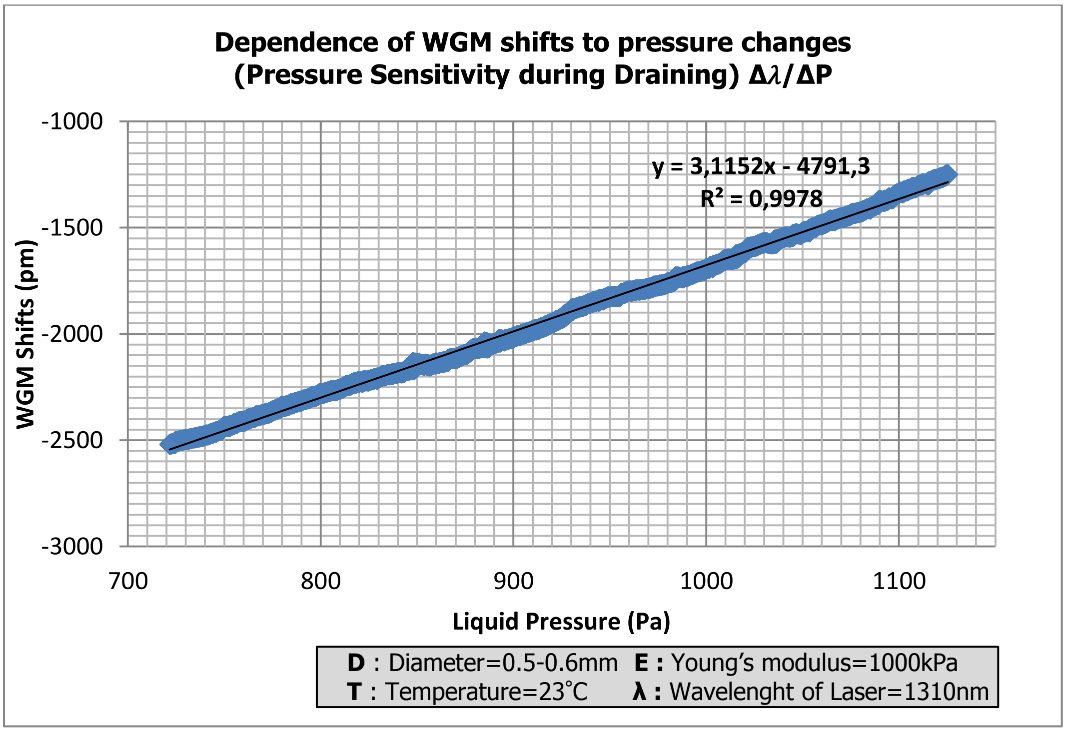

Figure 7.10 : The Dependence of WGM shifts to Liquid Pressure changes (Pa).

Y axis represents the resonance shifts in pm scale, while X axis represents the liquid levels in the container in mm scale. Again a nearly perfect (R^2=0,9967) linear dependence of WGM shifts due to liquid levels can be observed during draining water. Therefore it can be seen that for every Pa change, experimenters observe 3,2 pm shift in resonances.

To formulate the sensitivity dependence and resolution as mathematical expressions, because pm/pa value can be defined as sensitivity dependence [4]:

$$\frac{\Delta\lambda}{\Delta P} = S \tag{7.1}$$

By multiplying each sides with λ / λ which does not change the equalty:

$$S \cdot \frac{\lambda}{\lambda} = \frac{\Delta\lambda}{\Delta P} \cdot \frac{\lambda}{\lambda} \tag{7.2}$$

And as one of the inherent optical qualities of micro-sphere resonators is the very large values of $\lambda / \Delta\lambda$ ratios one can obtain. (Here λ is the resonant wavelength and $\Delta\lambda$ is the width of the resonance wavelength). This ratio is called the "Quality Factor" (or Q-factor). Therefore:

$$S = \frac{1}{Q} \cdot \frac{\lambda}{\Delta P} \tag{7.3}$$

The equation defining the resolution of the sensor becomes:

$$\Delta P = \frac{1}{Q} \cdot \frac{\lambda}{S} \tag{7.4}$$

Where Q is the Quality factor, S is the sensitivity (Dependence of WGM shifts to Liquid Level Changes) of the sensor, ΔP can be accepted as the Resolution (Resolution), and λ is the laser's wavelength.

In this case, the laser wavelength is 1310 nm, quality factor can vary between 10^6 and 10^7 according to previous studies [4], and the dependence of WGM shifts to Liquid leves vary according to different measurements and usage of different sensors. By using the formula above, it might be might be estimated to have a wide range of pressure resolutions varying between 0,04Pa to 0,9 Pa for different measurements, when the spheres used with Q factors between 10^7 and 10^6. But other than the calculated resolution values, the experiments always shows a strong correlation between WGM shifts and Liquid levels.

Therefore for when the X and Y axis switches sides, the graphs give a better idea about the resolution without including the effect of Q factor, directly the dependence of liquid levels per mm to WGM shifts (pm).

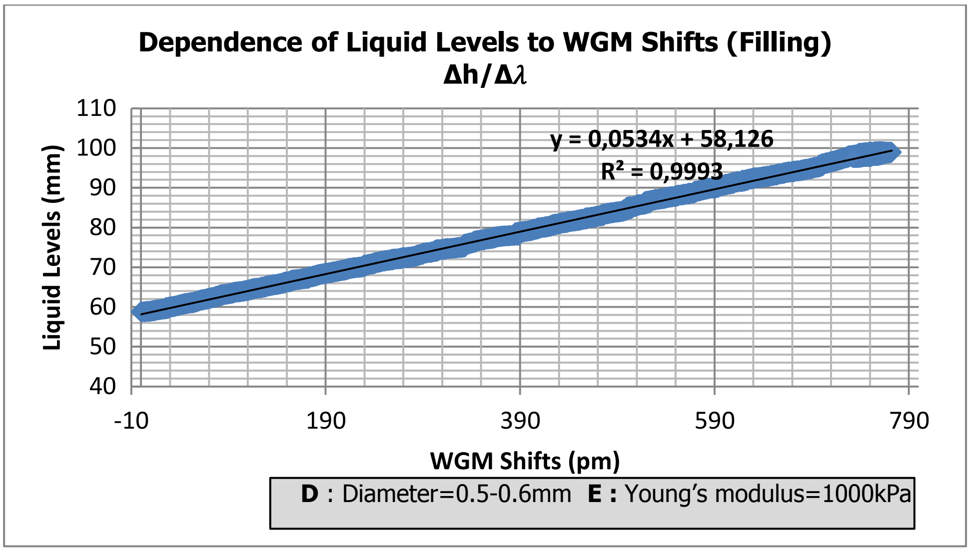

Figure 7.11 : The Dependence of Liquid Levels to WGM shifts (Filling).

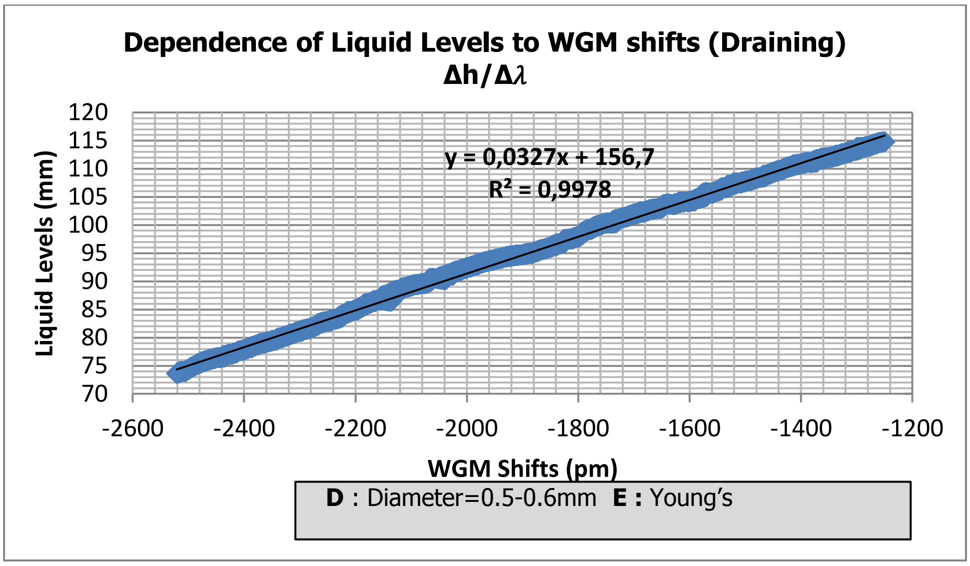

Figure 7.12 : The Dependence of Liquid Levels to WGM shifts (Draining).

As shown in the graphs above, there is a strong correlation between WGM shifts and the Liquid levels. The resonance shifts appear as a function of liquid levels with a linear response with no discernible hysteresis in the pressure range tested.

7.2.3 Accuracy and uncertainity

In engineering and science, the accuracy of a measurement system has been defined as the degree of closeness of measurements of a quantity to that quantity's true value [62,21].

It is considered, measurements made by calibrated instruments for which all known systematic errors have been removed. However, even the most carefully calibrated instruments will have errors associated with the measurements [29].

Error is the difference between the experimentally determined value and the true value, therefore accuracy increases as error approaches zero. In practice, the true values of measured quantities are rarely known, thus an error should be estimated, where this estimation is called uncertainity [4].

$$w_R = \left[\left(\frac{\partial R}{\partial x_1} w_1 \right)^2 + \left(\frac{\partial R}{\partial x_2} w_2 \right)^2 + ... + \left(\frac{\partial R}{\partial x_n} w_n \right)^2 \right]^{1/2} \qquad \textbf{(7.9)}$$

According to this formula [9], error in the resulting value is the result of errors in the variables. When neglecting the errors of the devices such as laser source, laser diode controller, function generator, DAQ card, computer, photodiodes, and the fibers, the accuracy measurement can ben derived by using the sensitivity value obtained at the end of the experiments. The sensitivity dependence has been already defined as $\frac{\Delta\lambda}{\Delta P} = S$, therefore the uncertainity error value of S becomes:

$$w_S = \left[\left(\frac{\delta S}{\delta \Delta\lambda} w_{\Delta\lambda} \right)^2 + \left(\frac{\delta S}{\delta \Delta P} w_{\Delta P} \right)^2 \right]^{1/2} \qquad \textbf{(7.10)}$$

By deriving each term:

$$\frac{\delta S}{\delta \Delta\lambda} = \frac{1}{\Delta P} \text{ and } \frac{\delta S}{\delta \Delta P} = \frac{-\Delta\lambda}{(\Delta P)^2} \qquad \textbf{(7.11)}$$

and , as a result:

$$w_S = \left[\left(\frac{1}{\Delta P} w_{\Delta\lambda} \right)^2 + \left(\frac{-\Delta\lambda}{(\Delta P)^2} w_{\Delta P} \right)^2 \right]^{1/2} \qquad \textbf{(7.12)}$$

can be evaluated.

In this equation the accuracy of pressure transducer is known as ±1,0%, so $w_{PT} = w_{DV_Filling} = 2{,}845$V x 0,01=0,0285V, and $w_{PT} = w_{DV_Draining} = 3{,}079$V x 0,01=0,03079V which gives an idea about $w_{\Delta P}$ value, but adding the error coming from the liquid level reading as 0,5mm/300mm=±0,166%, $w_{Ruler\,Reading} = w_{SC} = w_{SlopeOfConversion_Filling} = 39{,}668$mm x 0,00166=0,065mm, and $w_{Ruler\,Reading} = w_{SC} = w_{SlopeOfConversion_Draining} = 40{,}94$mm x 0,00166=0,0679mm thus the error or uncertainity term of the resonance shifts tracking should be obtained by 14 bit DAQ card where seven step software tracking algorithm.takes place, resulting a certainity of 2^{14} means an error of

$$\sum_{n=7} \frac{1}{2^{14}} = \frac{7}{16384} = \pm 0{,}043\%.,$$

where uncertainity value becomes:

$$w_{\Delta\lambda\_Filling} = (761{,}85 - 0{,}228)x\frac{7}{16384} = 0{,}325\text{pm}$$

$$w_{\Delta\lambda\_Draning} = (2515{,}55 - 1249{,}50)x\frac{7}{16384} = 0{,}541\text{pm}$$

When taking the results of the latest experiment during filling having ${\Delta\lambda}/{\Delta P} = 1{,}9083\ pm/Pa$, and during draining ${\Delta\lambda}/{\Delta P} = 3{,}115\ pm/Pa$ for finding the $W_{\Delta P}$, the uncertainities of the reading and pressure transducer should be calculated as one:

$P = \rho h$ and by differantiating both sides: $\Delta P = (\rho.g).\Delta h$ where ρ is the Density, and g is the Acceleration of Gravity, which both are constant.

$$\frac{\delta\Delta h}{\delta Sc} = \Delta V \text{ and } \frac{\delta\Delta h}{\delta\Delta V} = Sc, \text{ therefore: } w_{\Delta h} = \left[(\Delta V \cdot w_{Sc})^2 + (Sc \cdot w_{\Delta V})^2\right]^{1/2}$$

Because $\Delta P = \rho g.\Delta h$, $w_{\Delta P} = \left[(\rho g \cdot w_{\Delta h})^2\right]^{1/2}$

$$w_{\Delta P} = \left[(\rho g \cdot \Delta V \cdot w_{Sc})^2 + (\rho g \cdot Sc \cdot w_{\Delta V})^2\right]^{1/2}$$

$$w_{\Delta P\_Filling} = \left[(9{,}80 \cdot 2{,}845 \cdot 0{,}065)^2 + (9{,}80 \cdot 14{,}013 \cdot 0{,}0285)^2\right]^{1/2} = 4{,}31Pa$$

$$w_{\Delta P\_Draining} = \left[(9{,}80 \cdot 3{,}079 \cdot 0{,}0679)^2 + (9{,}80 \cdot 13{,}204 \cdot 0{,}03079)^2\right]^{1/2} = 4{,}48 Pa$$

in other words an uncertainity level of ±1,10% for filling, and ±1,11% for draining.

When this equation is used in the Formula 7.12:

$$w_S = \left[\left(\frac{1}{\Delta P} w_{\Delta\lambda}\right)^2 + \left(\frac{-\Delta\lambda}{(\Delta P)^2} w_{\Delta P}\right)^2\right]^{1/2}$$

$$w_{S\_Filling} = \left[\left(\frac{1}{389{,}047} \cdot 0{,}325\right)^2 + \left(\frac{761{,}622}{(389{,}047)^2} 4{,}31\right)^2\right]^{1/2} = 0{,}0217 \, {}^{pm}\!/_{Pa}$$

$$w_{S\_Draining} = \left[\left(\frac{1}{401{,}882} \cdot 0{,}541\right)^2 + \left(\frac{-1266{,}05}{(401{,}882)^2} 4{,}48\right)^2\right]^{1/2} = 0{,}0351 \, {}^{pm}\!/_{Pa}$$

resulting a total error or in other words uncertainity of ±1,137% for filling, and ±1,126% for draining.

In general it can be said that resulting dependence of WGM shifts to liquid pressure change is a function of resonance shifts tracking, Voltage to Liquid level conversion, and Pressure transducer signal as follows:

$$\Delta\lambda/_{\Delta P} = \mathrm{F}(\Delta\lambda, Sc, DV) \quad \textbf{(7.13)}$$

Therefore, the latest experiment during draining water with $\boldsymbol{\Delta\lambda}/_{\boldsymbol{\Delta P}}$ value of 3,115 pm/Pa, resulting an uncertainty of ±1,126%, while during filling water with $\boldsymbol{\Delta\lambda}/_{\boldsymbol{\Delta P}}$ value of 1,9083 pm/Pa, resulting an uncertainty of ±1,137%.

8. CONCLUSIONS

In this work a novel liquid level sensor has been developed. It has been estimated to reach sensitivities as high as 5,93 pm/Pa for the air pressure measurements. In the liquid level measurements, values reaching 2,19 pm/Pa have been obtained diring filling the container, and values as high as 3,12 pm/Pa have been obtained during draining. When stating these values, it should be noted that there is a nearly perfect linear dependence of WGM shifts to liquid levels or liquid pressure. Because the R^2 values obtained from the data are around 0,9967-0,9993, the correlation of linear relationship between WGM and Pressure values assumed to be perfect. It should also be noted that the linear dependence does not affected by the liquid heights; thus resulting a linear dependence valid within the experimental range.

The dependence of WGM shifts to liquid levels can be assumed perfectly linear, where a Pa change in liquid pressure, results as high as 3,12 pm WGM shifts. As observed during the liquid level experiments, it is estimated that there is 0,033-0,053 mm liquid (water) level change per pm WGM shift of the Laser Spectrum, again with a perfect linear correlation.

As the uncertainity calculations has been performed for liquid level measurements, a total uncertainity value of ±1,126% for draining, and ±1,137% for filling have been obtained. The pressure transducer, which acts as the reference device used in the experiments has ±1,0% accuracy, limits the total value. Any alternative device with better accuracies, would definetely help the future researchers to reach better uncertainity values.

Although the values obtained from the experiments would vary according to the experiment parameters, it has been observed that there is a strong correlation between WGM shifts and liquid levels. Therefore the resonance shifts appear as a function of liquid levels with a linear response in the pressure range tested. This relationship, results a dependence of WGM shifts to pressure changes as high as 3,12 pm/PA, which appears with a linear correlation of R^2=0,9978.

Due to the ruggedness of the newly developed sensor, which uses laser optics technology, it can work in any environment without being affected by the availability of flammable liquids and gasses etc. Thus, this novel liquid level sensor has a wide range of applications including automotive, aerospace & aviation industries, medicine, defense, civil engineering, and many other fields all around the globe.

9. DISCUSSION AND FUTURE WORK

As indicated in the experimental results, by using PDMS microspheres with base-to-curing agent volume ratio of 10:1, a very high linear dependence of WGM shifts to liquid levels can be achieved. Each geometry and material for building the microspheres has different measurement ranges, therefore for a given sphere material; although the level of applied force must stay within the elastic deformation range, different sensitivity values can be achieved according to the composition of the material and the diameter of the sphere. Therefore many different kinds of sensors can be build by using the same design, just by changing the resonator shape, size and material, resulting totally different sensitivities.

For example a base-to-curing agent volume ratio of 60:1 can help to obtain higher sensitivity values, in other words, enables the sensor to detect even lower values by means of force as mm of liquid height, while decreasing the measurement ranges, especially lowering the upper boundary because of the material's lower elasticity modulus.

Also as seen in some other studies, hollow spheres can be produced and used in the same design but with greater sensitivity. The hollow sphere resonators can detect the changes in the surrounding medium directly with greater sensitivities; and many other changes can be made to the current design for different purposes.

It has been considered that measurements have been performed with calibrated instruments like laser source, function generator, DAQ card, etc. all known systematic errors have been removed. Although when the issue of accuracy and error calculations arise, it can be said that the reference signal device in the experiments, which is the pressure transducer with ±1,0% accuracy, limits the minimum accuracy of the sensor measurements. The combined accuracy value reaches ±1,126% for draining, and ±1,137% for filling, therefore most of the error seems to come from the pressure transducer. Although this fact, the sensor showed a highly sensitive behavior reaching values of 3,12 pm/Pa, and was capable of detecting any small steam of air during the door openings in the lab, or just whistling through the sensor. Therefore it can be advised that, experiments in the future should be continued with different kinds of equipments with higher accuracy.

It has been shown that, the dependence of WGM shifts to liquid levels is always linear with very high R^2 values, so is not affected by the liquid heights; and is valid through the experimental range. But it should be evaluted that, what happens when a demand for using different liquids arise.

Liquids with higher densities, would definetely lead to higher deformations on the sphere resonators. Therefore when measuring the levels of a liquid with higher density, even higher sensitivity values or higher WGM shift values should be obtained for the same liquid height differences, with the same sensor design. As an example, when using an oil with higher density, the sensor would detect even lower liquid level height differences, and as a result give larger WGM shifts to same liquid level differences, when compared to the current experiments performed under water.

The microshere resonators used in the experiments, should be in elastic deformation range to obtain WGM shifts as expected. If the liquid density becomes too high, or the expected measurement range gets too wide resulting the sphere resonators pass beyond the elastic deformation region, a microsphere with a higher elasticity modulus should be used.

On the other hand, to be able to detect the same level differences with a low density liquid like alcohol, either the sphere should be hollow, or the material should be selected with a lower leasticity modulus. If the sphere remains the same, despite the loss in sensitivity, the measurement limits will be widened allowing to make measurements with a borader range.

Another important part of this novel sensor is the elastic membrane, which transfers the outside pressure on to the microsphere without leaking any fluid or gas inside. The elasticity of this membrane has a critical importance. For example, if stiffer materials with higher elasticity modulus such as thin metal sheets, or stiffer plastics used instead of latex, the microspheres will have the same deformations, but this time under much more higher loads. In other words when the stiffness of the membrane material increases, the sensor becomes less sensitive for low pressures, nevertheless it will be suitable for the measurement of higher pressure values. Therefore by changing the material of the membrane, the sensor can be used under very high loads, such as underwater applications like submarines, or even in civil engineering.

Although there was no distinguishing effects of the flow rate in a controlled medium, it has been observed that the novel sensor due to its sensitivity, can be affected by the vibrations and turbulance caused by high flow rates. For this aim, when measurements are required under turbulance, the usage of stiffer membranes will be helpful, but by loosing some part of the micro scale sensitivity.

For widening the application range, vibration effects should be added to the future experiment setups, which will help the researchers to differentiate the vibrations of the surrounding medium out of sensor signals, and help to modify the sensor for harsh environmental conditions without loosing it’s sensitivity.

Another significant advantage of this novel sensor is that, there is no threshold value for this sensor, which it starts measuring instantly and directly from ground zero.

As expressed in this study, spark free characteristics and exceptional sensitivity will lead the novel liquid level sensor to achieve greater success in many areas. With further improvements, it will take its place in automotive, aeronautics and space industries, civil and naval engineering, conventional and renewable energy systems, advanced medicine, Nano-robotics and many more.

REFERENCES

[1] **Adamovsky G., Ötügen V.,** (2008). Morphology-Dependent Resonances and Their Applications to Sensing in Aerospace Environments, *J. Aerosp. Comp.* Comm. & Info, Vol. **5**, pp. 409-424.

[2] **Aiyer R. C., Karekar R.C., Kulkarni, A., (**2005). Liquid Level Sensor, *Review of Scientific Instruments*, Vol. **26**, pp.105-108.

[3] **Ayaz U.K., Ioppolo T., Ötügen M.V.,** (2009). Tuning of whispering gallery modes of spherical resonators using an external electric field, *Optics Express*, Vol. **17**, 19, pp. 16465-16479.

[4] **Ayaz U.K., Ioppolo T., Ötügen M.V.,** (2009) . High Resolution Force Sensor Based on Morphology Dependent Optical Resonators Polymeric Spheres, *J. Appl. Physics*, Vol. **105**, 013535.

[5] **Bottacini M., Burani N., Foroni M., Poli F., Selleri S.**, (2005). All-plastic optical fiber level sensor, *Microwave and Optical Technology Letters*, Vol. **38**. no.6, pp. 520 -522.

[6] **Datta P., Kanak C.S., Nath P.,** (2007) . All Fiber-Optic Sensor For Liquid Level Measurement, *Microwave and Optical Technology Letters*, Vol. 50. no.7, pp. 1982 -1984.

[7] **Erdem M. E., and Güneş D.,** (2011). Liquid Level Sensor in Automotive Design, the Fifth International Conference on Sensor Technologies and Applications: SENSORCOMM 2011

[8] **Fleming W.J., (**2001). Overview of Automotive Sensors, *IEEE Sensors Journal*, Vol. **1**, no. 4, December 2001.

[9] **Geceli O.** (1998). *Ölçme Tekniği*, Birsen yayınevi, ISBN 975-511-113-1, Istanbul.

[10] **Haugen E.D., Hongerholt D.D., Huss C.G., Seidel G.A.,** (2001). Ultrasonic Technology For Non Intrusive Level Measurement On Commercial Aircraft, *Review Of Progress In Quantitative Nondestructive Evaluation*, Vol. **20**.

[11] **Hodges D.Y., Mazel D.S., Zuckerwar A. J.,** (1986). Ultrasonic Level Sensor For Liquids Under High Pressure, *Review of Scientific Instruments*, Vol. **57**, no 9.

[12] **llchenko V.S., Maleki L., Yao X.S.,** (1999). Pigtailing the High-Q Microsphere Cavity: A Simple Fiber Coupler for Optical Whispering-Gallery Modes, *Optics Letters*, Vol. **24**, pp.723–725.

[13] **Ioppolo T., Ötügen M.V.,** (2007). Pressure Tuning of Whispering Gallery Mode Resonators, *Applied Optics*, Vol. **47**, no. 16, pp.3009-3014.

[14] **Ioppolo T., Kozhevnikov M., Ötügen M. V., Sheverev V., Stepaniuk V.,** (2008) . A Micro-Optical Force Sensor Concept Based on Whispering Gallery Mode Resonators, *Appl. Optics*, Vol. **47** , 3009.

[15] **Ioppolo T., Marcis K., Ötügen M.V.,** (2010) . Magnetic Field-Induced Excitation and Optical Detection of Mechanical Modes of Micro-Spheres, *Journal of Applied Physics*, Vol. **107**.

[16] **Ioppolo T.,** (2011) . Whispering Gallery Mode-Based Micro Optical Sensors for Aerospace Applications, *Ph.D. Thesis*, PolyTechnic University.

[17] **Joshi S.G., Kuznetsov S.A., Kuznetsova I.E., Sakharov V.E., Zaitsev B.D.,** (2003). Liquid Level Sensor Using Ultrasonic Lamb Waves, *Ultrasonics*, Vol. **41** , no .4, pp. 319-322.

[18] **Johnson C. D.,** (2006). Process Control Instrumentation Technology, University of Houston, *Pearson Educational International*, ISBN: 0-13-197669-9, 8th Edition.

[19] **Url-1** *<http://www.ilxlightwave.com/pdfs/3700C_brochure_REV04.pdf>*, date retrieved 29. 11.2011.

[20] **Url-2** < http://www.ece.stevens-tech.edu/BoeschLab/Manpulsegenerators */HP8116-PulseFunctionGenerator/UsersManual-8116A.pdf >*, date retrieved 29.11.2011.

[21] **Url-3** *<http://www.churchsoundcheck.com/resolution2.html>*, date retrieved 04.01.2012.

[22] **Url-4** *<http://www.hella.com/hella-de-de/index.html>*, date retrieved 29.11.2011.

[23] **Url-5** *<http://www.valeo.com>*, date retrieved 29.11.2011.

[24] **Url-6** *<http://en.wikipedia.org/wiki/Modal_analysis_using_FEM>*, date retrieved 29.11.2011.

[25] **Url-7** *<http://www.timkelf.com/Research/ResearchWGM.html>*, date retrieved 10.02.2011.

[26] **Url-8** *<http://en.wikipedia.org/wiki/Fiber_optic_coupler>*, date retrieved 23.04.2011.

[27] **Url-9** *<http://www.sensorsmag.com/sensors/leak-level/a-dozen-ways-measure-fluid-level-and-how-they-work-1067>*, date retrieved

23.04.2011.

[28] **Url-10** <*http://www.engineering.uiowa.edu/~cfd/pdfs/References/uncert.pdf*> , accessed at 23.04.2011.

[29] **Url-11** <*http://www.iceweb.com.au/Technical/level_measurements_info_notes.htm*>, date retrieved 23.04.2011.

[30] **Url-12** <*http://en.wikipedia.org/wiki/Level_sensor*>, date retrieved 26.04.2011.

[31] **Url-13** <*http://www.ni.com/pdf/manuals/372121f.pdf*>. date retrieved 27.04.2011.

[32] **Url-14** <*http:// http://photonics.intec.ugent.be/download/mth_29.pdf* >. date retrieved 01.05.2011.

[33] **Url-15** <*http://www.hella.com/MicroSite/soe/sites/default/files/downloads/J00137_Oelniveausensoren_GB_TT_korr1.pdf*>, date retrieved 01.05.2011.

[34] **Url-16** <*http://www.hella.com/produktion/HellaUSA/WebSite/MiscContent/Download/AutoIndustry/Electronics/TI_Oelsensorik_GB_TT_05.pdf*, date retrieved 01.05.2011.

[35] **Url-17** <*http://www.autoshop101.com/forms/h15.pdf*>, date retrieved 01.05.2011

[36] **Url-18** <*http://en.wikipedia.org/wiki/Polydimethylsiloxane*>, date retrieved at 01.05.2011.

[37] **Url-19** <*http://en.wikipedia.org/wiki/Potentiometer*> date retrieved 01.05.2011.

[38] **Url-20** <*http://www.engineersedge.com/instrumentation/differential_pressure_level_detector.ht m* > date retrieved 01.05.2011.

[39] **Url-21** <*http://openticle.com/2007/12/09/level-detectors-conductivity-probe-method/* >, date retrieved 01.05.2011.

[40] **Url-22** < *http://www.nnin.org/doc/2005NNINreuTippie.pdf* >, date retrieved 01.05.2011.

[41] **Url-23** <*http://www.photosensor.co.kr/data/bubble.pdf* > date retrieved 01.05.2011.

[42] **Url-24** <*http://trs-new.jpl.nasa.gov/dspace/bitstream/2014/11624/1/02-0152.pdf* > date retrieved 01.05.2011

[43] **Url-25** <*http://ipnpr.jpl.nasa.gov/progress_report/42-162/162D.pdf*>, date retrieved 01.11.2011.

[44] **Url26** *<http://trs-new.jpl.nasa.gov/dspace/bitstream/2014/11624/1/020152. pdf>,* date retrieved 01.11.2011.

[45] **Url-27** < *http://en.wikipedia.org/wiki/Q_factor >,* date retrieved 01.11.2011.

[46] **Url-28** <*http://www.accessengineeringlibrary.com/mghpdf/0071738045_ar013.pdf* > date retrieved t 01.11.2011.

[47] **Url-29** <*http://en.wikipedia.org/wiki/Evanescent_wave>,* date retrieved 01.11.2011.

[48] **Url-30** <*http://www.faculty.iubremen.de/dknipp/c320352/Projects/Presentations%202005/CL%20Evanescent%20Fields.pdf* > date retrieved 01.11.2011.

[49] **Url-31** <*http://www.csir.co.za/lasers/basics_of_lasers.html>,* date retrieved 29.06.2010.

[50] **Url-32** <*http://kestro.com/pdf/Shanghai%20Kestro%20Polychem,%20Inc.-TDS A370P.pdf>,* date retrieved 29.11.2011.

[51] **Url-33** <*http://www.uta.edu/rfmems/Teralum_old/5742.pdf>,* date retrieved 01.11.2011.

[52] **Url-34** <*http://www.omega.com/Pressure/pdf/PX277.pdf>,* date retrieved 14.10.2010.

[53] **Url-35** <*http://arxiv.org/PS_cache/physics/pdf/0509/0509226v1.pdf>,* date retrieved 01.11.2011.

[54] **Url-36** <*http://dl.jbnu.ac.kr/dlsearch/dllocal/LOC/HTML/chonbuk/digital/IEICE/IEICE-TransactionsonElectronics/ieice_ietele_2005_e88-c07/1440.pdf>,* date retrieved 01.11.2011.

[55] **Url-37** < *http://doc.utwente.nl/23822/1/64.pdf*> date retrieved 01.11.2011.

[56] **Url-38** <*http://www.nano-optics.ethz.ch/publications/goetzinger03.pdf*> date retrieved 01.11.2011.

[57] **Url-39** <*http://daedalus.caltech.edu/publication/pubs/1272_ftp.pdf>,* date retrieved 01.11.2011.

[58] **Url-40** <*http://ipnpr.jpl.nasa.gov/progress_report/42-162/162D.pdf>,* date retrieved 01.11.2011.

[59] **Url-41** <*http://spie.org/documents/Newsroom/Imported/0585/0585-2007-02-15.pdf*> date retrieved 01.11.2011.

[60] **Url-42** <*http://books.google.com.tr/books?id=BwistUlpZ7cC&pg=PA316&lpg=PA316&dq=u+tube+liquid+physics&source=bl&ots=7_llgT9MqR&sig=Hy_tj7FlbUMzlU_Cw1gPZiRQtnA&hl=tr&ei=lrbeTr7KK4*

OzhAf7sNikBQ&sa=X&oi=book_result&ct=result&resnum=6&ved=0CGUQ6AEwBQ#v=onepage&q&f=false>, date retrieved 01.11.2011.

[61] **Url-43** < *http://www.ni.com/labview/*> date retrieved 01.11.2011.

[62] **Url-44** <*http://en.wikipedia.org/wiki/Accuracy_and_precision/*>,date retrieved 01.11.2011.

[63] **Url-45** <*http://en.wikipedia.org/wiki/Pressure>*, date retrieved 04.01.2012.

[64] **Url-46** <*http://en.wikipedia.org/wiki/Accuracy_and_precision>*, date retrieved 03.01.2012.

[65] **Url-47** <*http://en.wikipedia.org/wiki/Accuracy_and_precision>*, date retrieved 03.01.2012.

[66] **Url-48** <*http://whatis.techtarget.com/definition/0,,sid9_gci529971,00.html>*, date retrieved 04.01.2012.

[67] **Url-49** <*http://en.wikipedia.org/wiki/Linear*>, date retrieved 04.01.2012.

APPENDICES

APPENDIX A

Table A.1 : OLS_PA66GF35 Material Properties.

OLS-pa66-gf35	isotropic
Mass Density	1.41e-006 kg/mm^3
Young`s Modulus	12000000000 $Pa(N/m^2)$
Poisson`s Ratio	0.4
Yield Strength	200000000 $Pa(N/m^2)$
Ultimate Tensile Strength	150000000 $Pa(N/m^2)$
Thermal Expansion Coefficient	7e-005 1/K
Thermal Conductivity	0.35 W/m-K
Specific Heat	1500 J/kg-K
Plastic Strain Ratio	0.05
Fatigue Strength Coefficient	240 $N/mm^2(MPa)$
Fatigue Strength Exponent	-0.0666
Fatigue Ductility Coefficient	0.1235
Fatigue Ductility Exponent	-0.5502

Table A.2 : CUZN39PB3 Material Properties.

CuZn39Pb3	isotropic
Mass Density	8.46e-006 kg/mm^3
Young`s Modulus	97000 $N/mm^2(MPa)$
Poisson`s Ratio	0.3
Thermal Conductivity	123 W/m-K
Specific Heat	434000000 microJ/kg-K
Fatigue Strength Coefficient	141.91 $N/mm^2(MPa)$
Fatigue Strength Exponent	-0.07048
Fatigue Ductility Coefficient	0.1235
Fatigue Ductility Exponent	-0.5502

Table A.3 : Material Information.

Yield Strenght mN/mm² (kPa)		Ultimate Tensile Strenght mN/mm² (kPa)		Thermal Expansion Coefficient	
Temp.	Y.S.	Temp.	U.T.S.	Temp.	T.E.C.
20	480	20	575.79	20	1.78e-005
21.11	470.89	21.11	562.00	100	1.78e-005
23.89	470.89	23.59	562.00	107.22	1.88e-005
37.78	470.89	37.78	562.00	121.11	1.97e-005
135	470.82	51.67	562.00	135	2.06e-005
148.89	450.14	65.56	562.00	148.89	2.08e-005
162.78	454.45	79.44	562.00	162.78	2.09e-005
176.67	453.75	93.33	562.00	176.67	2.09e-005
190.56	453.07	107.22	562.00		
204.44	453.07	121.11	562.00		
218.33	450.31	135	562.00		
232.22	348.24	148.89	562.00		
246.11	346.17	162.78	562.00		
260	344.10	176.67	562.00		
273.89	341.34	190.56	562.00		
287.78	237.90	204.44	562.00		
301.37	234.45	218.33	562.00		
315.56	231.06	232.22	562.00		
329.44	227.56	246.11	562.00		
343.33	224.11	260	561.31		
357.22	220.67	273.89	560.62		
371.11	217.21	287.78	559.93		
385	213.77	301.67	557.87		
398.89	200.32	315.56	554.42		
412.78	180.15	329.44	549.59		
426.67	180.73	343.33	543.38		
		357.22	500.49		
		371.11	468.90		
		385	420.63		
		398.89	412.36		
		412.78	402.71		
		426.67	343.05		

APPENDIX B

Table B.1 : 1310nm DFB distributed feedback laser w/tec technical specifications [27].

Center Wavelength	1290-1330nm
Output Power	10mW minimum
Laser Linewidth	Less than 10MHz
Side Mode Suppression Ratio	> 45dB in CW, > 30dB (modulated)
Relative Intensity Noise	- 145dB/Hz
TEC Cooled	Yes
Optical Isolator	40dB minimum
Built-in Thermistor	Yes
Internal Bias T Input Impedance	75 Ohm
Modulation Type	Analog
Package Type	14-pin Butterfly
Fiber Type	SMF-28
Connectors	SC/UPC
Operation Temperature Range	-20 to +65˚C

Table B.2 : ILX Light Wave LDC-3724-C laser diode controller technical specifications [19].

Accuracy	0.05%
Operating Temperature	0 - 40.00° C
Stability	20ppm
Experiment temperature	22.99-23.00 C
Power Requirements (50-60Hz)	100-120 VAC (+-10%) 220-240 VAC (+-10%)
Compliance Voltage:	0–10V adjustable
Noise and Ripple- High Bandwidth Mode (rms):	<4μA
Noise and Ripple- Bandwidth Mode (rms)	<2μA
Compliance Voltage Adjust – Accuracy	±2.5%
Compliance Voltage Adjust – Resolution	50mV
Compliance Voltage Adjust – Range	0–10V
Photodiode Current	0–5000μA
Optical Power – Range	0.00–505.00mW

Table B.3 : HP 8116A 50MHz programmable pulse function generator technical specifications [20].

Frequency Range	1.00 mHz to 50.0 MHz
Resolution	3 digits, 10 μHz
Pulse width Range	10 ns tp 999 ms
Pulse width Resolution	3 digits, 100 ps (0.1 ns)
Pulse width Accuracy	±5 % ± 2 ns
Pulse width Jitter	0.2 % + 200 ps (width ≤ 10 μs) 0.1 % (width > 10 μs)

Table B.4 : Function / Arbitrary Waveform Generator 33220A technical specifications [20].

Frequency Range	1 μHz to 20 MHz
Noise Bandwidth	9 MHz typical
Pulse Frequency range	500 μHz to 5 MHz
Arbitrary Frequency Range	1 μHz to 6 MHz
Arbitrary Waveform length	2 to 64 k points
Accuracy	± (10 ppm + 3 pHz) in 90 days ± (20 ppm + 3 pHz) in 1 year
Resolution	1 μHz
Main Output Impedance	50 Ω typical
Main Output Isolation	42 Vpk maximum to earth
Protection	Short-circuit protected, overload automatically disables main output

Table B.5 : BNC Adapter for E/M/S analogue output series technical specifications [31].

BNC Connectors	15
Spring Terminal Block	30 positions
Wire Gauge	28-16 AWG wire
I/O connector	68 pin SCSI male connector
Operating temprature	0-70° C
Storage temperature	- 55 to 125 °C
Relative humidity	5 to 90%, noncondensing
Pollution Degree	2
Maximum altitude	2,000 m

Table B.6 : Omega PX277 differential pressure transducer technical specifications [52].

Excitation	12 to 35 Vdc
Output	0 to 5 or 0 to 10 Vdc selectable
Accuracy	±1.0% FS
Operating Temperature	-18 to 80°C
Compensated Temperature	-4 to 65°C
Thermal Effects	0.02% FS/°C
Proof Pressure	10 psi
Termination	Screw terminal block
Enclosure	Enamel coated, 18 GA steel

APPENDIX C

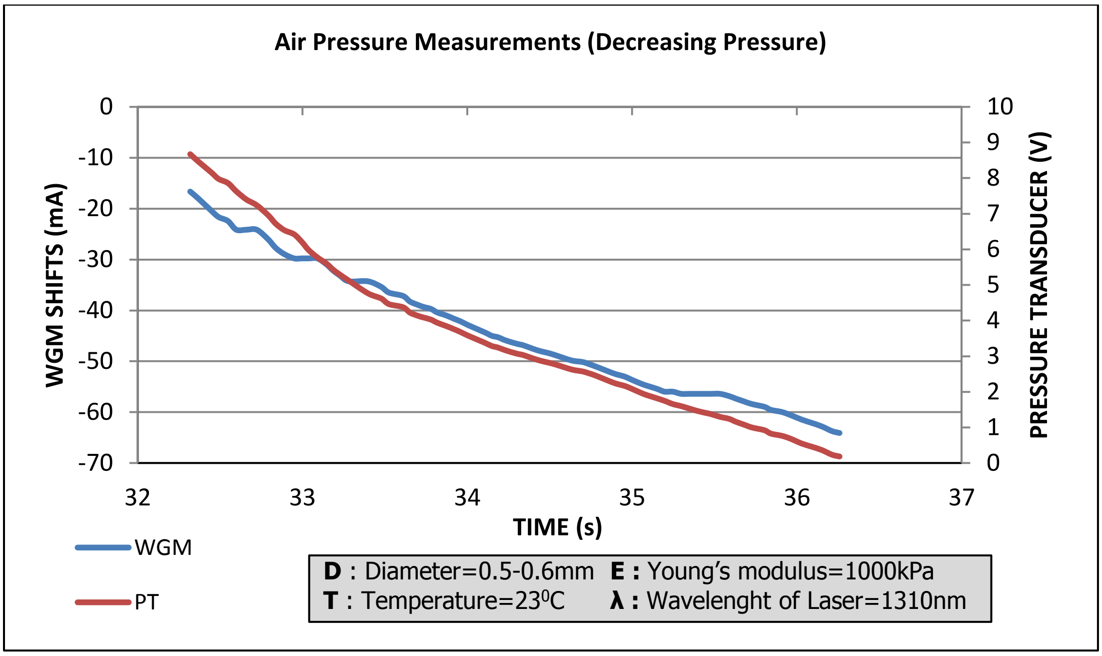

Figure C.1 : Air Pressure Measurements (1).

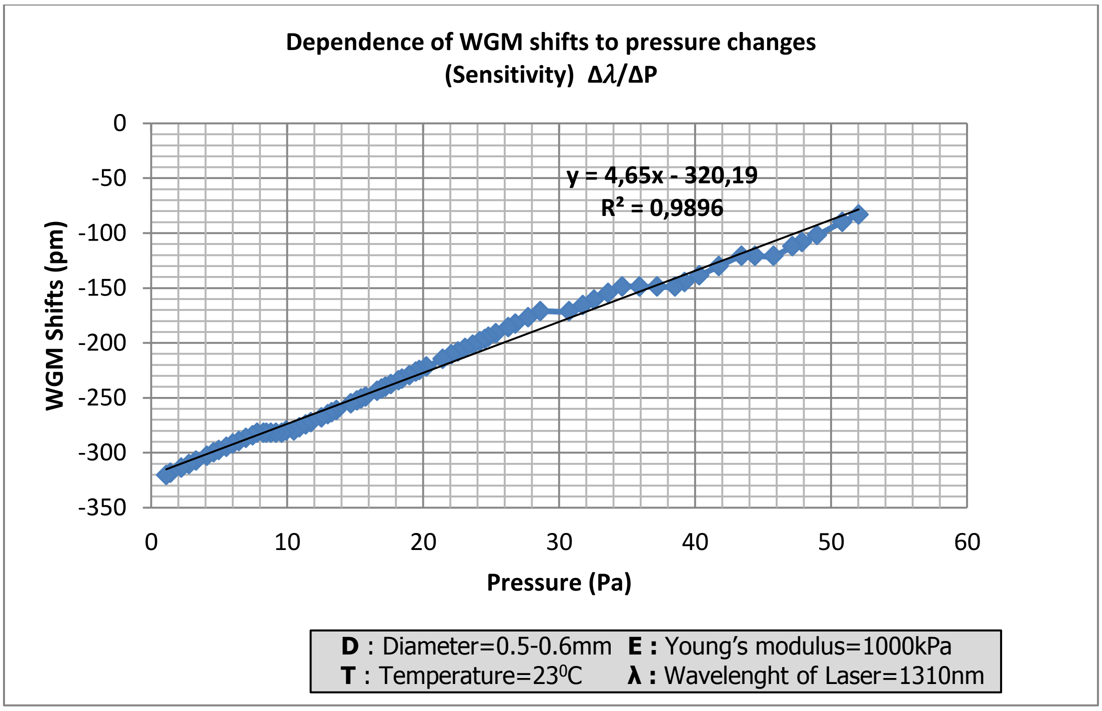

Figure C.2 : The dependence of WGM shifts to pressure changes (1).

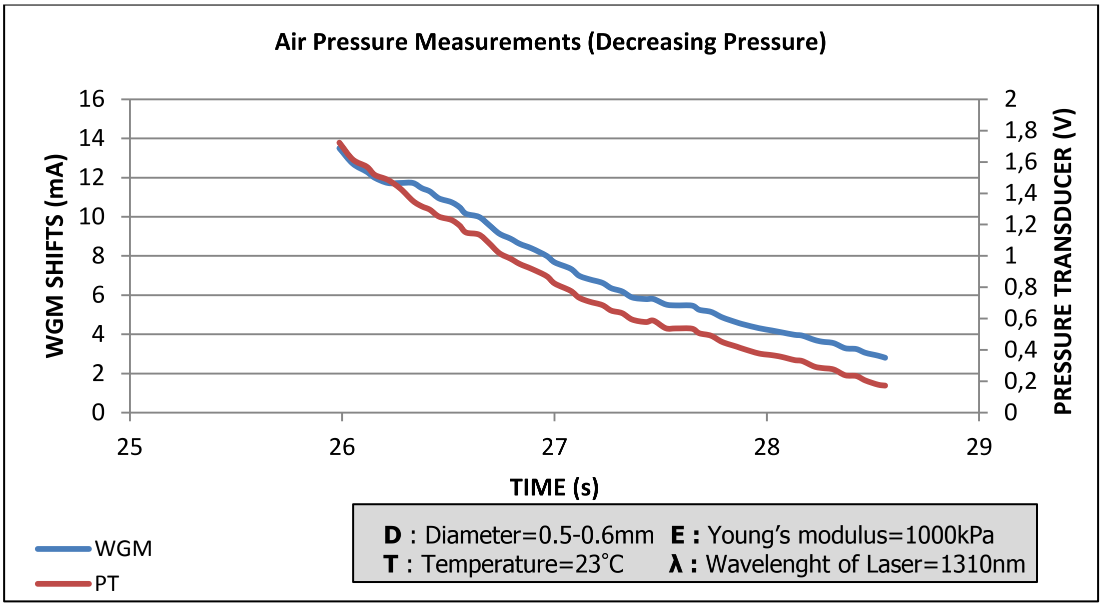

Figure C.3 : Air Pressure Measurements (2).

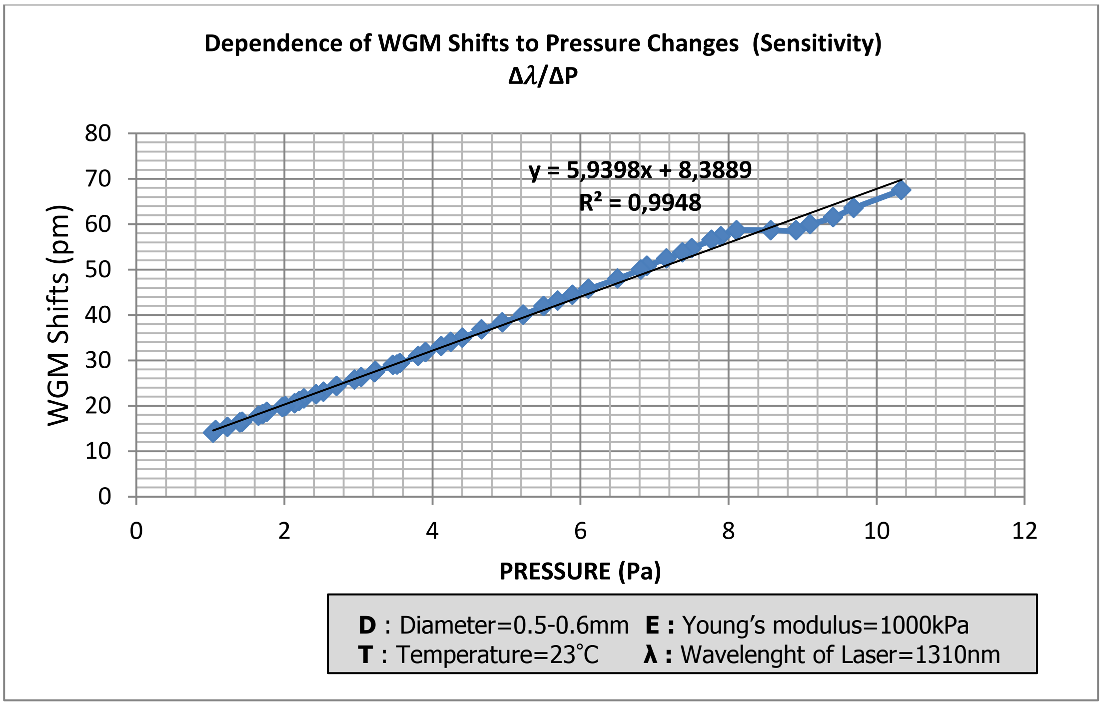

Figure C.4 : The dependence of WGM shifts to pressure changes (2).

APPENDIX D

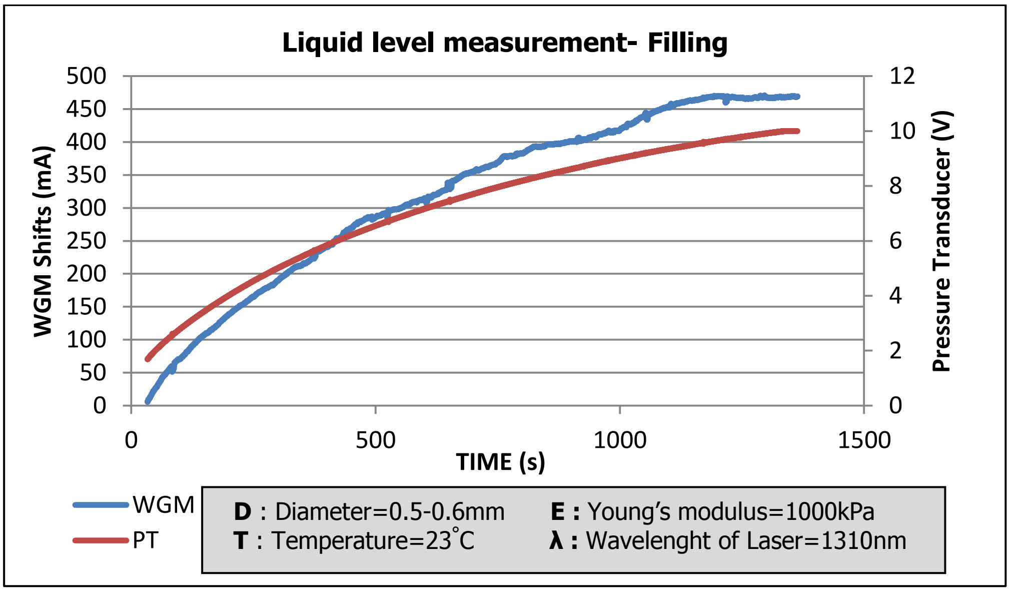

Figure D.1 : Liquid level measurement during increasing water levels (1)

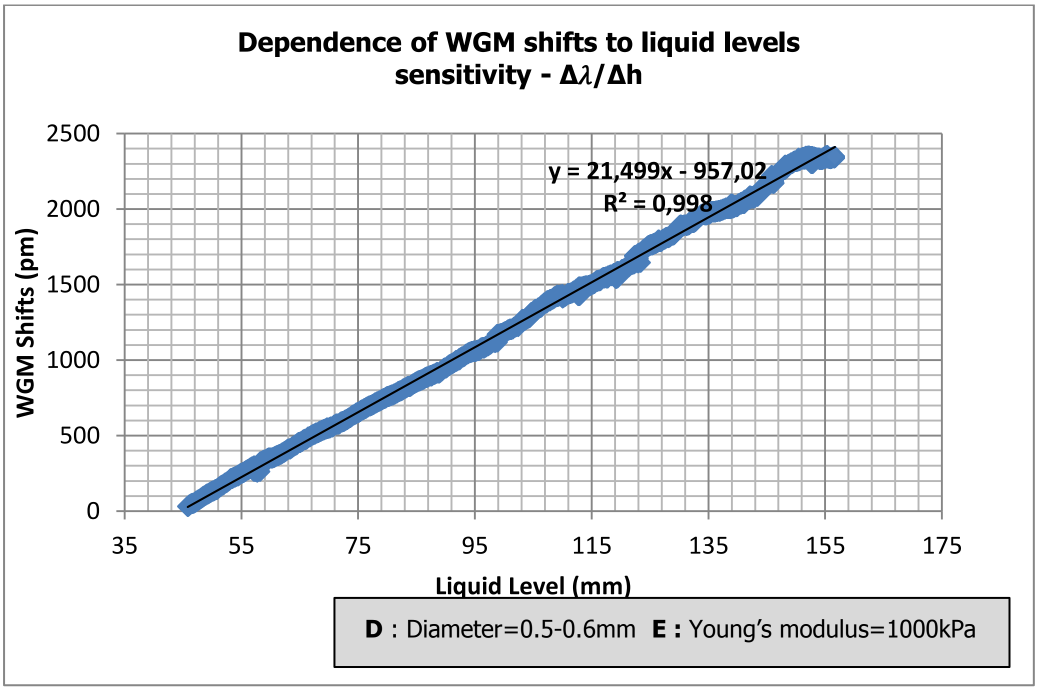

Figure D.2 : The sensitivity dependence of WGM shifts to liquid level measurements (1).

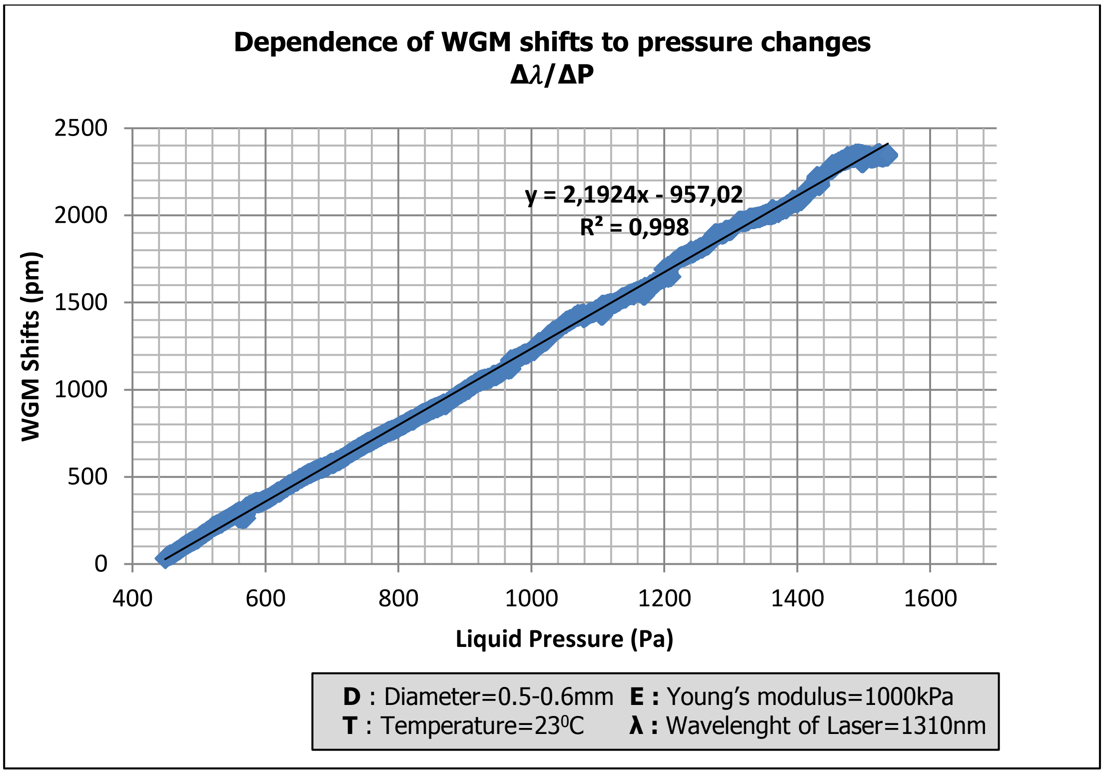

Figure D.3 : The dependence of WGM shifts to pressure changes (1).

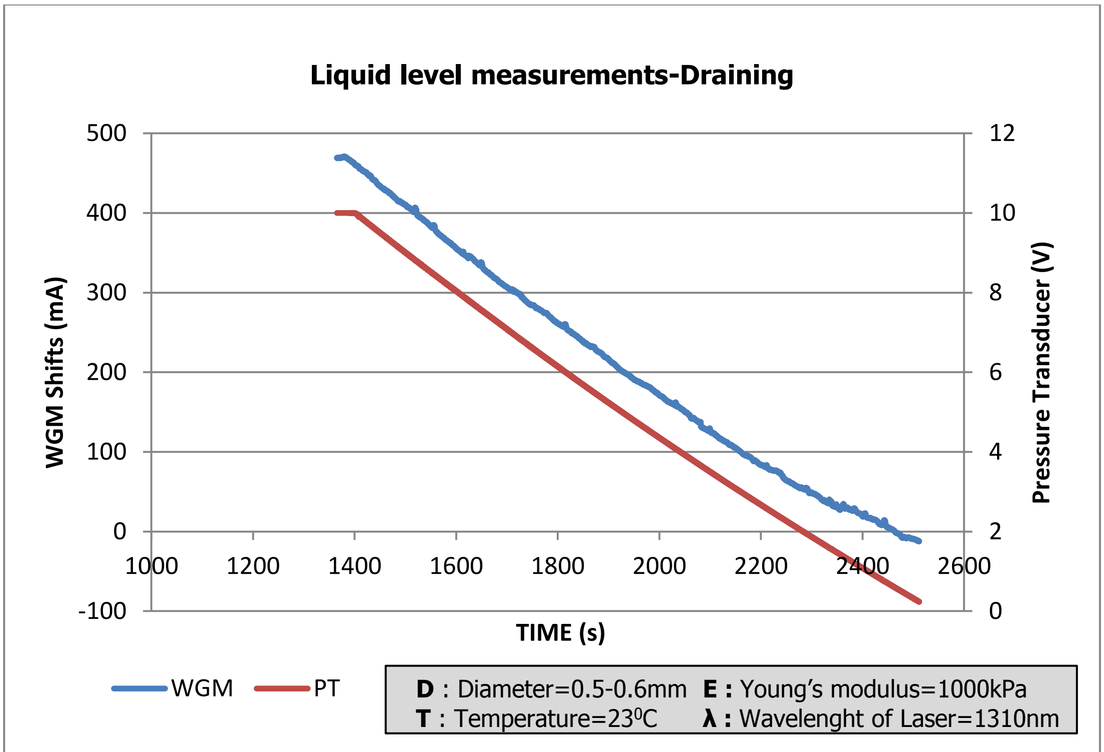

Figure D.4 : Liquid level measurement during draining water (2).

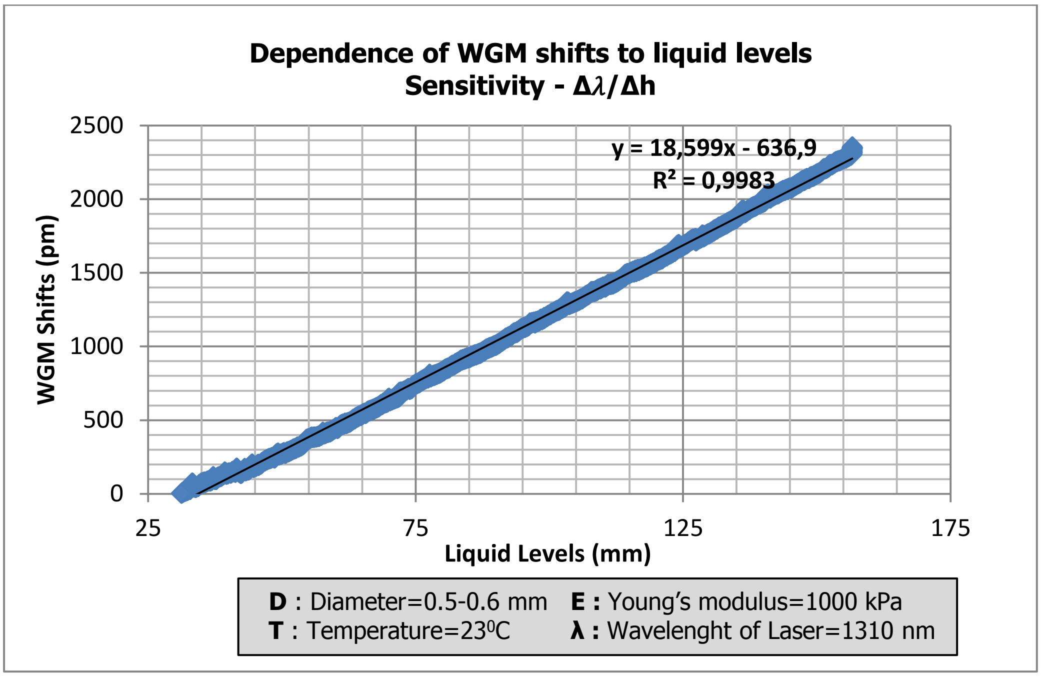

Figure D.5 : The sensitivity dependence of wgm shifts to liquid level measurements (2) .

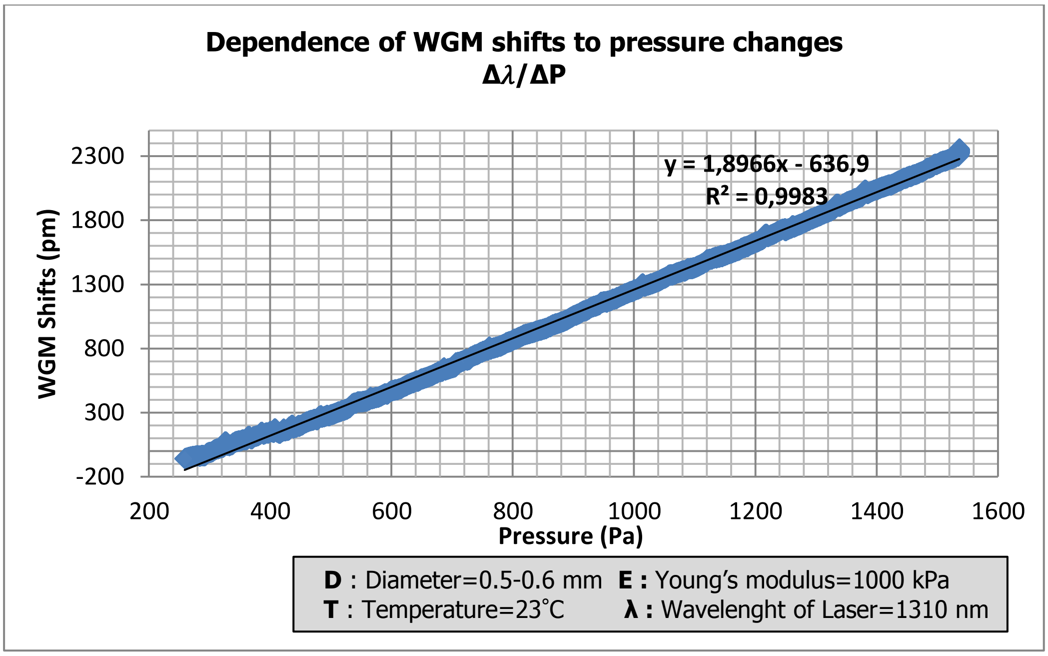

Figure D.6 : The dependence of WGM shifts to pressure changes (2).

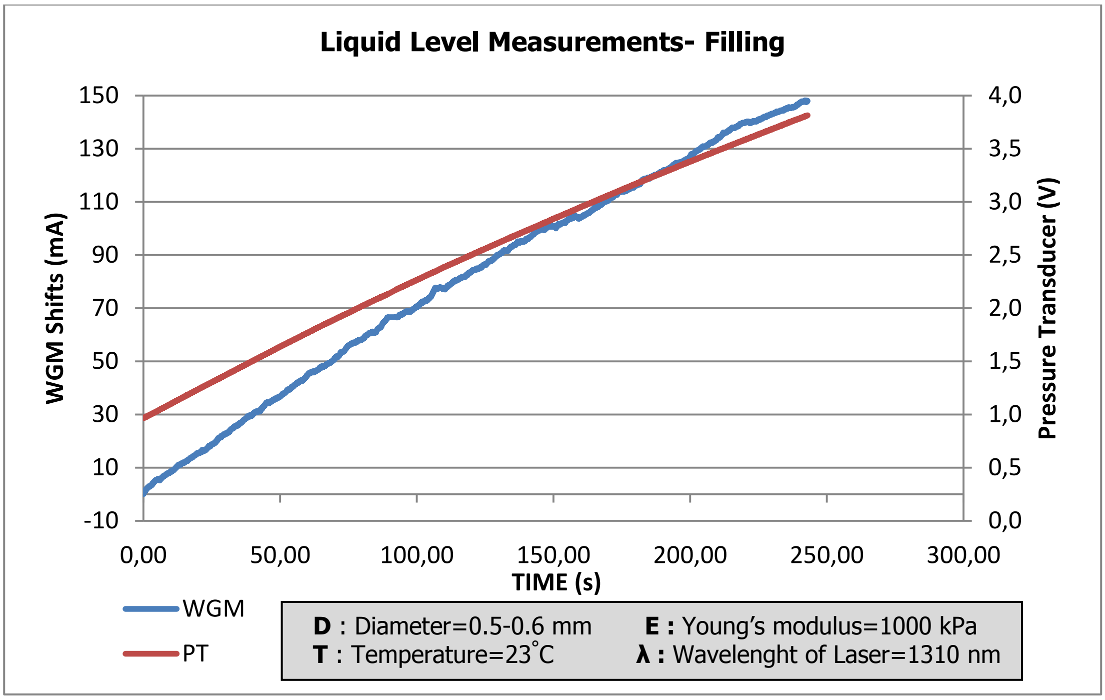

Figure D.7 : Liquid level measurement - Filling (3).

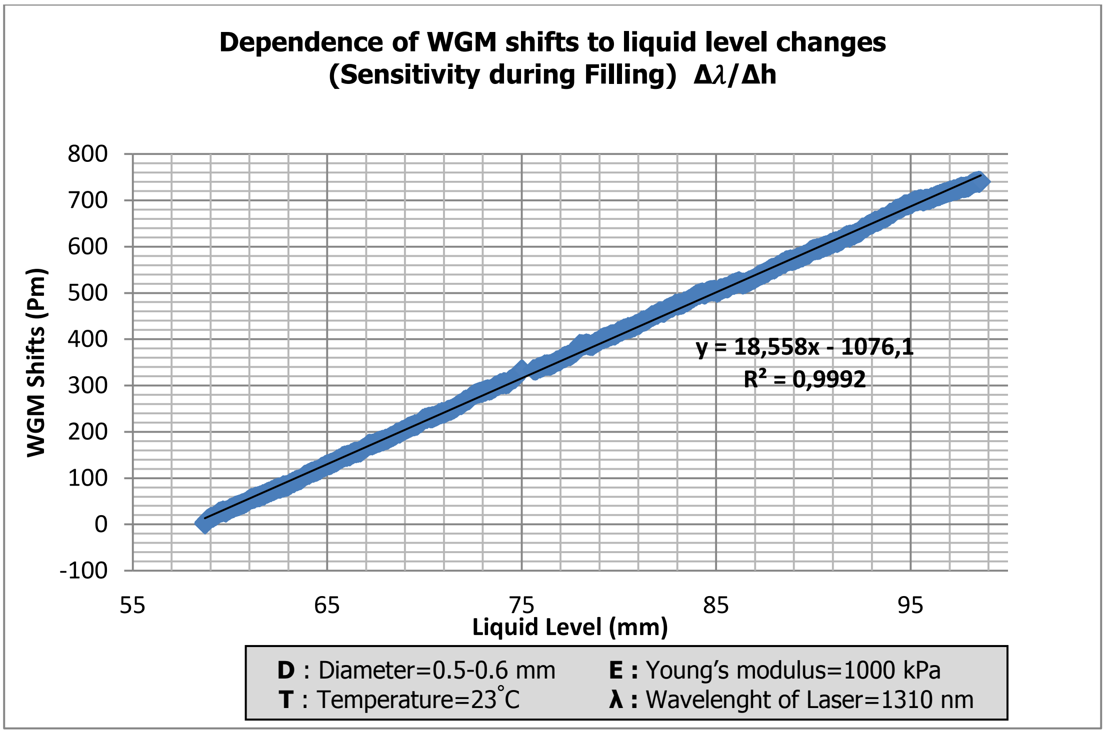

Figure D.8 : The dependence of WGM Shifts to Liquid Level Changes (3).

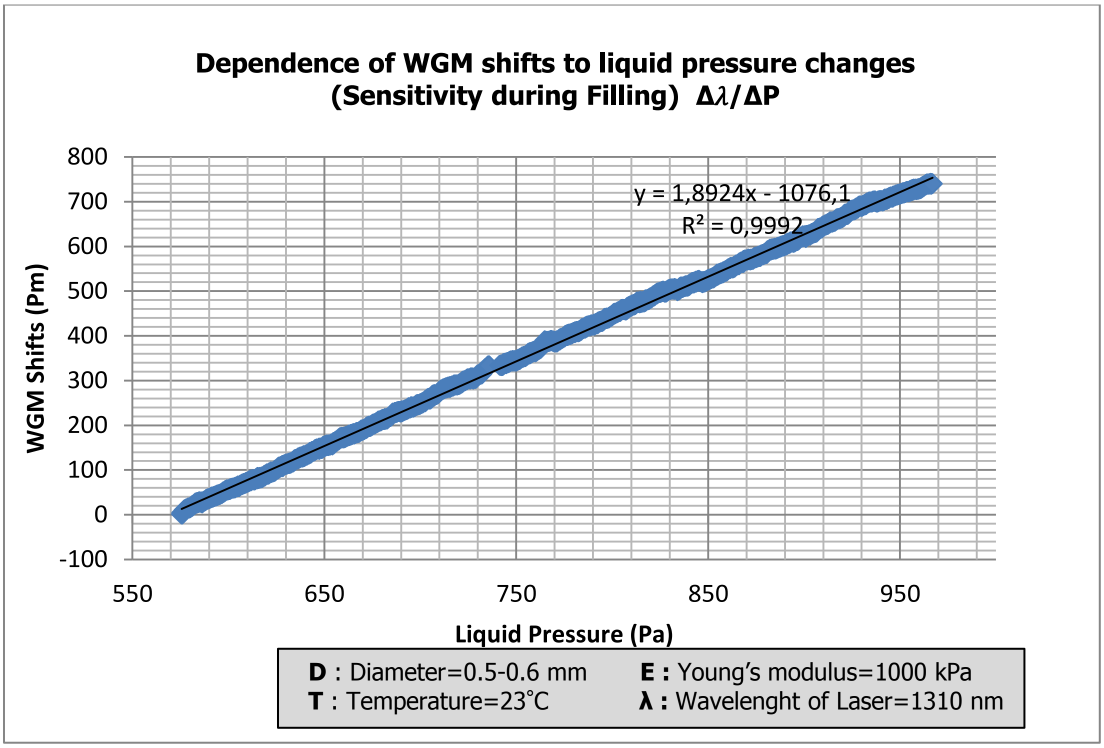

Figure D.9 : The dependence of WGM shifts to liquid pressure changes (3).

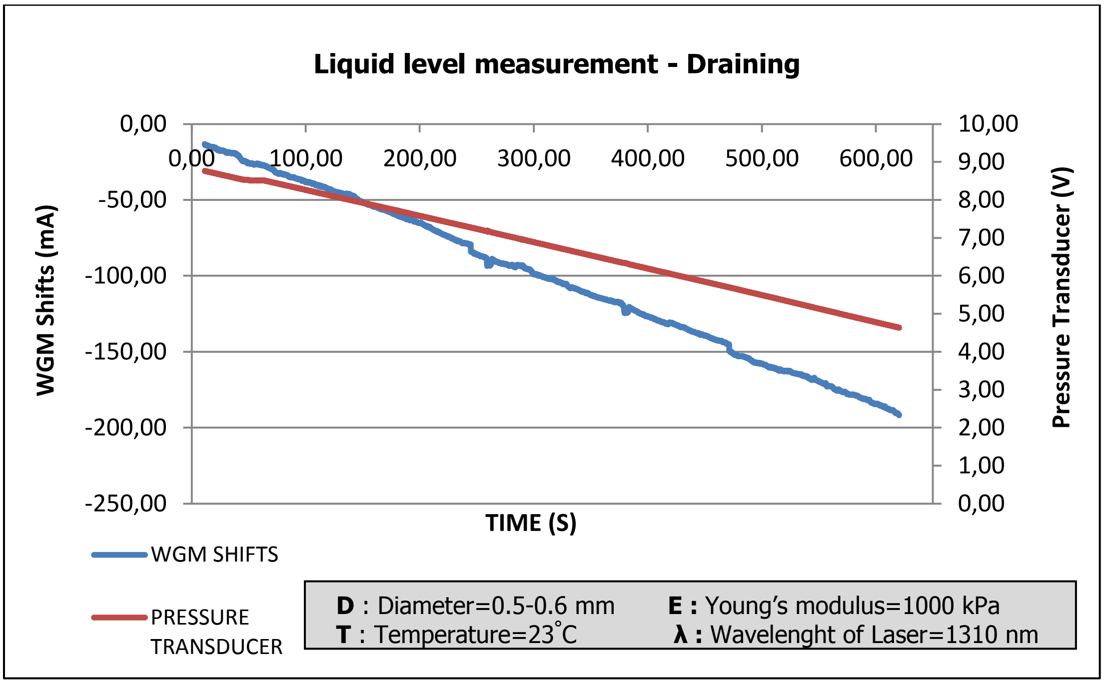

Figure D.10 : Liquid level measurement – Draining (4).

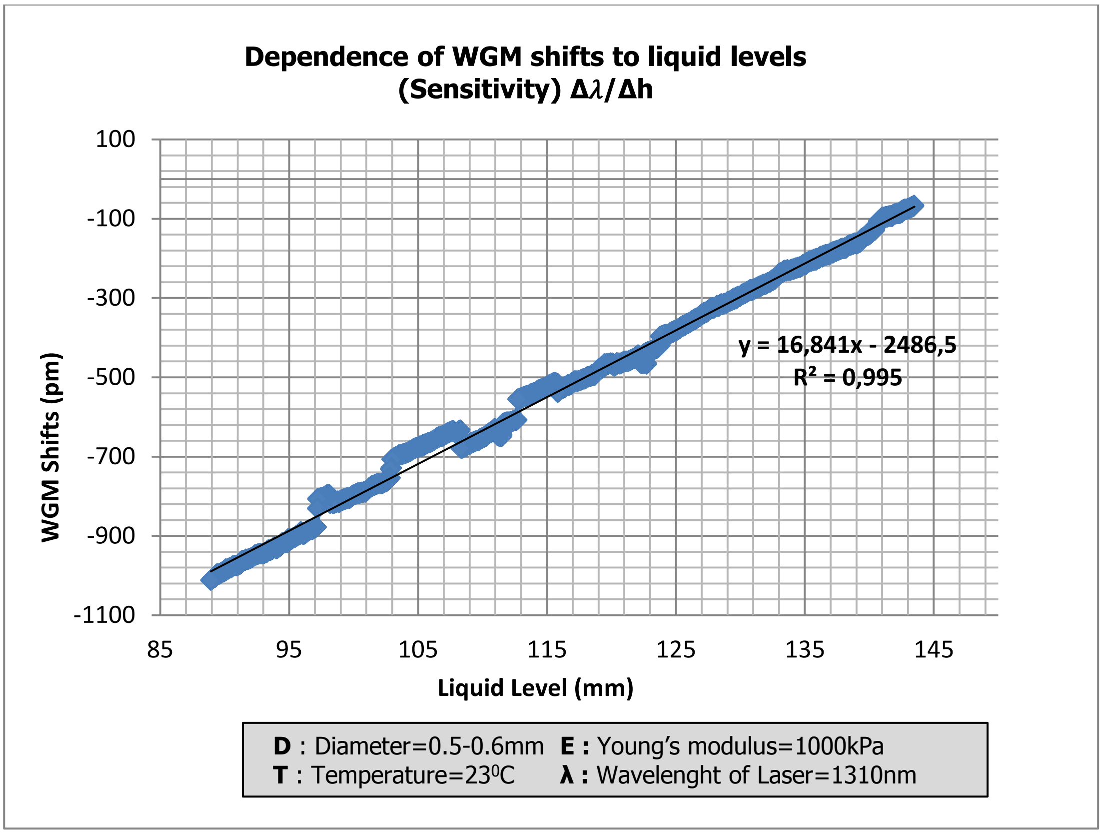

Figure D.11 : The sensitivity dependence of WGM shifts in liquid levels (4).

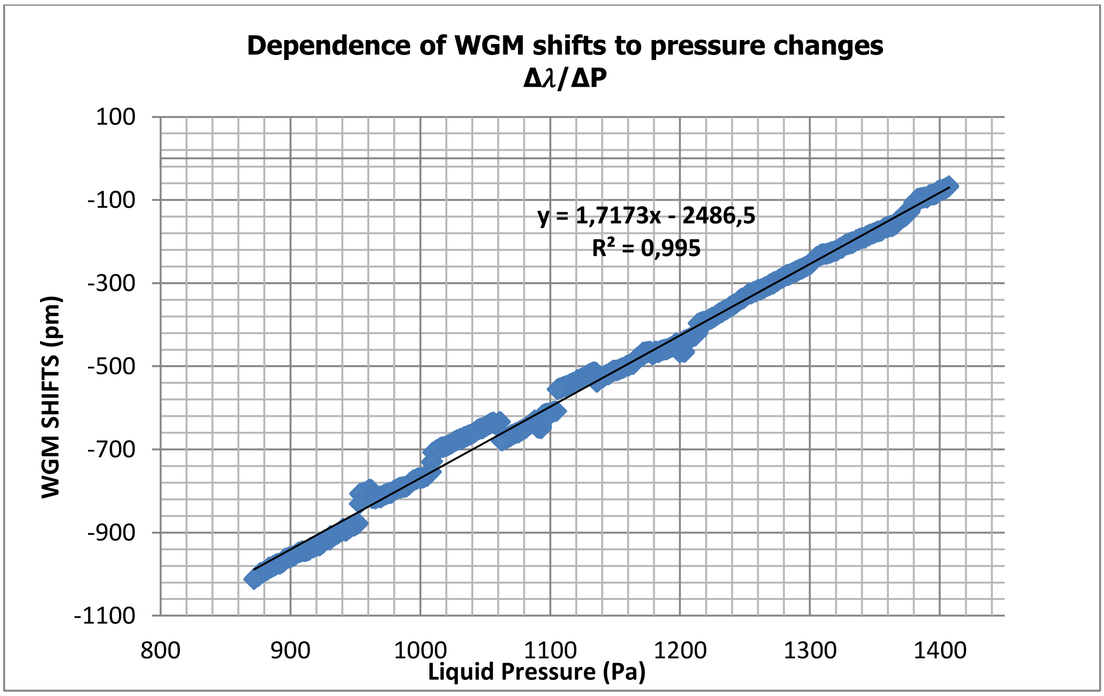

Figure D.12 : Dependence of WGM shifts to pressure changes (4).

CURRICULUM VITAE

Name Surname: Mehmet Emre Erdem

Place and Date of Birth: Istanbul 03/01/1979

E-Mail: emre_erdem@rocketmail.com

B.Sc.: 1997 – 2001 Istanbul Technical University,
Mechanical Engineering, BSc

M.Sc.: 2001 – 2004 Istanbul Technical University,
Mechanical Engineering, MSc

Mba: 2001 – 2004 Marmara University,
Mba on Management & Organization

List of Publications and Patents:

- *"A Novel Liquid Level Sensor Design Using Laser Optics Technology" Ph.D, 2012*
- *"Contribution Of Motivational Needs On the Internet Usage". MBA, 2004*
- *"Total Quality Management and An Application Example: MA-PA", MSc, 2004*
- *"Wind Energy Potential Of Turkey and An Application", BSc, 2001*

PUBLICATIONS/PRESENTATIONS ON THE THESIS

- *Erdem M. E. and Güneş D., 2011: "Liquid Level Sensor in Automotive Design,"* The Fifth International Conference on Sensor Technologies and Applications: SENSORCOMM 2011, ISBN: 978-1-61208-144-1
- *Erdem M. E. and Güneş D., 2012: "Lazer Optik Teknolojisi ile yeni bir Sıvı Seviye Sensörü",* İTÜ Dergisi / dMühendislik
- *Erdem M. E. and Güneş D., 2012: "A Novel Liquid Level Sensor Design Using Laser Optics Technology",* Sensors and Transducers Journal (ISSN 1726-5479), Vol.13, Special Issue, no.11, February 2012